MARMARA UNIVERSITY
INSTITUTE FOR GRADUATE STUDIES IN PURE AND APPLIED SCIENCES

EXPERIMENTAL INVESTIGATION OF INFLUENCES OF SUPPORT PLATES ON MICRO-DRILLING OF CFRP LAMINATES

AHMET DOĞRUSADIK

Ph.D. THESIS

Department of Mechanical Engineering

Thesis Supervisor
Assoc. Prof. Dr. Aykut KENTLİ

ISTANBUL, 2017

MARMARA UNIVERSITY
INSTITUTE FOR GRADUATE STUDIES IN PURE AND APPLIED SCIENCES

EXPERIMENTAL INVESTIGATION OF INFLUENCES OF SUPPORT PLATES ON MICRO-DRILLING OF CFRP LAMINATES

AHMET DOĞRUSADIK

(724611004)

Ph.D. THESIS

Department of Mechanical Engineering

Thesis Supervisor

Assoc. Prof. Dr. Aykut KENTLİ

ISTANBUL, 2017

MARMARA UNIVERSITY

INSTITUTE FOR GRADUATE STUDIES IN PURE AND APPLIED SCIENCES

Ahmet DOĞRUSADIK, a Doctor of Philosophy student of Marmara University Institute for Graduate Studies in Pure and Applied Sciences, defended his thesis entitled "**Experimental investigation of influences of support plates on micro-drilling of CFRP laminates**", on December 25, 2017 and has been found to be satisfactory by the jury members.

Jury Members

Assoc. Prof. Dr. Aykut KENTLİ (Advisor)
Marmara University ..... (SIGN) .....

Prof. Dr. Bülent EKİCİ (Jury Member)
Marmara University ..... (SIGN) .....

Prof. Dr. Abdülkerim KAR (Jury Member)
Marmara University ..... (SIGN) .....

Prof. Dr. Haydar LİVATYALI (Jury Member)
Yildiz Technical University ..... (SIGN) .....

Assoc. Prof. Dr. Mustafa BAKKAL (Jury Member)
Istanbul Technical University ..... (SIGN) .....

APPROVAL

Marmara University Institute for Graduate Studies in Pure and Applied Sciences Executive Committee approves that Ahmet DOĞRUSADIK be granted the degree of Doctor of Philosophy in Department of Mechanical Engineering on 22.01.2018.
(Resolution no: 2018/02-03)

Director of the Institute **Prof. Dr. Bülent EKİCİ**

ACKNOWLEDGEMENT

I would like to express my deepest gratitude to my supervisor Assoc. Prof. Aykut Kentli for his encouragement, support, and guidance. I am grateful to him for accepting me as a PhD student. I would like to thank my dissertation advisory committee members, Prof. Abdülkerim Kar and Assoc. Prof. Mustafa Bakkal. I am grateful to Assoc. Prof. Mustafa Bakkal for his support and advice to realize the cutting temperature and cutting forces experiments and, Prof. İsmail Lazoğlu who let me carry out the cutting force experiments in his research center, and Asst. Prof. Murat Çakan for his support and advice to realize the cutting temperature measurements.

I wish to express my appreciation to the evaluation committee members who have spared their valuable time for the assessment of this work.

I would like to thank my wife Nurdan for her endless support throughout my PhD study. Without her encouragement, I could not complete my PhD education. I am grateful to my parents who raised me with self-confidence and my sisters and brothers for their support.

This thesis was supported by Research Fund of the Marmara University. Project Number: FEN-C-DRP-080715-0343.

December 2017 **Ahmet DOĞRUSADIK**

TABLE OF CONTENTS

ÖZET

DESTEK PLAKALARININ KETP LAMİNALARIN MİKRO DELİNMESİ ÜZERİNE OLAN ETKİLERİNİN DENEYSEL OLARAK İNCELENMESİ

Delme nedeniyle oluşan delaminasyon ve takım aşınması Karbon Elyaf Takviyeli Plastik (KETP) laminaların mikro delinmesindeki iki temel problemdir. Delaminasyon yapının dayanımı ile ilgilidir ve önlenmelidir. Destek plakalarının kullanılması delme nedeniyle oluşan delaminasyonu azaltmak için kullanılan yöntemlerden biridir. Ancak destek plakalarının kullanılmasının delik çapı, dairesellik ve arta kalan elyaf alanı gibi işlem çıktıları üzerine bazı etkileri vardır. Bu çıktılar elyaf takviyeli kompozit malzeme üzerine delinmiş olan deliğin form kalitesini belirler. Destek plakalarının delaminasyon, delik form kalitesi ve takım aşınması üzerine olan etkileri çeşitli iş mili hızı ve ilerleme değerleri altında deneysel olarak incelenmiştir. Üç farklı deney seti kullanılmıştır. Birinci deney setinde, desteksiz KETP laminalar delinmiştir. İkinci deney setinde, alüminyum giriş plakası ve fenol çıkış plakası kullanılmıştır. Üçüncü deney setinde destek plakalarının malzeme etkisini incelemek için, pirinç giriş plakası ve ahşap çıkış plakası kullanılmıştır. Takım aşınmasının işlem çıktıları üzerine olan etkisini belirlemek için her bir deneyde çok sayıda delik delinmiştir. KETP laminaların mikro delinmesindeki delaminasyon hasarının sıradan delik delmedeki delaminasyon hasarından farklı olduğu ortaya çıkmıştır. Çap, dairesellik ve arta kalan elyaf alanının değişimleri her bir deney seti için değerlendirilmiştir. Destek plakalarının işlem çıktılarını genellikle geliştirdiği ve işlemi, işlem değişkenlerinin ve takım aşınmasının değişimine karşı daha az duyarlı hale getirdiği ortaya çıkmıştır. Ayrıca, ilerlemenin serbest yüzey aşınması üzerinde iş mili hızına göre daha etkili olduğu ortaya çıkmıştır. Ayrıca, KETP laminantların mikro delinmesinde kesme sıcaklığı ve kesme kuvvetlerini araştırmak için ayrı gruplar halinde deneyler gerçekleştirilmiştir.

ABSTRACT

EXPERIMENTAL INVESTIGATION OF INFLUENCES OF SUPPORT PLATES ON MICRO-DRILLING OF CFRP LAMINATES

Drilling induced delamination and tool wear are two major problems in micro-drilling of CFRP laminates. Delamination is concerning the strength of the structure and must be prevented. Using support plates is one of the methods to decrease the drilling induced delamination but also has some effects on the other process outputs such as hole diameter, roundness, and fiber overlap area. These outputs determine the form quality of a drilled hole on a fiber reinforced composite material. The effects of support plates on delamination, hole form quality, and tool wear were investigated experimentally under variable spindle speeds and feeds. Three different setups were employed. In the first setup, bare CFRP laminates were drilled. In the second setup, the entry board was aluminum plate and the backing board was phenolic plate. In the third setup, brass entry board and wooden backing board were used to inspect the material effect of the support plates. Numerous holes were drilled per an experiment to identify the effect of tool wear on the process outputs. It was revealed that the delamination damage in micro-drilling differs from the delamination damage in conventional drilling of CFRP laminates. Variations of diameter, roundness, and fiber overlap area were evaluated for each setup. It was concluded that the support plates generally improved the process outputs and made the process less sensitive to the change of the process variables and tool wear. It was also revealed that feed was more effective on flank wear than spindle speed. In addition, experiments were carried out to investigate the cutting temperature and cutting forces separately in micro-drilling of CFRP laminates.

CLAIM FOR ORIGINALITY

EXPERIMENTAL INVESTIGATION OF INFLUENCES OF SUPPORT PLATES ON MICRO-DRILLING OF CFRP LAMINATES

Use of carbon fiber reinforced plastic (CFRP) laminates is increasing in the industrial area. In parallel with this progress, complementary processes such as machining must be investigated to reduce the cost of production and to improve the quality of the products. Mechanical micro-drilling is one of them and can be applied to a wide range of workpieces to produce micro holes. However, there are some challenges in the process concerning delamination and tool wear. Abrasive carbon fibers cause rapid wear of the micro drill. Delamination is another challenge for the mechanical drilling operation. In the application, using the support plates is one of the methods to decrease the drilling induced delamination damage. In this dissertation, effects of support plates on process outputs such as delamination, hole diameter, roundness, fiber overlap area, and tool wear in micro-drilling of CFRP laminates were investigated experimentally under variable spindle speeds and feeds. Three setups were employed to inspect the effects of support plates, and the following innovations and findings were obtained.

- Unlike the previous studies, the delamination factors in micro-drilling of CFRP laminates were precisely calculated and compared for supported and unsupported cases.
- Fiber overlap area was calculated for micro-drilling of CFRP laminates.
- Brass entry board was used for the first time in micro-drilling of CFRP laminates.
- Effect of tool wear on process outputs for both supported and unsupported cases was investigated.
- Wear of the micro drill in micro-drilling of CFRP laminates was investigated by taken into account the effects of support plates.

SYMBOLS

α : Delamination damage weight coefficient

A_0 : Nominal area of the hole (μm^2)

A_d : Delamination area (μm^2)

A_{del} : Cumulative peripheral damage area (μm^2)

β : Delamination damage weight coefficient

D_0 : Nominal diameter of micro-drill (μm)

D_d : Diameter of delamination zone (μm)

f : Feed (μm/rev)

F : Feed Rate (mm/min)

F_a : Two-dimensional delamination factor

F_d : Delamination damage

F_{da} : Adjusted delamination factor

S : Spindle speed (rpm)

ABBREVIATIONS

ANOVA : Analysis of Variance

CAD : Computer Aided Drafting

CFRP : Carbon Fiber Reinforced Plastic

DF : Degree of Freedom

GFRP : Glass Fiber Reinforced Plastic

MS : Mean Squares

PCB : Printed Circuit Board

PCD : Polycrystalline Diamond

RGB : Red, Green, Blue

SEM : Scanning Electron Microscopy

SS : Sum of Squares

LIST OF FIGURES

PAGE

LIST OF TABLES

PAGE

1. INTRODUCTION

1.1. Overview

Demand for micro components (Figure 1.1) is increasing significantly for the areas such as automotive, medical, aerospace, electronics, etc. Production of miniature parts requires the higher dimensional accuracy, precision, and surface quality. One of the fields which requires the micro components was watch production industry in the past. Today, there are many fields which require the micro components. Printed circuit boards, fuel injection nozzle for automobiles, and medical tools contain micro holes and forms. Micromachining is one of the key technologies which can meet the requirements for micro components. Micro components by the process of micromachining can be obtained by means of the improvements in cutting technology [1,2].

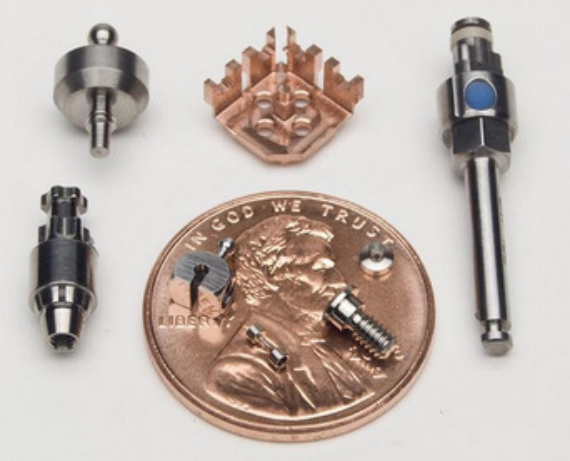

Figure 1.1. Sample parts produced by micromachining [3].

CFRP is a remarkable composite material for key industries due to its excellent properties such as high strength, low density, resistance to corrosion etc. It is known that advanced composite materials make about 50% of the structural weight of Boeing 787 and Airbus A350XWB [4]. In particular, CFRP has been a major material in the recently developed aircrafts because of its resistance to corrosion and high loads while reducing the weight of the structural parts [5]. As a superior material, CFRP usually requires complementary processes to obtain finished parts in the applications. Machining is cost effective and widely used solution to derive finished parts from the raw materials.

Machining operations such as drilling, milling and turning processes are used for shaping CFRPs. In addition, mechanical micro-drilling as a micromachining process is used to form micro holes on the CFRP laminates.

One of the application areas where the micro-drilling of CFRP is necessary is that carbon fabric laminated parts of an aircraft such as nacelles, wings and tail surfaces are provided with micro-holes (micro perforations) to reduce the airflow turbulence by delaying the formation of the boundary layer separation. Thus, the laminar flow is extended which leads to reduced fuel consumption [2]. Another application area of the micro-drilling of CFRP is printed circuit boards (PCBs). PCB is an essential part of any electronic product. CFRP laminate is one of the candidates that can replace the currently used boards due to its superior properties in extreme applications. It was demonstrated that the CFRP core PCB provided higher heat dissipation and lower thermal expansion than the conventional PCB [6]. Ogawa et al. stated that in addition to high strength and low density, CFRP is a candidate for PCBs with its higher thermal conductivity [7].

Mechanical micro-drilling is widely used among various micro-hole-making processes. Because, it is independent of workpiece properties, subject to less thermal deformation and minimizes finishing work [8]. The process brings some advantages such as high form quality of the hole, ease of process, widespread usage, low cost, and less thermal deformation to the workpiece but also brings some disadvantages such as drilling induced delamination and tool wear. Abrasive carbon fibers cause rapid wear of the micro drill [9]. Wear of the micro drill cannot be eliminated but can be reduced by selecting the proper cutting parameters [10]. Performance of the cutting tool is the key factor for the cost effective manufacturing. For the micro scale, it is harder to estimate the lifetime of the micro tools due to their gentle structures. Delamination is another challenge, because it is related to the strength of the structure [11]. Experimental researches have shown that using support plates which are placed front and rear sides of the workpiece decreases the delamination damage when drilling micro holes on the CFRP (Carbon Fiber Reinforced Plastic) laminates [12]. Support plates are also called as entry board for the front side and backing board for the rear side. Effect of the support plates on decreasing the drilling induced delamination damage has already been known and used for drilling the printed circuit boards (PCB) which require huge amount of micro holes [13]. As compared to the GFRP (Glass Fiber Reinforced Plastic) which is

used as printed circuit board material, abrasive nature of the CFRP which is not desired due to the rapid wear of the cutting tool puts another problem [2]. Therefore, the effects of the support plates on micro-drilling of CFRP laminates must be investigated to identify the characteristics of the process.

Mechanical micro-drilling differs from the conventional drilling with some aspects. The ratios of the web thickness and chisel edge length of the micro drills to the tool diameter are greater when compared to the ordinary drills to increase the stiffness of the micro drill [14]. Drill nomenclature is shown in Figure 1.2. However, it makes the chip evacuation difficult, and increasing the chisel length causes the higher thrust force during drilling due to the negative rake angle of the chisel edge [15]. The chisel edge contributes significantly to the total thrust force which causes delamination [16]. Moreover, in micro-drilling, uncut chip thickness is small and comparable to the cutting edge radius. This situation brings size effect in the process, and insufficient uncut chip thickness causes ploughing as opposed to cutting. Ploughing influences the surface roughness, chip formation, burr formation, and residual stress state [17]. Size effect in mechanical micromachining has been investigated by several researchers using FEM simulation [18] and slip-line field model [19]. Recently, an experimental study revealed that the different deformation mechanisms occur with the variations of the cutting angle and depth of cut in the orthogonal cutting experiments of the unidirectional CFRP laminate [20].

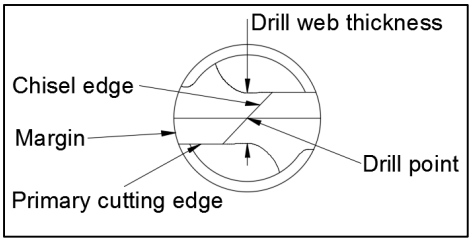

Figure 1.2. Drill nomenclature.

It is obvious that delamination is primary concern when drilling the composite laminates due to its negative effects on the strength [21]. There are several methods which decrease the delamination damage during drilling the composite laminates such as using support plates [22], application of variable drilling conditions [23], changing drill geometry [23, 24], using special drill bits [25] and using pilot hole [26]. But, using pilot hole increases the machining time. Production of special drill bit such as core drill is difficult due to the micro size.

When the support plates are used, drilling process becomes more complex due to the existence of the different structures. Support plates are usually aluminum board for the entry side and phenolic, wooden, or plastic boards for the exit side. For this kind of arrangement, micro drill cuts the entry board, CFRP laminate, and backing board respectively. The first phase is metal, and the following phases are composite materials. Therefore, cutting mechanism changes drastically during operation. There is also an interaction between the delamination and tool wear. Wear of the drill's cutting edges causes higher thrust force and thus higher delamination damage [27, 28].

Using support plates is one of the methods to decrease the drilling induced delamination in micro-drilling of CFRP laminates but also has some effects on the other process outputs such as hole diameter, roundness, and fiber overlap area. These outputs determine the form quality of a drilled hole on a fiber reinforced composite material. For a drilling operation of multiple holes, it is desired that the variation of the hole diameters is small, and the diameters of the drilled holes are close to the drill diameter. Additionally, roundness error value of the holes must be small. Furthermore, fiber overlap area which can be described as the occupation area of the residual fibers must be small for a fiber reinforced composite laminate.

To increase the productivity in a drilling operation without changing the tool path, the only way is to get the higher feed rate (mm/min) which is derived by the product of the following cutting parameters; spindle speed (rpm) and feed (rev/min). However, there are some limitations concerning the hole quality and tool life due to the excessive thrust force and torque. Overburdening the cutting tool causes the rapid wear and sudden breakage. Possible reason of sudden breakage is that cutting forces may exceed the values that the tool can withstand, or worn cutting edge causes the increase of the cutting forces. To improve the tool life, wear mechanisms are investigated. Tool wear is usually inspected by SEM or optical microscopes after drilling sufficient number of holes or can be detected indirectly. As cutting tool wears, thrust force and torque increase. Thus, the measurement of them gives some information about the tool wear condition [29, 30]. The change in consumed power can be attributed to the tool wear [31]. Acoustic emission [32] and vibration [33] were also reported to detect the tool condition in the literature. Indirect methods are usually named as on-line tool condition monitoring. There are also some tool wear detection methods without disassembling the tool from the machine. In a

mass production system such as CNC machine, a tool is changed for one machining operation. After the operation the tool is released to the magazine of the machine, and the tool waits for the next operation. During this period, a touch sensor, laser, or camera system may be used to compensate the tool wear. When the maximum tolerable amount of wear is reached, the tool is changed with the new one. These are the methods which can be used to detect the tool wear, but also increase the investment cost. Tool life is usually determined as the maximum number of holes that can be drilled in mass production. When this number is reached, cutting tool is changed regardless of the tool condition. If tool wear is unstable, it is difficult to determine the tool life. In such a case, tool life is determined as over conservative to eliminate the tool failure. Therefore, indirect methods have some advantages. However, some of the indirect methods cannot be used for the present to estimate the condition of micro drills because of very small force, torque or sensitivity [32]. Rapid wear of the cutting tool increases the production cost, deteriorates the hole quality, affects the burr formation specially for the metals and delamination damage for the fiber reinforced composites.

1.2. Objective and Motivation

Micro-drilling of CFRP laminates is emerging due to demands for several applications. In this area, there are not enough experimental studies in the literature. Micro-drilling of CFRP laminates must be investigated to provide the cost effective and quality products. It is obvious that delamination is primary concern to increase the hole quality as usual for all fiber reinforced composites. There are several techniques which limit the delamination damage during drilling of the CFRP laminates such as using support plates, application of variable drilling conditions, changing drill geometries and using pilot hole. There are several articles about micro-drilling of CFRP laminates. However, a comprehensive study is not produced about the influences of support plates on micro-drilling of CFRP laminates. In this experimental work, influences of support plates are particularly investigated under variable drilling conditions. With the guidance of this experimental study, it is aimed to find out distinctive relationships between the process inputs such as support plates, cutting speed, feed and the process outputs such as delamination, hole form quality, tool wear, cutting temperature, and cutting forces.

1.3. Literature Survey

Literature about the subject of the micro-drilling of CFRP laminates is limited. Only a few articles which have been studied experimentally can be found. Therefore, literature about the conventional drilling of CFRP has been revised in addition to the literature about the micro-drilling of CFRPs.

It is obvious that the delamination is primary concern when studying the drilling of the CFRPs [21]. König et al. have introduced a critical thrust force approach. According to this approach, delamination starts when the thrust force exceeds a critical value [34]. Hocheng and Dharan have proposed the first analytical model to calculate the critical thrust force [35]. Hocheng and Tsao have proposed analytical models and also applied analytical models for different types of drills [22, 25]. They have extended their study by using exit back-up which increases the critical thrust force [36]. It is seen that the support plates drastically decrease the delamination in drilling. Capello stated that the additional sacrificial ply can be used under CFRP laminate to reduce the delamination. He also stated that the support plate may contain pre-drilled hole which is coaxial with the drill [37]. There are many parameters which affect the thrust force for a drilling operation such as spindle speed, feed, drill geometry, tool wear, etc. It is seen from the experimental investigations which have been conducted to inspect the conventional drilling of fiber reinforced composites that effect of spindle speed on the thrust force is not significant, and thrust force slightly decreases as spindle speed increases, but effect of feed on the thrust force is significant and thrust force increases as feed increases [38-43].

Experimental studies have been extensively conducted to reveal the effects of spindle speed and feed on the delamination damage. According to the experimental studies, delamination damage increases as feed increases [28, 44-52]. However, there is no consensus for the effect of spindle speed. It was reported in one group of researches that delamination damage increases as spindle speed increases [44-48], vice versa for another group [28, 49-54].

As for micro-drilling of CFRP laminates, Rahamathullah and Shunmugam have realized experiments on micro-drilling of CFRP laminates [2]. It is known that support plates have significant effects on the hole quality when drilling thin laminates. These effects

have been introduced experimentally as an application to micro-drilling of CFRP laminate with high speed drilling process by Ogawa et al. [12]. Anand et al. have carried out experimental study for micro-drilling of CFRPs with taking into account the size effect [55]. Ogawa et al. realized an experimental study by using diamond coated tools to show the cutting tool coating effect on the micro-drilling of CFRP plates [7]. According to their study, diamond coated cutting tools showed superior performance. Anand and Patra developed a mechanistic model to predict the thrust force and torque for micro-drilling of CFRP laminates by taking into account the cutting tool edge radius and layered structure of CFRP laminates as fabric plies and epoxy resin matrix instead of an equivalent homogeneous material. They also validated their study by the experimental results [56].

Among the experimental studies, only Ogawa et al. used support plates [12]. However, in their study, the cutting speed and the setup of the support plates were not changed and the delamination factor was not calculated. The effect of the support plates was just shown visually. A comprehensive study must be considered to discover the support plate effects for different support plate setups and cutting conditions. Therefore, the support plate effects on the hole quality will be studied in particular. The effects of cutting speed and feed will also be examined for different support plate setups.

1.3.1. Literature review of tool wear

Following findings were reported in the literature to identify the wear modes in drilling the CFRP laminates and similar composites. The process temperature in CFRP machining is lower as compared to the metal machining due to the chip formation mechanism which occurs in the form of fracture, and thus diffusion wear does not take place [57]. Rawat and Attia [58] stated that chipping and abrasion were the wear mechanisms which deteriorate the carbide drill in their experimental study. Zheng et al. [59] investigated the wear mechanisms of the cemented tungsten carbide micro drills which used for drilling printed circuit boards, and revealed that the broken glass fiber chips, reinforcing fillers, and diffusion of cobalt caused the abrasion which was main wear mechanism. Usually, fiber reinforced composite laminates are not drilled alone. Combinations of CFRP/Ti and CFRP/Al stacks for the aerospace industry, Cu/GFRP printed circuit boards for the electronics, and metal, plastic, or composite entry and exit

boards which decrease the delamination damage are common arrangements. Wang et al. [60] stated that drilling CFRP/Ti stacks improved the tool life more than three times compared to the drilling Ti plate due to the fact that carbon fibers brush off the Ti adhesion and smoothing the cutting edge, and also stated that edge rounding is primary tool wear mode when drilling CFRP laminates. Lin and Chen [61] carried out an experimental study by using a carbide drill in the diameter of 7 mm and revealed that tool wear increased drastically with increasing spindle speed, and the tool wear increased the thrust force. Chen [62] realized drilling experiments on CFRP laminates by using carbide drills with a diameter of 5 mm and concluded that increased flank wear caused higher delamination damage due to increase of the generated thrust force. Shyha et al. [23] carried out an experimental study by using 1.5 mm carbide drill to inspect the effects of the drill geometry and cutting parameters in drilling CFRP laminates, and revealed that higher feeds increased the tool life. Tsao and Hocheng [27] used the plate-bending theory and linear elastic fracture mechanics to model the thrust force considering the chisel edge wear for the worn drill and realized experiments to validate the model. They concluded that although the critical thrust force increased with the wear, the delamination was more probable to occur due to the excessive increase of the actual thrust force with wear. Zitoune et al. [63] carried out an experimental study which compares the double cone drill to the ordinary twist drill and stated that the double cone drill decreases the thrust force and wear, sustains the hole quality for more holes. Faraz et al. [64] proposed the cutting edge rounding as a wear criterion for drilling CFRP laminates with various kinds of carbide drill geometries and stated that the cutting edge rounding based wear measurement is easier than the flank wear measurement when different tool geometries were used. Raj and Karunamoorthy [65] carried out an experimental study to inspect the wear of 6.35 mm carbide drills when drilling CFRP laminates, and concluded that although the cutting edge radius is constant along the cutting edge length for a new drill, it does not form a perfect circle and varies non-uniformly from the center to the periphery as tool wears. Liu [66] used the flank wear area instead of flank wear height to measure the magnitude of the flank wear of the drill, and stated that the flank wear height did not provide stable range for the consecutive drills according to the trials. Su et al. [67] developed an automated flank wear inspection method for the micro drills which are used in drilling PCB boards, and stated that the

vision system measures the flank wear area, average flank wear height, maximum wear height, and height of the cutting plane. Imran et al. [68] proposed the wear map approach which was a two dimensional graph with the spindle speed and feed axis to find out the safe zones against the flank wear of the micro drill in micro-drilling of nickel-based super alloy. Wear map approach may be helpful to choose the eligible cutting conditions against the wear when a general trend does not occur.

1.3.2. Literature review of thermal investigations

Thermal investigations about the machining of CFRP laminates can be summarized as follows. Chen [62] carried out an experimental study to measure the flank surface temperature of the drill with embedded thermocouple method in drilling of CFRP laminates and stated that flank surface temperature increases as cutting speed increases and feed rate decreases. Brinksmeier at al. [69] used pyrometer method to measure the cutting temperature in drilling CFRP laminates, and stated that the maximum temperature increased with increasing cutting speed, and vice versa for the feed. Yashiro et al. [70] demonstrated several temperature measurement methods as tool-workpiece coupling method to measure the tool tip temperature, infrared thermography method to measure end mill surface temperature, and thermocouple method to measure the machined surface temperature in milling of CFRP laminates and stated that high cutting speeds up to 300 m/min did not influenced the resin matrix as a result of SEM observations of the machined surface. Wang et al. [71] used the tool-workpiece coupling method to measure the cutting temperature in milling of CFRP laminates and concluded that spindle speed is the most influential parameter on temperature among the other parameters of feed rate and radial depth of cut, and increase in the spindle speed increases the cutting temperature. Pinho et al. [72] stated that peel-up delamination decreases as temperature increases at the beginning of the process in drilling of CFRP laminates with diamond-coated drill. Zitoune et al. [73] pointed out that thrust force decreases as spindle speed increases due to fact that elevated temperature on the cutting edge of the drill reduces the cutting resistance of epoxy. Ghafarizadeh et al. [74] stated that cutting speed and fiber orientation are influential on the cutting temperature in milling of unidirectional CFRP laminates, and maximum cutting temperature occurs for 90° fiber orientation whereas minimum cutting temperature occurs for the 0°fiber

orientation. Sorrentino et al. [75] measured both the drill and CFRP temperatures with K type thermocouples and stated that maximum drill temperature increases with increasing cutting speed and decreasing feed (μm/rev), and workpiece temperature in low cutting speed decreased with increasing feed, while it was almost found constant in high cutting speed. Wang et al. [76] placed K type thermocouples on the flank face of diamond coated cemented carbide drill to measure the temperature in drilling of CFRP/Al stacks, and stated that drilling temperature increased with increase of the spindle speed and decrease of the feed, and they also stated that drilling Al/CFRP stacks caused less maximum temperature as compared to the drilling CFRP/Al stacks. Merino-Pérez et al. [77] carried out an experimental study by using an uncoated cemented carbide double point angle drill on CFRP laminates and stated that high cutting speed caused severe matrix cracking and splintering on hole entry and exit according to the SEM inspection, and it was also found that types of reinforcement and polymer matrix have significant effect on the maximum developed temperature.

1.4. Methodology

To reveal the effects of support plates on process outputs such as delamination, hole diameter, roundness, fiber overlap area, and tool wear in micro-drilling of CFRP laminates, an experimental study is planned. Also, to identify the effects of cutting parameters of spindle speed and feed on the process outputs, three levels of the experiment variables were employed. Three levels of the support plates were applied to reveal the material effect of the support plates. To inspect the effects of the cutting parameters and support plates on tool wear, the number of holes to be drilled was increased under same conditions for each experiment. Results of the experiments were evaluated for each process output.

1.4.1. Structure of report

In Chapter 2, experimental study is explained. Chapter 3 deals with the results of the experimental study. Conclusions are given in Chapter 4.

2. MATERIALS AND METHODS

2.1. Problem Description

Drilling induced delamination and tool wear are two major problems in micro-drilling of CFRP laminates. Using the support plates is one of the methods to decrease the drilling induced delamination but also has some effects on other process outputs. The aim of this study is to reveal the effects of support plates the on process outputs such as delamination, hole diameter, roundness error, fiber overlap, and tool wear.

2.2. Experimental Setup

Experimental layout is shown in Figure 2.1.

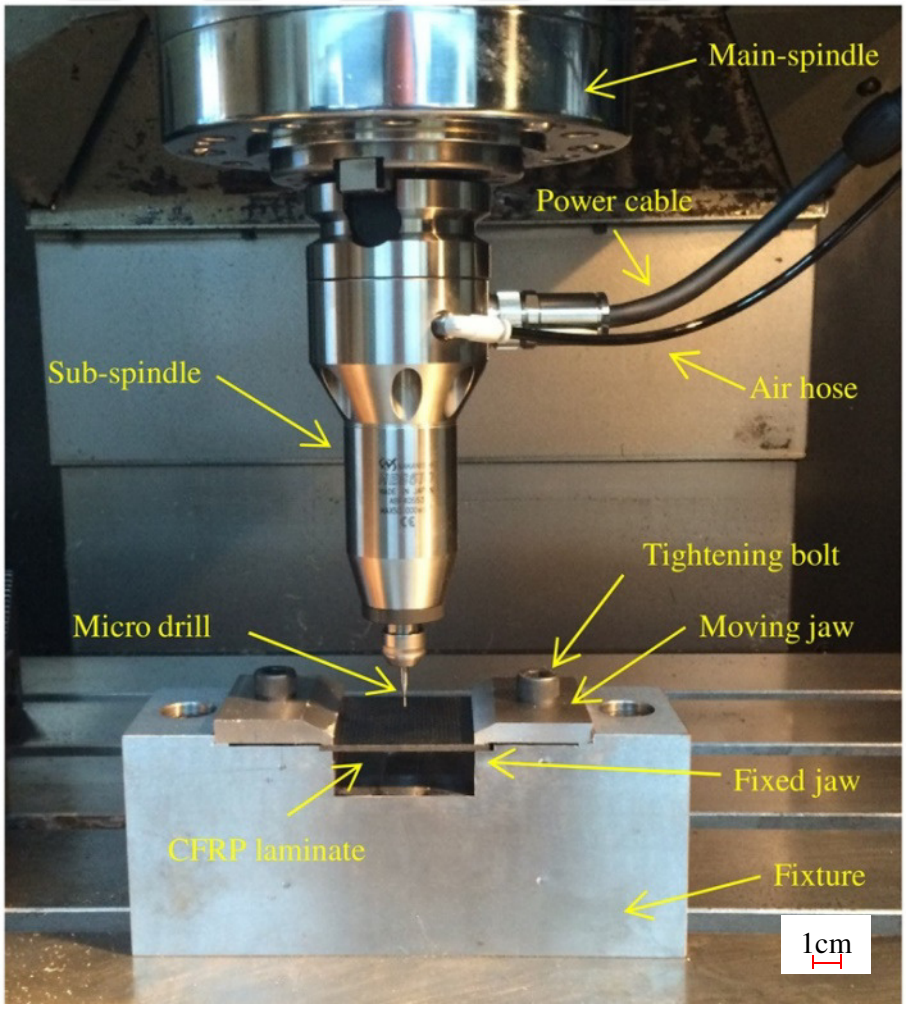

Figure 2.1. Experimental layout.

2.2.1. Material

2 mm thick CFRP laminate was used (Figure 2.2). Each ply was made of 245 g/m2 plain woven fabrics. Tow size of the fibers was 3K. DowAksa-made Aksaca 3K A-38 fibers were used. Fiber properties are shown in Table 2.1. The CFRP laminate was produced by vacuum resin infusion method. Epoxy content of the CFRP laminate was 40 percent. Each CFRP laminate was cut into 60 mm x 60 mm dimensions for placement into the fixture. Through all experiments, mold side of the CFRP laminate was placed upwards and vacuum bag side was placed downwards.

Table 2.1. Fiber properties.

Properties	Value
Tensile strength	3800 MPa
Tensile modulus	240 GPa
Density	1,78 g/cm^3
Yield	200 g/1000m
Strain	1,6 %

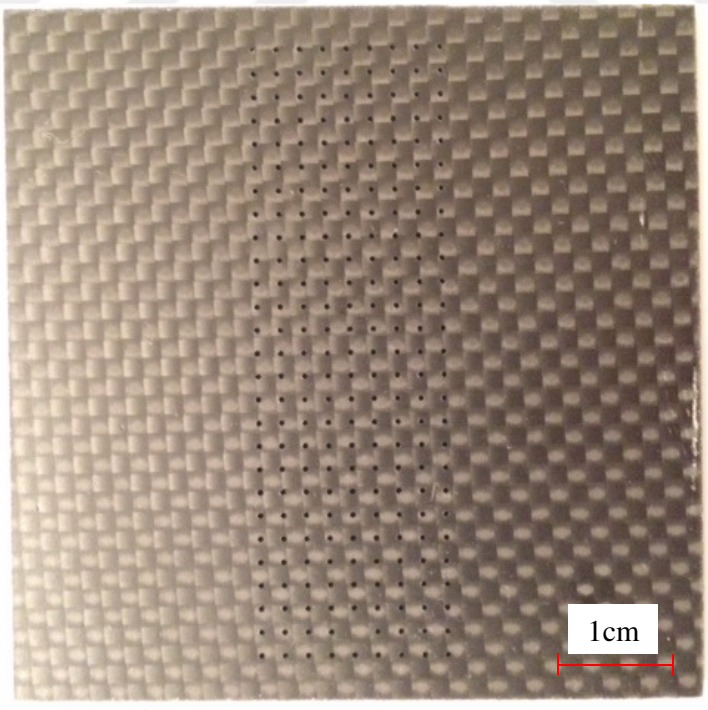

Figure 2.2. CFRP laminate.

2.2.2. Cutting tool

Uncoated solid carbide micro-drills (Figure 2.3) which had been made by Seco Tools were used. Diameter of the micro drill was 0.5 mm. Point angle was 130°. Maximum drilling depth was 3.2 mm.

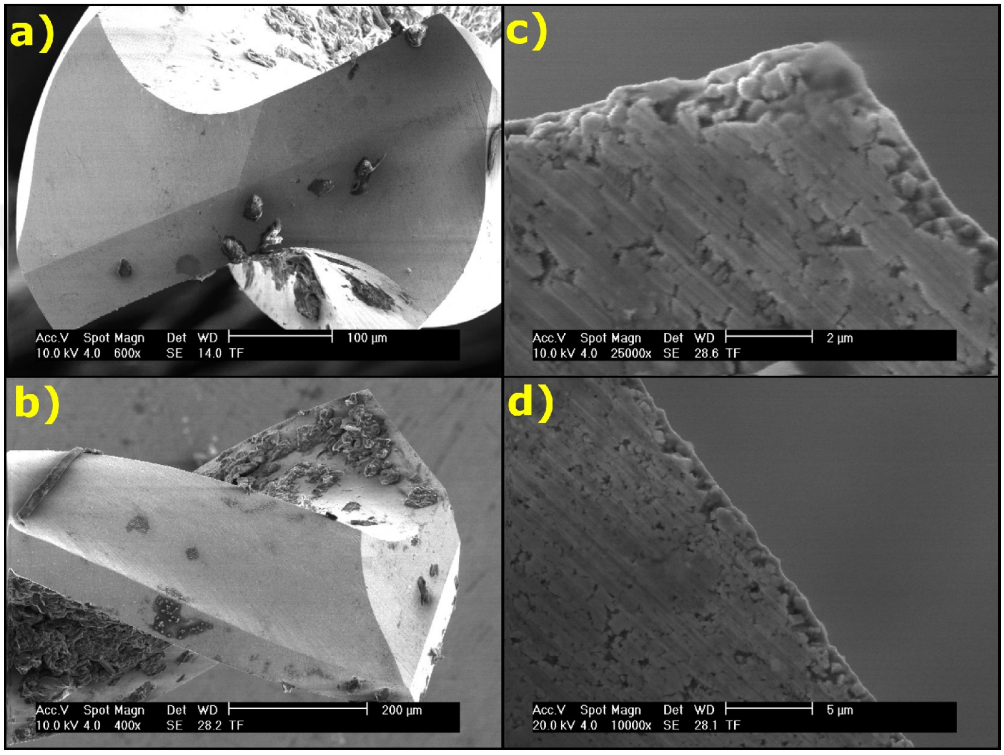

Figure 2.3. Micro drill: (a) top view, (b) side view, (c) corner radius, (d) cutting edge.

2.2.3. Machine tool

Three axes vertical CNC machining center Kent Industrial KMV-11VC (Figure 2.4) was used to perform the micro-drilling process. Due to limited spindle speed of the CNC machine tool, an electrically excited sub-spindle (Nakanishi HES-510) was used to deliver high speed. This kind of sub-spindle ensures the low level of the vibration and noise in comparison with mechanically excited sub-spindles. During operation, spindle of the CNC machining center did not rotate. Cutting speed was provided via sub-spindle.

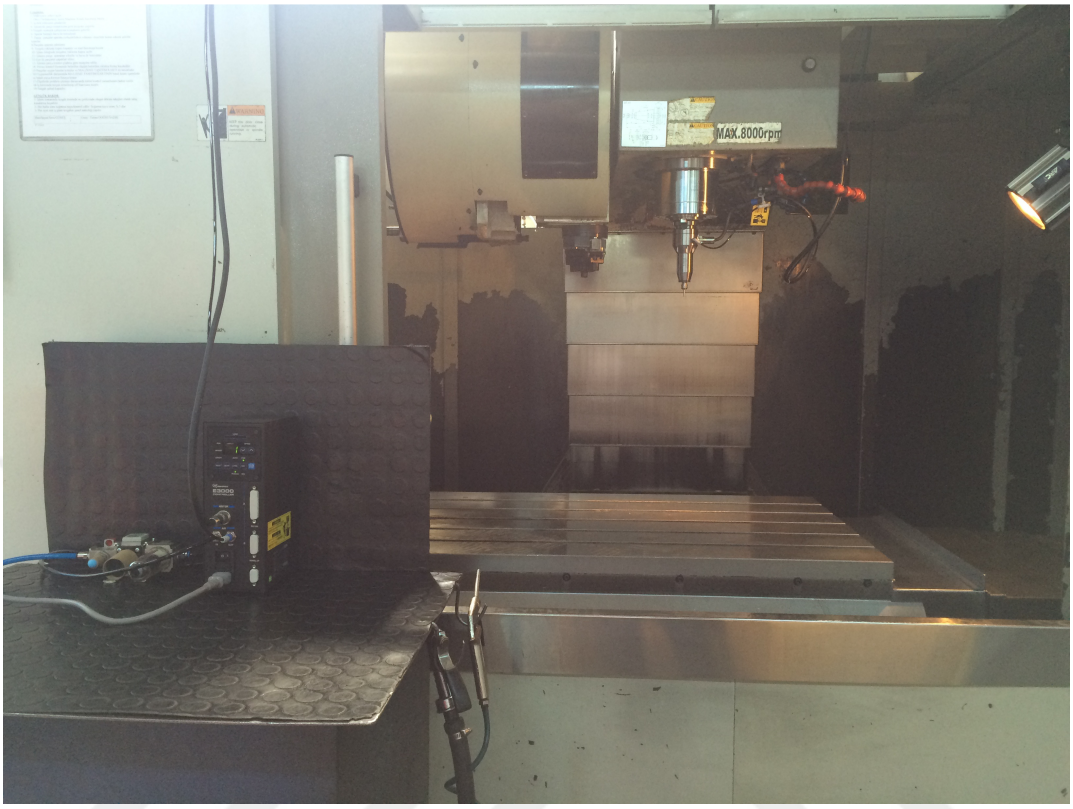

Figure 2.4. Machine tool.

2.2.4. Fixture

A dedicated fixture was designed and manufactured for the samples that must provide the sufficient aligning and fixing tasks for each experiment sample. As bolts are tightened, moving jaws fix the CFRP laminate. The fixed jaws of the fixture were modified after completing bare CFRP laminate setup experiments for the condition where support plates were used to provide enough gap for the assembly of the CFRP laminate, support plates and thrust plate.

2.2.5. Support plates

According to the performed experimental studies, delamination is worse in the rear side where the drill exits the laminate than the front side where the drill enters the laminate [12]. Therefore, different setups of the backing board are getting importance. In the first level, support plates were not used to provide comparison to the situations which support plates were used in the other levels (Figure 2.5). Because there are not enough studies

concerning influences of support plates in micro drilling of CFRP laminates, application of support plates used for GFRP laminates having similar structure was imitated. Since GFRP laminates are often used in the production of printed circuit boards in electronics, many studies have been performed in this area for a long time [78]. The most common assembly of support plates in micro drilling of GFRP laminates is that the entry board is aluminum plate and the backing board is phenolic or wooden plate. Therefore, it was decided to use 0.5 mm thick aluminum plate (1050A H14) as entry board and 4 mm thick phenolic plate as backing board (Figure 2.6). To decrease deflection of the backing boards during operation, thicker plates were used. As a composite material, the structure of phenolic plate is very close to the structure of the CFRP laminate. Only difference is that textile fabrics are used as reinforcement instead of carbon fiber fabrics. Thus, structural resemblance of the workpiece and the backing board is ensured.

Also, to inspect the influence of materials of support plates on the delamination, a third group of experiments were carried out. 0.5 mm thick brass plate (MS 70 - %70 Cu – balance Zn – others max %0.5) was used as entry board and 5 mm thick fir wood plate was used as backing board in the third setup (Figure 2.7). Brass was chosen as entry board because of its good machinability and widespread accessibility in the industry as a thin sheet metal. Due to its anisotropic structure, wood plate was placed longitudinally on the fixture by taking into account the fiber orientation to decrease deflection during operation.

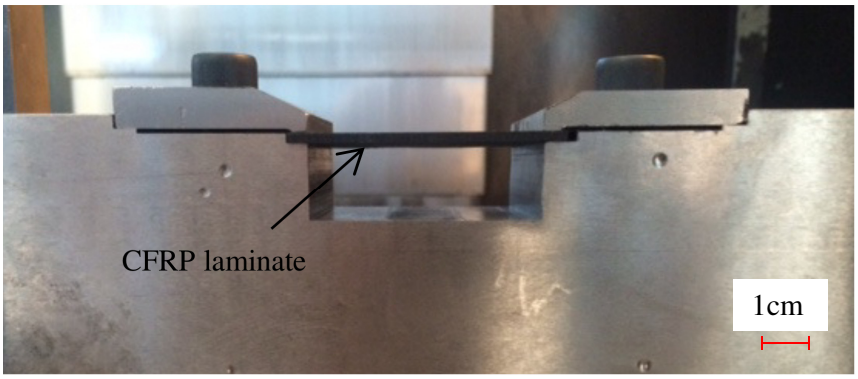

Figure 2.5. Experimental setup in case of bare CFRP laminate.

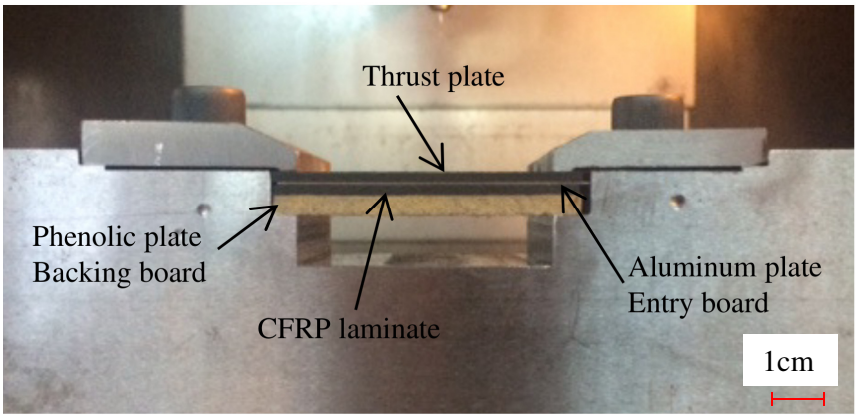

Figure 2.6. Experimental setup in case of aluminum-phenolic support plates.

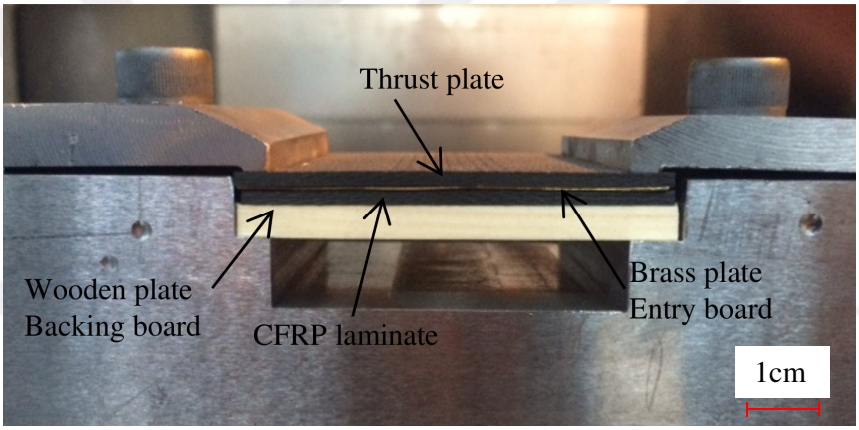

Figure 2.7. Experimental setup in case of brass-wood support plates.

During initial trials, clamping the support plates together with CFRP laminate brought a deflection problem because of the thin structure of the entry board. A thrust plate (Figure 2.8) was used on aluminum and brass entry boards to overcome the deflection of the entry board. One of the unused CFRP laminate of the experiment samples was sacrificed and 242 holes with diameter of 1.2 mm were drilled in sequence of samples which would be drilled during experiments. Because, it was thought that CFRP laminate was an appropriate candidate for thrust plate thanks to its excellent flexural rigidity.

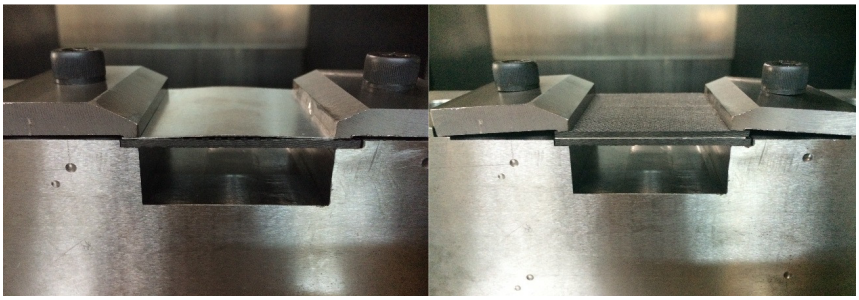

Figure 2.8. Influence of thrust plate.

2.2.6. Inspection

Nikon SMZ 745T trinocular stereo microscope which had been equipped with Toupcam 5.1 MP camera was used to take the hole images of the samples. Each hole was 80 times magnified optically before snapshot. Two-armed cold light source was used. ToupView software was used to extract the positional and areal data from the images of the holes.

2.2.6.1. Delamination

Delamination factor (F_d) is described as the ratio of the delamination zone diameter to the cutting tool diameter [62].

$$F_d = \frac{D_d}{D_0} \tag{1}$$

where, D_d is the diameter of the delamination zone. D_0 is the nominal diameter of the micro-drill. There are several formulas for the delamination factor calculations. Used formula is the most common form. Other forms usually include the delamination damage area [64, 79]. This provides a better comparison in case of different delamination trends occur. But it was not preferred due to the regular forms of the delamination. Two-dimensional delamination factor (F_a) is the ratio of the cumulative peripheral damage area to the nominal hole area [64].

$$F_a = \left(\frac{A_{del} - A_0}{A_0}\right)\% \tag{2}$$

where A_{del} is the cumulative peripheral damage area, A_0 is the nominal area of the hole. Adjusted delamination factor is also proposed to calculate the magnitude of the delamination damage [79].

$$F_{da} = \alpha \frac{D_d}{D_0} + \beta \frac{A_d}{A_0} \tag{3}$$

where A_d is the delamination area which is calculated by using the maximum damage diameter, α and β are weight coefficients.

$$A_d = \pi \frac{D_d^2}{4} \tag{4}$$

$$A_0 = \pi \frac{D_0^2}{4} \tag{5}$$

By substituting equations (1),(4), and (5) into equation (3) gives:

$$F_{da} = \alpha F_d + \beta F_d^2 \tag{6}$$

Davim et al. [79] stated that β can be considered as the ratio of the damage area (A_{del} - A_0) to the delamination area (A_d) minus nominal hole area (A_0) and α is complement of β.

$$\alpha = 1 - \beta \tag{7}$$

Equation (6) can be rewritten as:

$$F_{da} = F_d + \frac{A_{del} - A_0}{A_d - A_0} \ (F_d^2 - F_d) \tag{8}$$

If damage area (A_{del} - A_0) approaches the delamination area (A_d) minus nominal hole area (A_0), then adjusted delamination factor (F_{da}) approaches the square of delamination factor (F_d^2). If damage area (A_{del} - A_0) approaches 0, then adjusted delamination factor (F_{da}) approaches the delamination factor (F_d). Graphical representation of distinctive zones to quantify the delamination is shown in Figure 2.9.

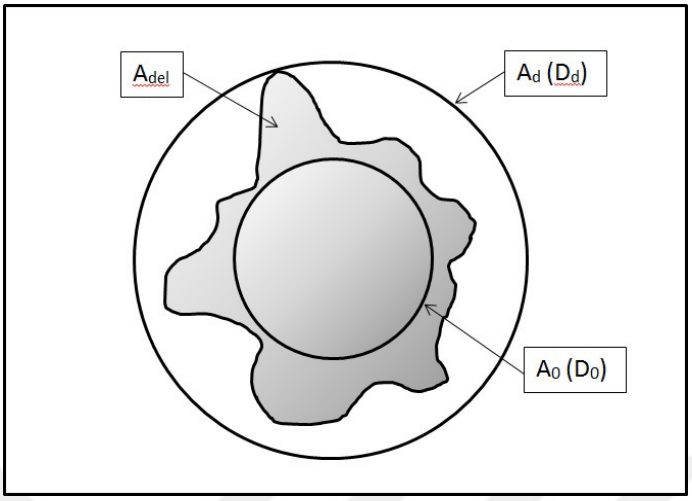

Figure 2.9. Description of distinctive zones.

Following process was repeated to calculate the delamination factor for each hole. First of all, eight points were located around the borderline of drilled hole by the software (Figure 2.10). Center of the hole was determined by using the coordinates of these points with least squares method. Then, a point was located on the picture where the delamination ends. Finally, delamination zone diameter was derived by calculating the distance between the hole center and the delamination end point.

It was preferred to use eight points to form a circle, instead of using three points or drawing a circle on the hole. Thus, center coordinates of the hole which do not belong to a perfect circle is determined precisely.

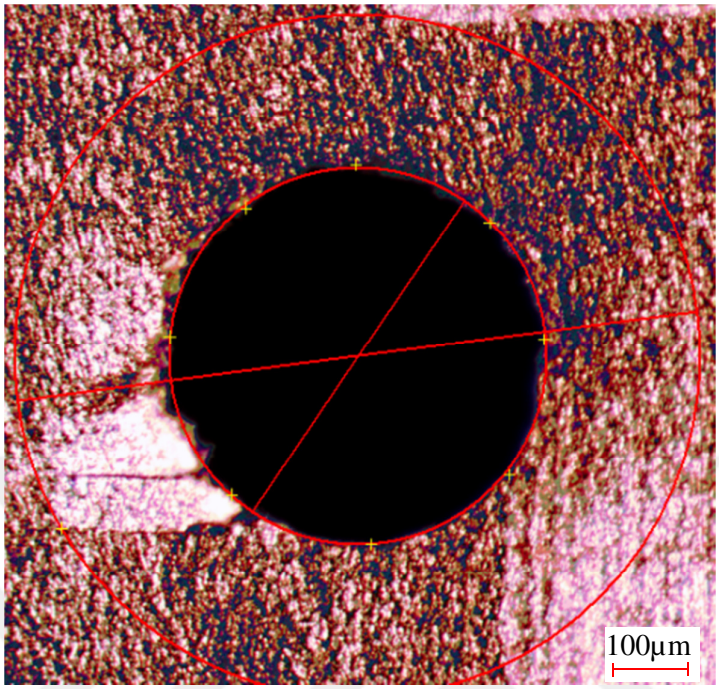

Figure 2.10. Determination of delamination factor.

The eight points were located outside the delamination zone. Because, it might cause miscalculation of the hole center. Also, points were tried to locate with close intervals.

During inspection of the holes, it was observed that burrs of the aluminum and brass support plates had penetrated to the CFRP laminate and formed a ring shaped cavity around the hole as micro-drill entered the material (Figure 2.11). This is another kind of damage and may not be desired for some application areas. Though, this damage is not significant as much as the delamination which affects the strength of the structure. This damage was not observed on the exit side of the CFRP laminates.

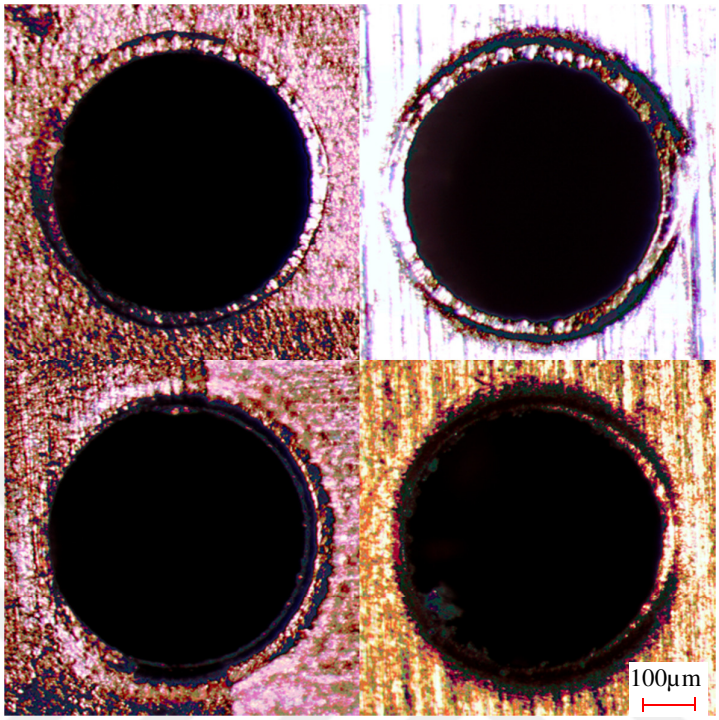

Figure 2.11. Typical ring shaped cavity around the hole (top-left: CFRP laminate in case of aluminum entry board, top-right: aluminum plate, bottom-left: CFRP laminate in case of brass entry board, bottom-right: brass plate)

2.2.6.2. Diameter

The hole images which had been taken by using the digital microscope were used to determine the hole diameters precisely. It was preferred to locate the enough quantity of points on the hole borderline to calculate the diameter of the drilled holes, instead of using direct measurement by means of the software. It was decided by trial that eight points satisfy the circle approximation. Least squares method was used to fit a circle for the selected points. The method provides the diameter and the center coordinates of the fitted circle. A sample fitted circle is seen in Figure 2.12.

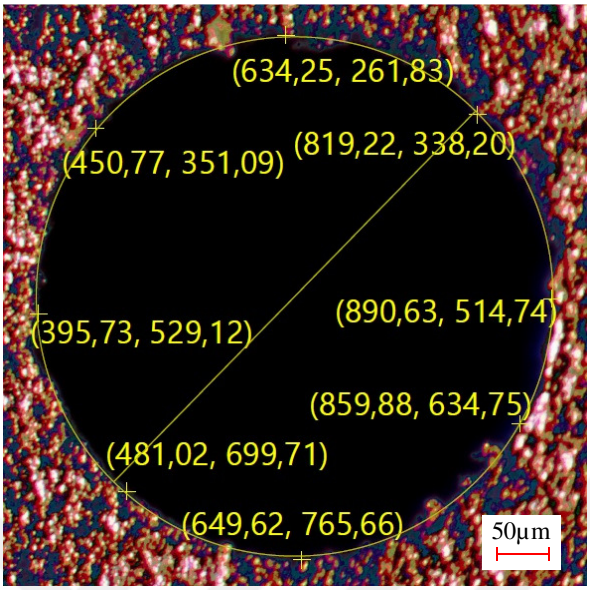

Figure 2.12. Fitted circle by means of the least squares method.

2.2.6.3. Roundness error

Roundness error is an important factor for the hole form quality. There are several approaches to calculate the roundness error of a hole. These can be ordered as follows; least squares circle method, minimum zone circle method, minimum circumscribed circle method, and maximum inscribed circle method. The least squares circle method was used due to the fact that same method was also selected for the diameter calculation. To calculate the roundness error of a hole, eight points which had been used for the diameter calculation were used again. The farthest two points to the fitted circle from the inside and the outside were selected among them, and two concentric circles were produced by using these two points and center point of the fitted circle. Finally, roundness error was derived by calculating the distance between the produced circles. Same procedure was repeated for each hole.

2.2.6.4. Fiber overlap

Drilling fiber reinforced composites may cause residual fibers which are not desired on the hole. Fiber overlap area can be described as the occupation area of the residual fibers on the hole. Fiber overlap was calculated as the ratio of fiber overlap area to the entire hole area and denoted as percentage fiber overlap. Gaugel et al. [80] calculated the fiber

overlap area successfully for the conventional drilling of CFRP laminate by using segmentation process. Similar procedure was applied. To measure the fiber overlap area, the digital image processing tools of the software were used. There are several tools to choose the interested area of the image. One of them is using color cube selection tool. If the hole image is inspected, it is seen that the hole has a dark area which red, green, and blue (RGB) contents are very small. By determining the tolerances for the RGB contents, interested area can be selected by visual inspection. The segmentation area is obtained after the process. Fiber overlap area is derived by subtracting the segmentation area from the hole area which has been calculated by using the fitted circle diameter. In Figure 2.13, images of the sample holes from the front and rear sides are seen before and after the segmentation process.

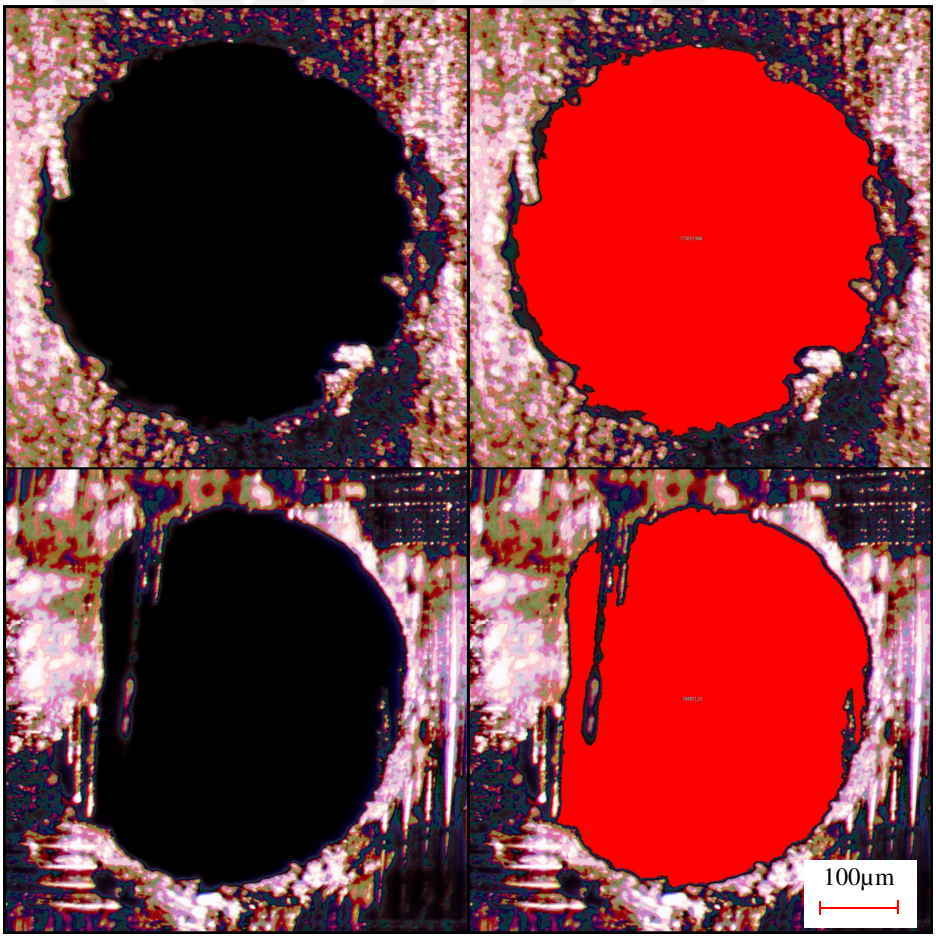

Figure 2.13. Illustration of the segmentation process for the last hole with 30000 rpm and 3 µm/rev feed. (top: front side, bottom: rear side)

2.2.6.5. Tool wear

Nikon SMZ 745T trinocular stereo microscope equipped with Toupcam 5.1 MP camera was used to take the flank face images of the micro drills. A specially designed angled stand (Figure 2.14a) was used to orient the one of the flank face of the micro drill to the objective of the microscope. Each image was 100 times magnified optically before snapshot. Two-armed cold light source was used. The light direction is very important to reflect the interested area as seen in the Figure 2.14b. The flank face images were used to quantify the flank wear area of the micro drills. The boundaries of the remaining flank face area (Figure 2.14c) were redrawn with the lines and arcs on the image by using the image processing software, and the drawing was transferred to CAD software to calculate the remaining flank face area. Flank wear area was derived by subtracting the remaining flank area from the entire flank area which was calculated by using the unused micro drill.

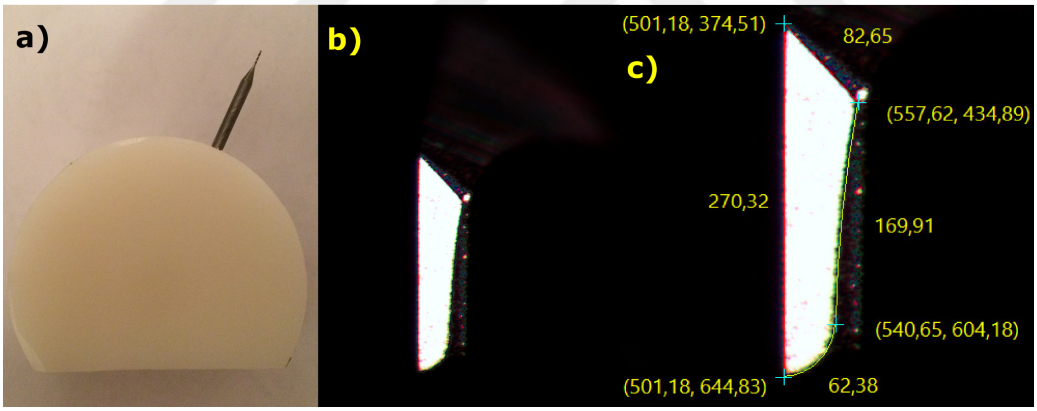

Figure 2.14. Flank wear quantification: (a) micro drill stand, (b) flank face, (c) surrounding the remaining flank face area.

2.2.6.6. Chip morphology

Due to the brittle structure of the carbon fibers, chips are formed as powder during cutting. Some single small fibers are also seen. As for the cases of the support plates, chips of the support plates are also formed. In the experimental study, it is seen that chips of the CFRP laminates in cases of the support plates differ from the chips in case of the bare CFRP laminate. In the result and discussion section, types of the chips are presented.

2.3. Experimental Method

Three setups were planned for micro-drilling experiments under variable cutting speeds and feeds. These are bare CFRP laminate setup, CFRP laminate with aluminum plate as entry board and phenolic plate as backing board setup and CFRP laminate with brass plate as entry board and wood plate as backing board setup. Micro-drilling experiments were realized in random order for each setup. The number of holes to be drilled per experiment with the same tool was determined by finding the worst case with initial trials. Tool breakage was observed among various trials with the spindle speed of 20000 rpm and the feed of 7 µm/rev. The tool breakage did not occur at higher spindle speeds after drilling the same number of holes with the same feed. Also, tool breakage was not observed in case of support plates for the same conditions. Finally, it was determined to limit the number of holes to 242 holes per experiment to prevent the tool breakage. Already, this number of holes sufficed to wear the micro drill. Holes were drilled through CFRP laminate's thickness. In case of setups of support plates, backing board was also drilled at least 0.3 mm depth. At the end of the drilling of a hole, spindle was not stopped and cutting tool was withdrawn rapidly with a feed rate of 2000 mm/min. Drilling sequence (Figure 2.15) was designed by taking into account the symmetrical location of the holes. The first hole was located to the bottom raw and middle column. Drilling order was along columns and every column was started to drill from the bottom raw. Columns were ordered one from right and one from left to balance the structure.

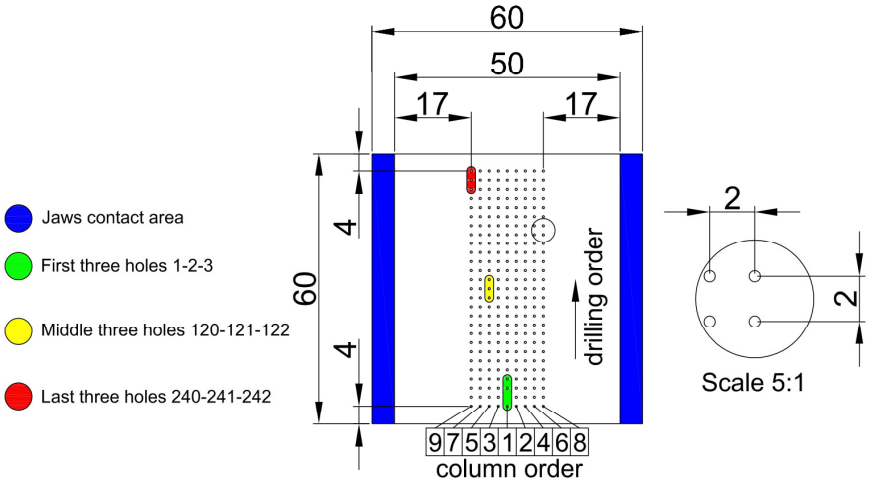

Figure 2.15. Drilling sequence.

Horizontal and longitudinal distances between the holes were determined by trial. Distance of 1 mm between the hole centers caused the merging of the delamination damages of the adjacent holes (Figure 2.16). But it was not observed with the distance of 2 mm. Thus, sufficient unaffected area provided for each hole by using a distance of 2 mm.

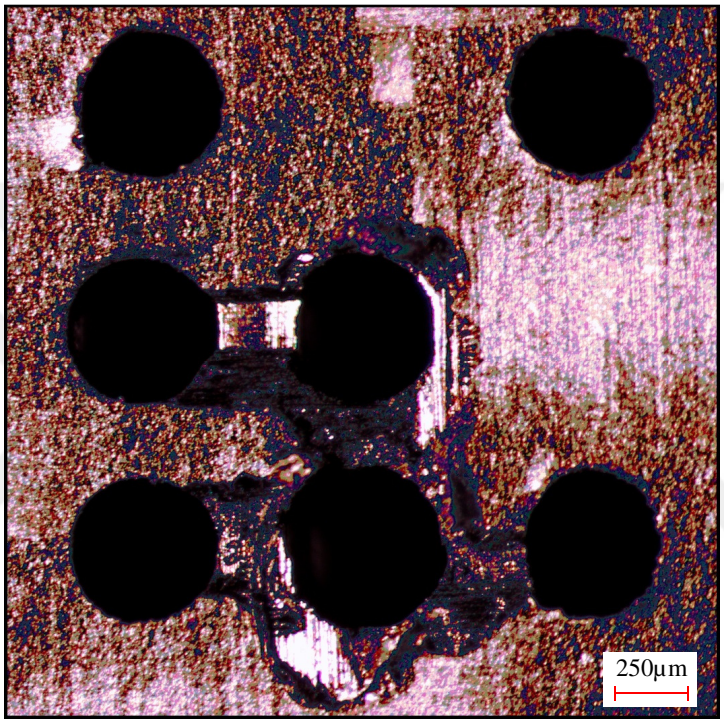

Figure 2.16. Merging of the adjacent delamination damages.

It is known that cutting edge radius of the drill affects the drilling process. If the feed per flute is lower than a critical value which is a function of the cutting edge radius, then the size effect occurs. Lower feeds can cause ploughing as opposed to shearing [81]. Therefore, size effect has been considered during the determination of the feed levels. SEM was used to measure the cutting edge radius (Figure 2.17). It was thought that cutting edge usually does not form a radius, but forms a distance instead. If the SEM picture is inspected, grinding lays which have been formed during the manufacturing of micro drill are seen. These lays are interrupted toward to the cutting edge. Therefore, the mean distance between the borderline of these lays and the cutting edge was assumed as the cutting edge radius. In this case it is calculated as 1.5 µm. Thus, 3µm/rev was decided for the first level. Second and third levels of the feed have been determined as

greater than the first level as expected. Three levels of feed are 3, 5 and 7µm/rev.

Figure 2.17. SEM picture of the cutting tool.

Spindle speed is one of the most important parameters in any machining operation. Therefore, different levels of the spindle speed must be examined for different arrangements of the support plates. Thus, the effect of the spindle speed will be revealed for each level of the support plates. Determining the levels of the spindle speed is more difficult than the determination of the levels of other parameters because chatter phenomenon reveals with increasing spindle speed. Chatter models have been successfully developed for the conventional drilling [82] but not for micro-drilling yet. Since primary concern of the study is the comparative assessment of the influences of the support plates on delamination in micro-drilling of CFRP laminates, different levels of the spindle speed have been used in the experiments, but it is not aimed to find out the spindle speeds which chatter does not occur. Process time decreases with increasing spindle speed due to the feed rate which is determined as feed per revolution. Thus, the productivity increases. Therefore, high cutting speeds were preferred. Besides, the sub-spindle can supply high speeds precisely. If the studies are taken into consideration which have been published in the field of micro-drilling of CFRP laminates, it is found that the spindle speed varies between the 3820 rpm and 40000 rpm [2,12,55]. Finally, three levels of spindle speeds were determined as 20000, 30000 and 40000 rpm which correspond to 31.42, 47.12 and 62.83 m/min cutting speeds respectively.

Each experiment was repeated three times with the same spindle speed and feed for the bare CFRP laminate setup and the setup of the CFRP laminate with aluminum-phenolic support plates. As for the setup of the CFRP laminate with brass-wood support plates, each experiment was repeated two times because of the consistent results of previous

experiments. Totally, 72 experiments were conducted by drilling 17424 holes. 648 holes were chosen and pictures of both sides were inspected. In Table 2.2, levels of the experiment variables are seen.

Table 2.2. Levels of the experiment variables.

		Levels		
Factors	**Units**	**1**	**2**	**3**
Speed	Rpm	20,000	30,000	40,000
Feed	µm/rev	3	5	7
Support Plates	Entry	-	Aluminum	Brass
	Backing		Phenolic	Fir Wood

2.4. Experimental Work for Cutting Temperature

2.4.1. Introduction

General temperature measurement methods which are used in cutting processes are thermocouple, tool-workpiece coupling, infrared thermography, heat sensitive paint and fiber optic pyrometer [83, 84]. Thermocouples which are based on the principle of contact measurement are usually located to the nearest place to the tool tip on the cutting tool or workpiece, and heat conduction model is used to predict the temperature distribution over the cutting tool and workpiece. Infrared thermography fulfills its mission successfully if the heat source does not move and cutting is not interrupted such as in the case of turning. For the interrupted cutting operations such as milling, heating and cooling periods occur consecutively, and heat source rotates. Therefore, infrared thermography method cannot detect the variation of the temperature. In tool-workpiece coupling method, a potential difference in millivolts develops between the cutting tool and workpiece due to the Seebeck Effect as temperature increases, and potential difference is associated to the temperature. Tool-workpiece coupling method requires the isolation of the cutting tool and workpiece from the environment, and calibration of the system is also difficult. In fiber optic pyrometer method, fiber optic is usually embedded into the cutting tool and connected to the pyrometer. This method cannot provide the tool tip temperature, either. Heat sensitive paint changes its color as temperature varies, and

thus temperatures can be identified by calibrating the colors. Each heat-sensitive-paint responds to a specific range of temperatures, and this method is usually applied to the accessible surfaces of the cutting tool and workpiece. Due to the uncertainties in temperature measurements of cutting processes, multiple temperature measurement systems are deployed for verification. Thermocouple which is embedded into the cutting tool or workpiece is the most used temperature measurement method in the application. However, this method cannot provide the tool tip temperature and requires heat conduction modelling to predict the temperature distribution over cutting tool and workpiece. It is also difficult to build the thermal model of the process by means of moving heat source, three-dimensional heat conduction, and transient heat conduction regime due to the instant process. To measure the drill temperature in a drilling process, thermocouple is placed at the nearest point to the cutting edge. A cavity is usually formed on the drill body to place the wires of the thermocouple, or through-hole coolant holes of the drill are used. If the wires of the thermocouple are connected to the data acquisition system directly, the workpiece is rotated instead of drill. Otherwise, a wireless communication system is required, or a miniature data acquisition device which rotates with the drill may be used. However, mentioned methods to place the thermocouple to the micro drill cannot be applied due to the very small size.

Heat is generated in three distinctive zones in cutting as primary deformation zone between the workpiece and chip, secondary deformation zone between the rake face of the cutting tool and chip, and tertiary deformation zone between the workpiece and flank face of the cutting tool. Elastic-plastic deformation in the primary deformation zone, plastic deformation and friction in the secondary deformation zone, and elastic deformation and friction in the tertiary deformation zone are responsible for the heat generation [85]. Additional heat is also generated in some cutting operations such as the heat generation due to the friction between the drilled hole wall and drill margin in drilling process. Chips are produced during the cutting processes, and generated heat is partitioned among the chip, cutting tool, and workpiece.

On the other hand, thermal conductivity of the workpiece is a measure of its machinability. The workpiece which has a good thermal conductivity dissipates the generated heat easily. Thus, cutting temperature decreases. If the thermal conductivity of the workpiece is poor such as the titanium and nickel-based alloys, then higher cutting

temperatures occur, and vast majority of the generated heat flows to the cutting tool and causes thermal stresses which accelerate the fracture, wear, or chipping [86].

Using cutting fluids is another aspect of the cutting processes. Many times, cutting fluids are used to dissipate the generated heat. However, some workpieces such as CFRP (Carbon Fiber Reinforced Plastic) laminates require the dry cutting due to absorption of the cutting fluids which have detrimental effects on the static and fatigue performance of the structure [87], and cutting fluids may cause swelling of polymer which deteriorates the dimensional accuracy and degradation of the structure due to the chemical reaction [88].

Elevated temperatures are detrimental for both cutting tool and workpiece. The increased temperature weakens the wear resistance of the cutting tool, degrades the surface integrity of the workpiece, causes residual stresses, and so on. Nakagawa et al. [89] stated that surface roughness of hole wall increased with the increasing drill temperature caused by workload due to the friction between the drill margin and hole wall in micro-drilling of aramid fiber reinforced plastic and glass fiber reinforced plastic laminates. Lin and Chen [61] pointed out that higher cutting temperature at higher cutting speed could be responsible of rapid drill wear in drilling CFRP laminates. Weinert and Kempmann [88] carried out an experimental study on drilling of fiber reinforced plastic composites with cemented carbide drill and stated that cutting temperature affected the hole diameter accuracy due to radial expansion of the drill, tool wear due to the decomposition of cemented carbides from the cobalt binder, and surface integrity due to the pyrolysis or decomposition of the polymer matrix.

Heat generation in cutting processes is particularly important for the CFRP laminates. If the cutting temperature is greater than the glass transition temperature which is starting from 180°C for the most carbon fiber – epoxy systems, structure of the CFRP laminate may be degraded [9].

In this section, it is aimed to find out the relationships between the generated temperatures and process variables as spindle speed and feed and effects of drill margin friction and tool wear on the generated temperatures. Due to the mentioned difficulties, the temperature measurement has been performed on the workpiece side with the thermocouple and infrared thermography methods.

2.4.2. Experimental setup

As similar to the previous setup, 2 mm thick plain woven CFRP laminates with 3K tow size were used in the experiments. Tensile strength of the fibers is 3800 MPa, and tensile modulus of the fibers is 240 GPa. Epoxy content of the workpiece is 40 percent.

0,5 mm uncoated cemented carbide micro drills with point angle of 130° were used. Experiments were performed on Kent Industrial KMV-11VC vertical CNC machining center with an electrically exited sub-spindle (Nakanishi HES-510), which supplies rotational speeds up to 50000 rpm.

Process variables in the experiments were determined as spindle speed and feed. Two levels of each variable were employed. Levels of the spindle speed are 20000 rpm and 40000 rpm. Levels of the feed are 3 µm/rev and 7 µm/rev. Experiments were also performed with the supported case. Only entry board was used for the supported case due to the backing board which prevents the installing of the thermocouple. It was also thought that backing board does not contribute significantly to the generated temperature due to the limited drilling depth of the micro-drill on the backing board. 0,5 mm thick 1050A H14 grade aluminum plate was used as entry board. Each experiment was repeated 4 times. Experimental setup is shown in Figure 2.18.

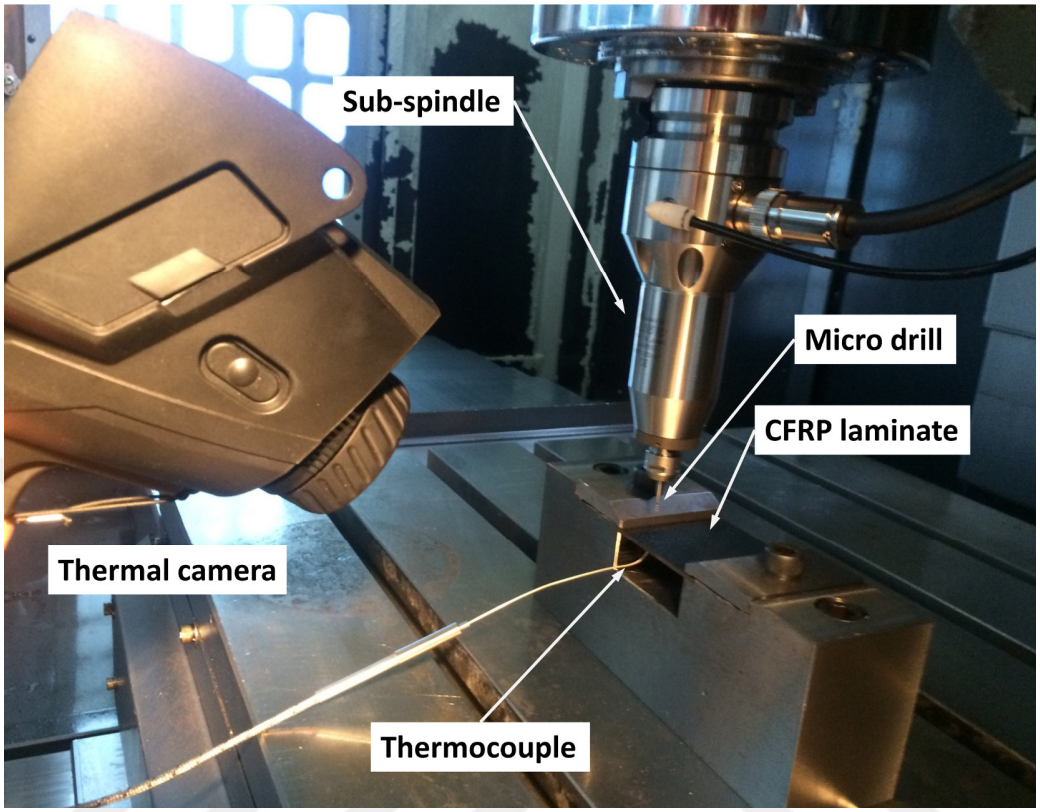

Figure 2.18. Experimental setup.

Two different methods as thermocouple and infrared thermography were used to measure the generated temperature during micro-drilling of CFRP laminates. J type thermocouple with 1 mm head diameter was embedded into the CFRP laminate. Thermocouple hole was drilled through the thickness of the CFRP laminate and in a diameter which fits the thermocouple tightly. Thermocouple was connected to Delta ohm HD2328.0 thermometer to collect the data of measured temperatures. Measurement frequency was 1 Hz. The distance between the thermocouple and drilled hole was determined with an experiment by varying the distance. Experiments were carried out with the constant spindle speed and feed of 20000 rpm and 3 µm/rev to find out the most eligible position for the thermocouple. The distance between the boundaries of thermocouple and drilled hole was decreased from 1 mm to 0,25 mm with 0,25 mm intervals which correspond to central distances from 1,75 mm to 1 mm. It was found that generated maximum temperature changed significantly at the distance of 0,25 mm which is the nearest one to the drilled hole. Therefore, the distance of 0,25 mm was used in the experiments. Smaller distance was not preferred due to the probable delamination

damage. Graphical representation of the relationship between the temperature and thermocouple distance is shown in Figure 2.19. Process time is only 2 seconds for the selected drilling conditions. It must be noted that the maximum temperatures occur after process ends.

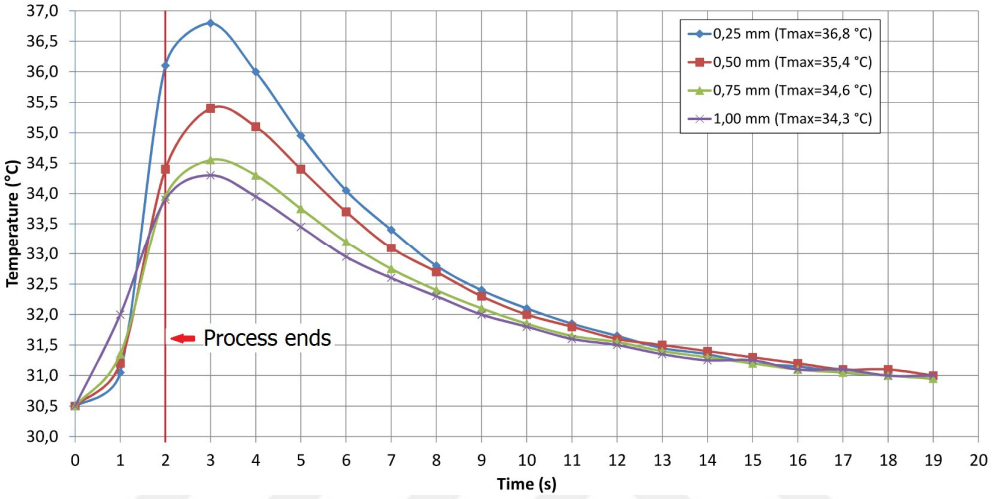

Figure 2.19. Temperature-time graph and effect of thermocouple distance.

Testo 875-1i infrared thermograph camera was used to measure the highest temperature during micro-drilling process. A sample thermal image is shown in Figure 2.20. Emissivity was adjusted as 0,95. The highest temperature which had been observed with the infrared thermography was recorded for each experiment. Infrared thermograph camera was positioned to measure the front side temperature of the CFRP laminate, but it was positioned to measure the rear side temperature of the CFRP laminate due to the entry board which prevents the direct temperature measurement on the front side.

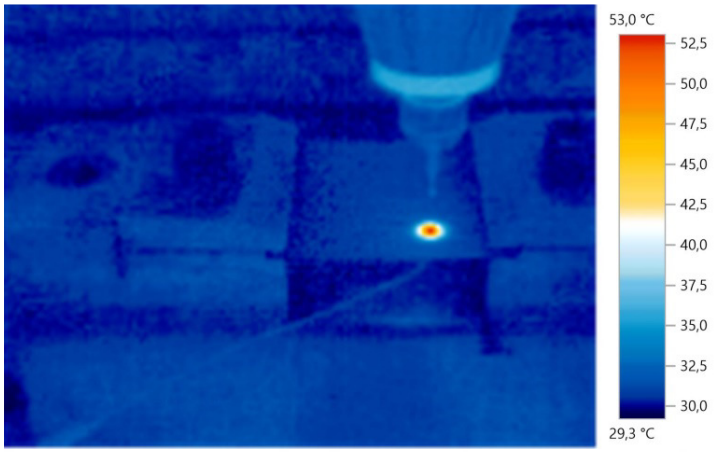

Figure 2.20. Sample image of infrared thermography measurement (S20000 rpm, f3µm/rev).

2.5. Experimental Work for Cutting Forces

2.5.1. Introduction

When investigating the delamination damage, thrust force is usually referred especially for the exit side delamination damage. It is thought that delamination does not occur below a critical thrust force [22]. To increase the critical thrust force, one of the methods is using the support plates. Exit delamination damage usually occurs at the last ply. If the backing board is used, critical thrust force increases and delamination is less probable to occur.

In this section, it is aimed to find out the relationships between the cutting forces and process variables as spindle speed and feed for both bare and supported CFRP laminates.

2.5.2. Experimental setup

As similar to the previous experiments, 2 mm thick plain woven CFRP laminates with 3K tow size were used in the experiments. Tensile strength of the fibers is 3800 MPa, and tensile modulus of the fibers is 240 GPa. Epoxy content of the workpiece is 40 percent.

0,5 mm uncoated cemented carbide micro drills with point angle of 130° were used. Experiments were performed on Mazak FJH-200 UHS vertical CNC machining center with an electrically exited sub-spindle (Nakanishi HES-810) which supplies up to 80000

rpm.

Process variables in the experiments were determined as spindle speed and feed. Two levels of each variable were employed. Levels of the spindle speed are 20000 rpm and 40000 rpm. Levels of the feed are 3 µm/rev and 7 µm/rev. Experiments were also performed for the supported case. 0,5 mm thick 1050A H14 grade aluminum plate as entry board and 4 mm thick phenolic plate as backing board were used. Each experiment was repeated 3 times. Experimental setup is shown in Figure 2.21.

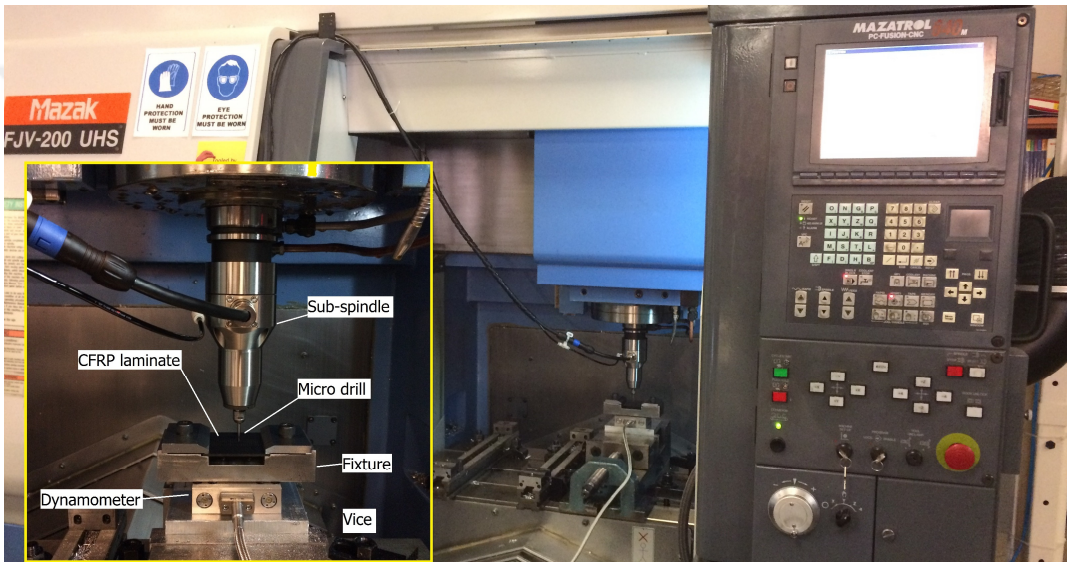

Figure 2.21. Experimental Setup.

Kistler 9256C1 mini dynamometer with 5070A multi-channel charge amplifier and National Instruments data acquisition board (USB-6259 BNC) was used to measure the cutting forces. Data acquisition system is shown in Figure 2.22. Sampling frequency was 30030 Hz for each experiment. Thrust force as F_z and drilling torque as M_z were recorded.

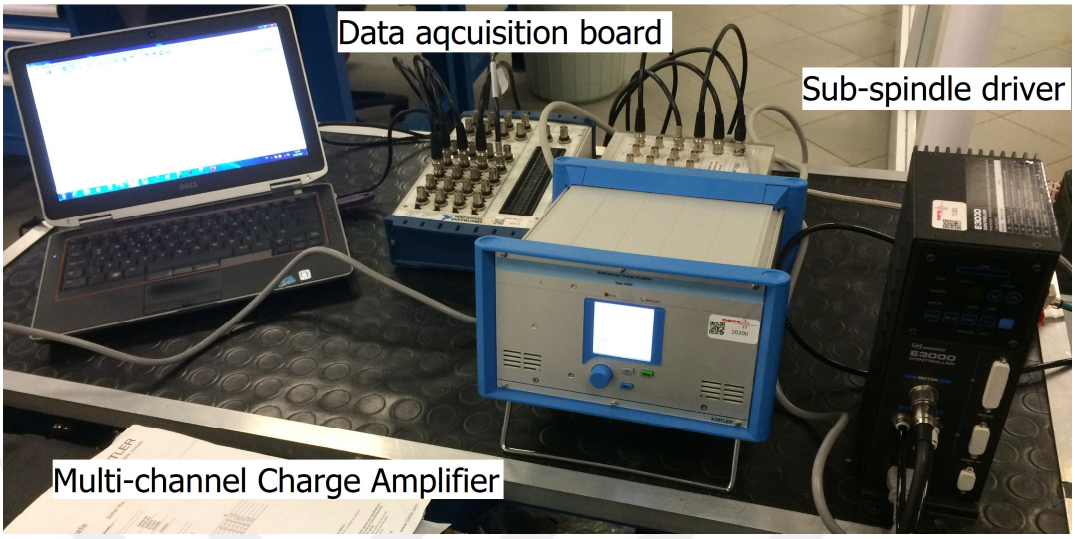

Figure 2.22. Data acquisition.

Thrust force and torque data were filtered by using a second order low pass filter with Butterworth topology. Cutoff frequency was varied between 20 Hz and 100 Hz.

3. RESULTS AND DISCUSSON

3.1. Delamination

Spindle speed and feed values are optimized in addition to analyzing the experimental results. Response surface method was used for the optimization. Minitab provides convenient tool for the method. Full quadratic functions which include the terms such as feed, spindle speed, square of feed, square of spindle speed and multiplication of feed and spindle speed were used to construct the curves. 95% confidence level was chosen for all intervals. Triangular desirability functions were selected. For each delamination factor, minimum and maximum delamination factors were appointed as upper and lower bounds. The goal was determined as minimizing the values of six delamination factors. Composite desirability value is the geometric mean of the individual desirability values. Software tries to find out the maximum composite desirability value to optimize the delamination factors.

3.1.1. Bare CFRP experiments

Effects of feed and spindle speed on the delamination damage were evaluated by using the results of the first group experiments which did not contain the support plates. Table 3.1 presents the calculated delamination factors. Shown values are the means of nine delamination factors (3 times repetitions and neighbored 3 holes). Delamination factors for the entry side and exit side were also given in Appendix 1-1 and Appendix 1-2.

Table 3.1. Delamination factors for bare CFRP laminate micro-drilling experiments.

Spindle speed (rpm)	Feed (µm/rev)	Resulting feed (mm/min)	Front Side Delamination Factors			Rear Side Delamination Factors		
			Hole numbers			Hole numbers		
			1-2-3	120-121-122	240-241-242	1-2-3	120-121-122	240-241-242
20000	3	60	1.044	1.195	1.380	1.347	1.426	1.514
30000	3	90	1.065	1.389	1.442	1.296	1.393	1.454
40000	3	120	1.051	1.360	1.303	1.204	1.324	1.331
20000	5	100	1.050	1.134	1.221	1.200	1.313	1.457
30000	5	150	1.060	1.171	1.219	1.177	1.487	1.508
40000	5	200	1.041	1.279	1.260	1.206	1.412	1.443
20000	7	140	1.061	1.236	1.174	1.294	1.418	1.461
30000	7	210	1.047	1.141	1.230	1.223	1.460	1.403
40000	7	280	1.069	1.240	1.338	1.126	1.312	1.355

In Figure 3.1 and Figure 3.2, graphical representations of front side and rear side delamination factors for bare CFRP laminate micro-drilling experiments are shown. In the plots, horizontal lines indicate the median values, plus signs indicate the mean values, multiplication signs indicate the outliers, and boxes indicate the interquartile ranges. Whiskers extend to the highest and lowest values within the limits. Upper limit equals to Q_3+1,5(Q_3-Q_1) and lower limit equals to Q_1-1.5 (Q_3 - Q_1).

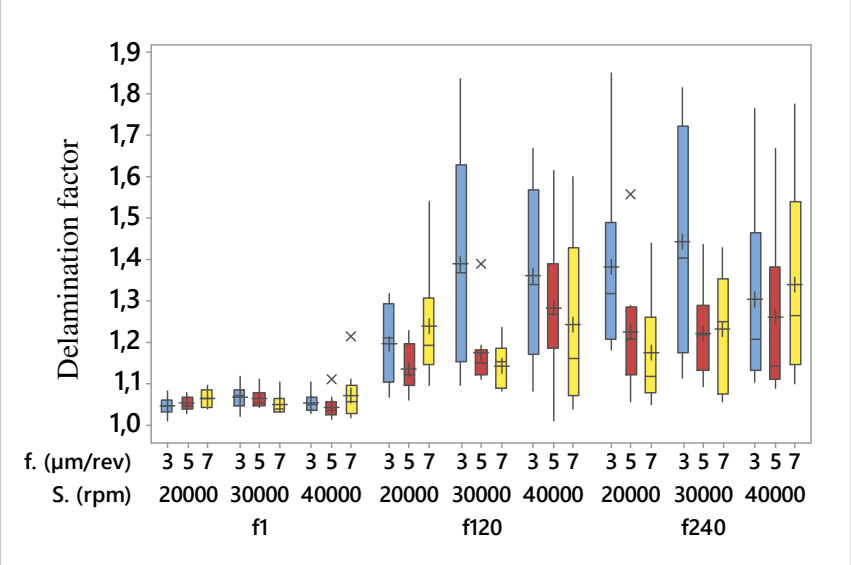

Figure 3.1. Box plots of the front side delamination factors for the bare CFRP experiments.

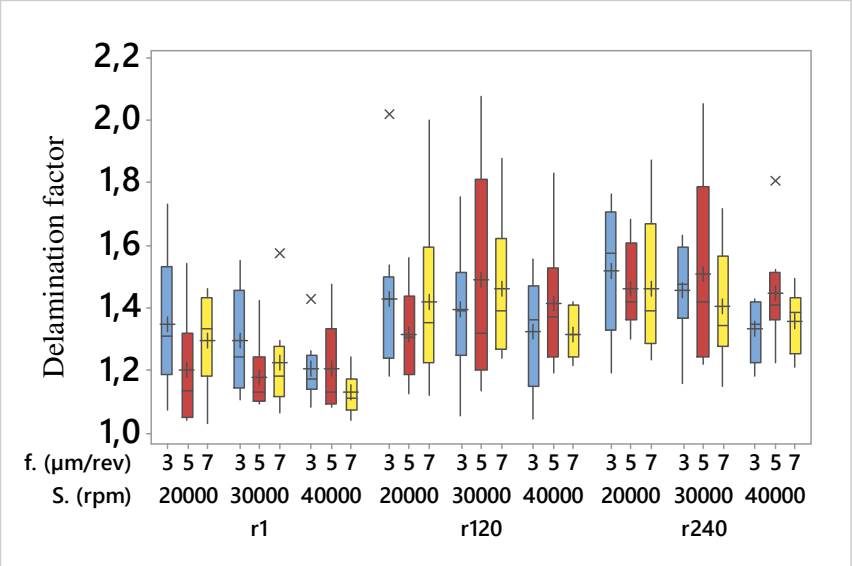

Figure 3.2. Box plots of the rear side delamination factors for the bare CFRP experiments.

Delamination factors increase from the first to the last hole for any individual experiment. Through all the bare CFRP experiments, it is observed that delamination in the first drilled holes does not change at all in case of any feed and cutting speed for the entry side.

Contour plots of the bare CFRP laminate experiments for entry and exit sides are shown in Figure 3.3 and Figure 3.4 respectively. If the results of the first group of experiments are inspected, it is seen that delamination shows different trends for the entry and exit sides. On the entry side, minimum value of the delamination is derived with the feed of around 5µm/rev, and the delamination decreases generally as spindle speed decreases for this feed. On the exit side, delamination decreases generally as spindle speed increases, but shows complicated behavior to the feed change. Delamination increases as feed increases from 3 µm/rev to intermediate feeds, and then decreases as feed increases to 7 µm/rev for the middle and last holes, vice versa for the first holes.

By using the response surface method, optimum values of the bare CFRP laminate experiments are derived as 5.6263 µm/rev for feed and 40000 rpm for spindle speed. By using these conditions, entry side delamination factors are obtained as 1.0514 for the first holes, 1.2266 for the middle holes and 1.2548 for the last holes, and exit side delamination factors as 1.1353 for the first holes, 1.3601 for the middle holes and 1.4067

for the last holes. Due to the contrary effect of the spindle speed on the delamination for the entry and exit side, delamination factors are relatively high for the entry side as compared to the exit side. By using the same feed and 20000 rpm spindle speed, delamination factors for the entry side can be decreased to 1.0488 for the first holes, 1.1470 for the middle holes and 1.1753 for the last holes. Though, it is not convenient using different spindle speeds for entry and exit sides of a hole during the drilling in practice, because acceleration requires time and may bring other problems.

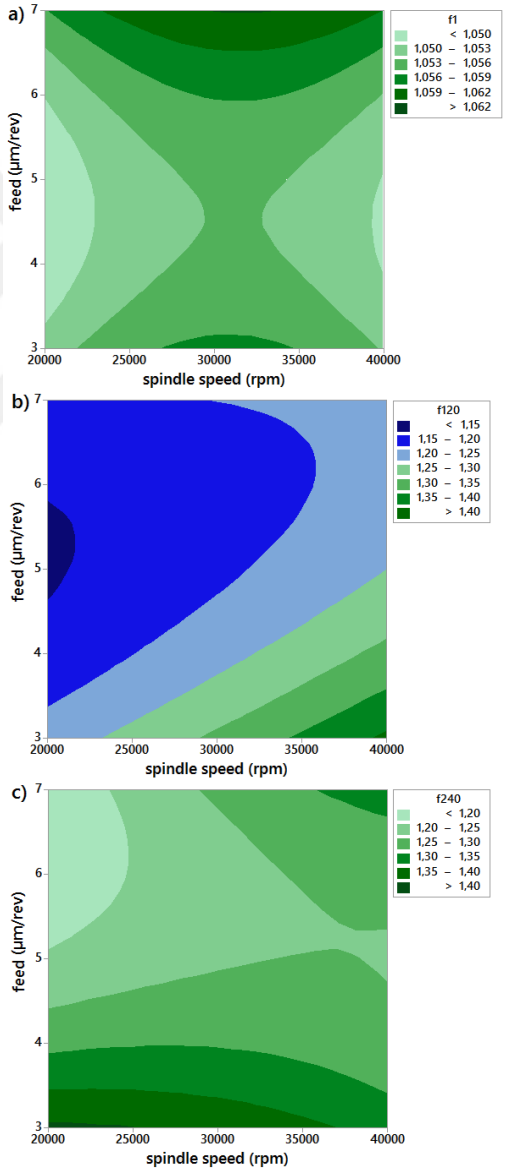

Figure 3.3. Contour plots of the delamination factors for the bare CFRP entry side. (a - f1:the first holes, b - f120:the middle holes, c - f240:the last holes)

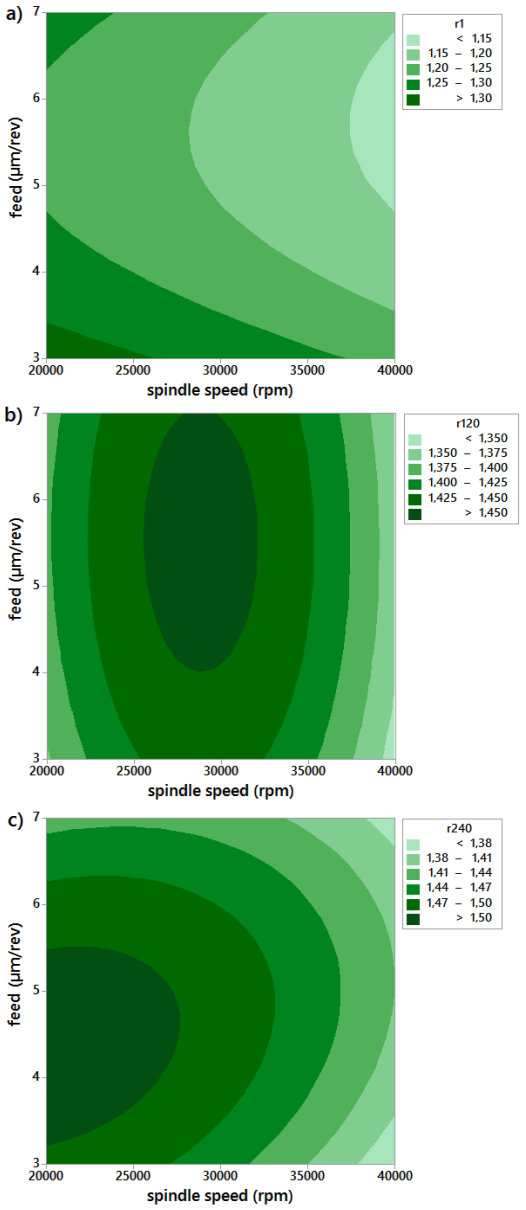

Figure 3.4. Contour plots of the delamination factors for the bare CFRP exit side. (a - r1:the first holes, b - r120:the middle holes, c - r240:the last holes)

It is seen from the results that feed settle on an intermediate value to minimize the delamination for the entry side. This behavior may be related to the size effect. Ploughing occurs and causes the worse delamination damage when the feed per flute approaches the value of the cutting edge radius. As feed increases to intermediate values, size effect decreases and efficient cutting is achieved. Further increasing the feed increases the delamination due to the peel up effect as usual for all fiber reinforced

composites. As for the exit side delamination, similar feed trend for the first holes is seen. No doubt, different trends of the delamination for the first, middle and last holes are related to the tool wear. As cutting edge wears, cutting edge radius increases. Ploughing effect which causes the highest delamination damage for the middle and last holes is seen again, but this time for intermediate feeds. Obviously, tool wear increases the magnitude of the push out effect on delamination for the middle and last holes compared to the first holes.

Spindle speed exhibits contrary trends for the entry and exit side delamination damages. For the exit side delamination, higher spindle speeds provide less thrust force which will be validated in Chapter 3.6. Thus, exit side delamination decreases. For the calculated optimum feed, increasing the spindle speed causes higher delamination damage for the entry side. This behavior can be explained as increasing the spindle speed causes higher cutting temperature which causes matrix softening. Thus, delamination increases.

ANOVA (Analysis of Variance) table is shown for the front side first holes in the case of bare CFRP experiments in Table 3.2. According to the results, p-value of the lack of fit error is equal to 0,116 which is greater than 0,05. Therefore, it reveals that full quadratic model fits the data adequately. P-value of the model is 0,902 which is greater than 0,05. It indicates that failure of the model is more probable. R-sq value indicates that the model accounts for 2,07% of the variability in the model. Adjusted sum of squares (Adj. SS) value is a measure of deviation from the mean. According to the results, feed components have greater adjusted sum of squares values than those of spindle speed.

Table 3.2. Analysis of variance table of response surface regression for the front side first holes in the case of bare CFRP experiments.

Source	DF	Adj. SS	Adj. MS	F-Value	P-Value
Model	5	0,001518	0,000304	0,32	0,902
Linear	2	0,000463	0,000232	0,24	0,786
S. (rpm)	1	0,000073	0,000073	0,08	0,783
f. (µm/rev)	1	0,000390	0,000390	0,41	0,526
Square	2	0,001049	0,000524	0,55	0,581
S. (rpm)*S. (rpm)	1	0,000393	0,000393	0,41	0,524
f. (µm/rev)*f. (µm/rev)	1	0,000656	0,000656	0,68	0,411
2-Way Interaction	1	0,000006	0,000006	0,01	0,936
S. (rpm)*f. (µm/rev)	1	0,000006	0,000006	0,01	0,936
Error	75	0,071971	0,000960		
Lack-of-Fit	3	0,005629	0,001876	2,04	0,116
Pure Error	72	0,066342	0,000921		
Total	80	0,073489			

S	R-sq	R-sq(adj)	R-sq(pred)
0,0309776	2,07%	0,00%	0,00%

ANOVA table is shown for the front side middle holes in the case of bare CFRP experiments in Table 3.3. According to the results, p-value of the lack of fit error is equal to 0,126. Therefore, it reveals that full quadratic model fits the data adequately. P-value of the model is 0,008. It indicates that the model is very successful. R-sq value indicates that the model accounts for 18,53% of the variability in the model. According to the results, spindle speed (S.) and feed (f.) terms are statistically significant due to their p-values which are 0,020 and 0,015 consecutively.

Table 3.3. Analysis of variance table of response surface regression for the front side middle holes in the case of bare CFRP experiments.

Source	DF	Adj. SS	Adj. MS	F-Value	P-Value
Model	5	0,44451	0,088903	3,41	0,008
Linear	2	0,30897	0,154487	5,93	0,004
S. (rpm)	1	0,14841	0,148409	5,69	0,020
f. (µm/rev)	1	0,16056	0,160565	6,16	0,015
Square	2	0,07690	0,038450	1,48	0,235
S. (rpm)*S. (rpm)	1	0,00095	0,000950	0,04	0,849
f. (µm/rev)*f. (µm/rev)	1	0,07595	0,075951	2,91	0,092
2-Way Interaction	1	0,05864	0,058641	2,25	0,138
S. (rpm)*f. (µm/rev)	1	0,05864	0,058641	2,25	0,138
Error	75	1,95452	0,026060		
Lack-of-Fit	3	0,14826	0,049420	1,97	0,126
Pure Error	72	1,80626	0,025087		
Total	80	2,39903			

S	R-sq	R-sq(adj)	R-sq(pred)
0,161432	18,53%	13,10%	4,65%

ANOVA table is shown for the front side last holes in the case of bare CFRP experiments in Table 3.4. According to the results, p-value of the lack of fit error is equal to 0,653. Therefore, it reveals that full quadratic model fits the data adequately. P-value of the model is 0,029. It indicates that the model is very successful. R-sq value indicates that the model accounts for 15,03% of the variability in the model. According to the results, feed (f.) term is statistically significant due to its p-value which is 0,017.

Table 3.4. Analysis of variance table of response surface regression for the front side last holes in the case of bare CFRP experiments.

Source	DF	Adj. SS	Adj. MS	F-Value	P-Value
Model	5	0,48843	0,097686	2,65	0,029
Linear	2	0,24250	0,121251	3,29	0,043
S. (rpm)	1	0,02339	0,023387	0,64	0,428
f. (µm/rev)	1	0,21912	0,219116	5,95	0,017
Square	2	0,11463	0,057315	1,56	0,218
S. (rpm)*S. (rpm)	1	0,00561	0,005615	0,15	0,697
f. (µm/rev)*f. (µm/rev)	1	0,10902	0,109015	2,96	0,089
2-Way Interaction	1	0,13130	0,131296	3,57	0,063
S. (rpm)*f. (µm/rev)	1	0,13130	0,131296	3,57	0,063
Error	75	2,76107	0,036814		
Lack-of-Fit	3	0,06136	0,020454	0,55	0,653
Pure Error	72	2,69971	0,037496		
Total	80	3,24950			
S	R-sq		R-sq(adj)	R-sq(pred)	
0,191870	15,03%		9,37%	0,44%	

As a result, analysis of variance revealed that feed is more dominant on delamination damage for the front side holes in the case of bare CFRP experiments.

ANOVA table is shown for the rear side first holes in the case of bare CFRP experiments in Table 3.5. According to the results, p-value of the lack of fit error is equal to 0,285. Therefore, it reveals that full quadratic model fits the data adequately. P-value of the model is 0,053. It indicates that the model is successful. R-sq value indicates that the model accounts for 13,32% of the variability in the model. According to the results, spindle speed (S.) term is statistically significant due to its p-value which is 0,014.

Table 3.5. Analysis of variance table of response surface regression for the rear side first holes in the case of bare CFRP experiments.

Source	DF	Adj. SS	Adj. MS	F-Value	P-Value
Model	5	0,25662	0,051325	2,30	0,053
Linear	2	0,20256	0,101281	4,55	0,014
S. (rpm)	1	0,14052	0,140517	6,31	0,014
f. (µm/rev)	1	0,06204	0,062044	2,79	0,099
Square	2	0,05270	0,026351	1,18	0,312
S. (rpm)*S. (rpm)	1	0,00009	0,000087	0,00	0,950
f. (µm/rev)*f. (µm/rev)	1	0,05261	0,052615	2,36	0,129
2-Way Interaction	1	0,00136	0,001362	0,06	0,805
S. (rpm)*f. (µm/rev)	1	0,00136	0,001362	0,06	0,805
Error	75	1,67062	0,022275		
Lack-of-Fit	3	0,08515	0,028382	1,29	0,285
Pure Error	72	1,58548	0,022021		
Total	80	1,92725			
S	R-sq		R-sq(adj)	R-sq(pred)	
0,149248	13,32%		7,54%	0,00%	

ANOVA table is shown for the rear side middle holes in the case of bare CFRP experiments in Table 3.6. According to the results, p-value of the lack of fit error is equal to 0,376. Therefore, it reveals that full quadratic model fits the data adequately. P-value of the model is 0,744. It indicates that failure of the model is more probable. R-sq value indicates that the model accounts for 3,49% of the variability in the model. According to the results, spindle speed components have greater adjusted sum of squares values than those of feed. It indicates that spindle speed terms are more effective on the deviation of delamination damage from the mean.

Table 3.6. Analysis of variance table of response surface regression for the rear side middle holes in the case of bare CFRP experiments.

Source	DF	Adj. SS	Adj. MS	F-Value	P-Value
Model	5	0,13737	0,027473	0,54	0,744
Linear	2	0,02078	0,010389	0,20	0,815
S. (rpm)	1	0,01752	0,017519	0,35	0,558
f. (µm/rev)	1	0,00326	0,003259	0,06	0,801
Square	2	0,11656	0,058279	1,15	0,322
S. (rpm)*S. (rpm)	1	0,11262	0,112622	2,22	0,140
f. (µm/rev)*f. (µm/rev)	1	0,00394	0,003937	0,08	0,781
2-Way Interaction	1	0,00003	0,000029	0,00	0,981
S. (rpm)*f. (µm/rev)	1	0,00003	0,000029	0,00	0,981
Error	75	3,80121	0,050683		
Lack-of-Fit	3	0,15928	0,053092	1,05	0,376
Pure Error	72	3,64193	0,050582		
Total	80	3,93857			
S	R-sq		R-sq(adj)	R-sq(pred)	
0,225128	3,49%		0,00%	0,00%	

ANOVA table is shown for the rear side last holes in the case of bare CFRP experiments in Table 3.7. According to the results, p-value of the lack of fit error is equal to 0,616. Therefore, it reveals that full quadratic model fits the data adequately. P-value of the model is 0,284. It indicates that the model can fail. R-sq value indicates that the model accounts for 7,83% of the variability in the model. According to the results, spindle speed (S.) term is statistically significant due to its p-value which is 0,049.

Table 3.7. Analysis of variance table of response surface regression for the rear side last holes in the case of bare CFRP experiments.

Source	DF	Adj. SS	Adj. MS	F-Value	P-Value
Model	5	0,21869	0,043738	1,27	0,284
Linear	2	0,14713	0,073565	2,14	0,124
S. (rpm)	1	0,13759	0,137592	4,01	0,049
f. (µm/rev)	1	0,00954	0,009539	0,28	0,600
Square	2	0,05840	0,029201	0,85	0,431
S. (rpm)*S. (rpm)	1	0,01415	0,014149	0,41	0,523
f. (µm/rev)*f. (µm/rev)	1	0,04425	0,044253	1,29	0,260
2-Way Interaction	1	0,01316	0,013156	0,38	0,538
S. (rpm)*f. (µm/rev)	1	0,01316	0,013156	0,38	0,538
Error	75	2,57330	0,034311		
Lack-of-Fit	3	0,06299	0,020998	0,60	0,616
Pure Error	72	2,51031	0,034865		
Total	80	2,79199			
S	R-sq		R-sq(adj)	R-sq(pred)	
0,185231	7,83%		1,69%	0,00%	

As a result, analysis of variance revealed that spindle speed is more dominant on delamination damage for the rear side hole diameters in the case of bare CFRP experiments.

Experimental studies in the literature which were performed for conventional drilling of CFRP have revealed that delamination increases as feed increases due to the increase of the thrust force, and delamination slightly decreases as spindle speed increases [90, 91]. However, derived experimental results have shown that intermediate feed and low spindle speed for the entry side and intermediate feed and high spindle speed for the exit side are preferable to decrease the delamination damage.

3.1.2. Aluminum-phenolic support plates experiments

It was stated earlier that the entry side support plates (aluminum and brass) eliminated the delamination, but produced ring shaped cavity around the hole instead. In Table 3.8,

delamination factors for the exit side and the damage factors which have been calculated in the same manner as delamination are seen for the entry side. Shown values are the means of nine damage factor for the entry side and the means of nine delamination factors for the exit side (3 times repetitions and neighbored 3 holes). Damage factors for the entry side and delamination damage factors for the exit side were also given in Appendix 1-3 and Appendix 1-4.

Table 3.8. Damage factors for CFRP laminate with Aluminum-Phenolic support plate micro-drilling experiments

Spindle speed (rpm)	Feed (µm/rev)	Resulting feed (mm/min)	Front Side Damage Factors			Rear Side Delamination Factors		
			Hole numbers			Hole numbers		
			1-2-3	120-121-122	240-241-242	1-2-3	120-121-122	240-241-242
20000	3	60	1.196	1.166	1.210	1.366	1.436	1.436
30000	3	90	1.162	1.169	1.188	1.256	1.337	1.442
40000	3	120	1.171	1.178	1.192	1.274	1.403	1.423
20000	5	100	1.176	1.215	1.241	1.300	1.470	1.403
30000	5	150	1.196	1.187	1.222	1.267	1.382	1.398
40000	5	200	1.159	1.175	1.183	1.223	1.419	1.388
20000	7	140	1.204	1.194	1.210	1.347	1.493	1.470
30000	7	210	1.178	1.190	1.206	1.244	1.320	1.316
40000	7	280	1.163	1.182	1.202	1.228	1.329	1.510

In Figure 3.5 and Figure 3.6, graphical representations of front side damage and rear side delamination factors for CFRP laminate with Aluminum-Phenolic support plates micro-drilling experiments are shown.

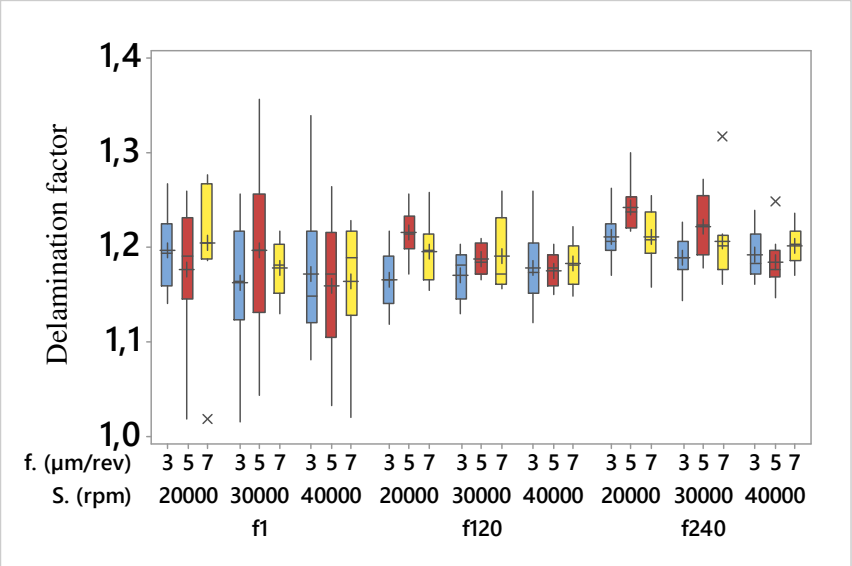

Figure 3.5. Box plots of the front side damage factors for CFRP laminate with Aluminum-Phenolic support plates micro-drilling experiments.

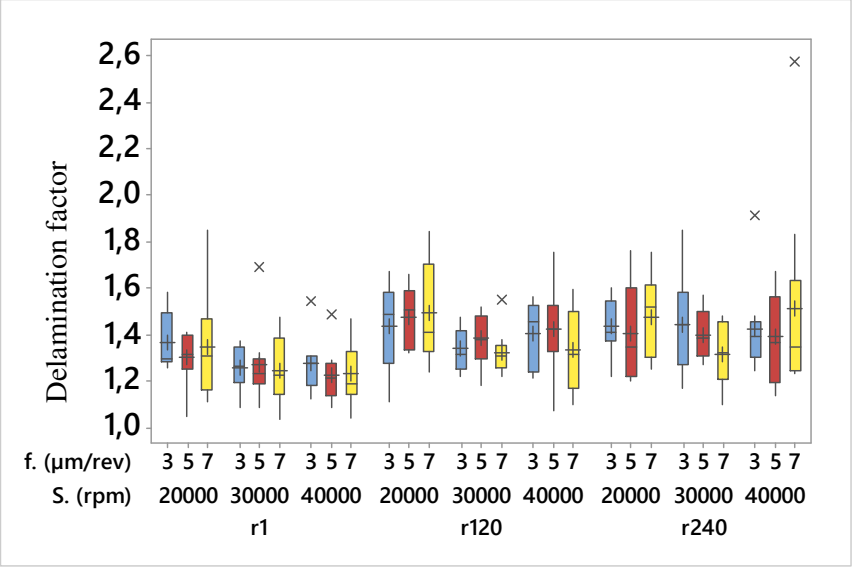

Figure 3.6. Box plots of the rear side delamination factors for CFRP laminate with Aluminum-Phenolic support plates micro-drilling experiments.

If the entry side damage factors are inspected, it is seen that they are changed slightly and between the values of 1.159 and 1.241. Response surface method contour plots of the damage factors for the entry side are seen in Figure 3.7. This damage occurs with the same mechanism for each case by means of the exit burrs of the entry support plates during drilling. If it is assumed that this damage is tolerable, only exit side delamination

factors can be considered for the optimization.

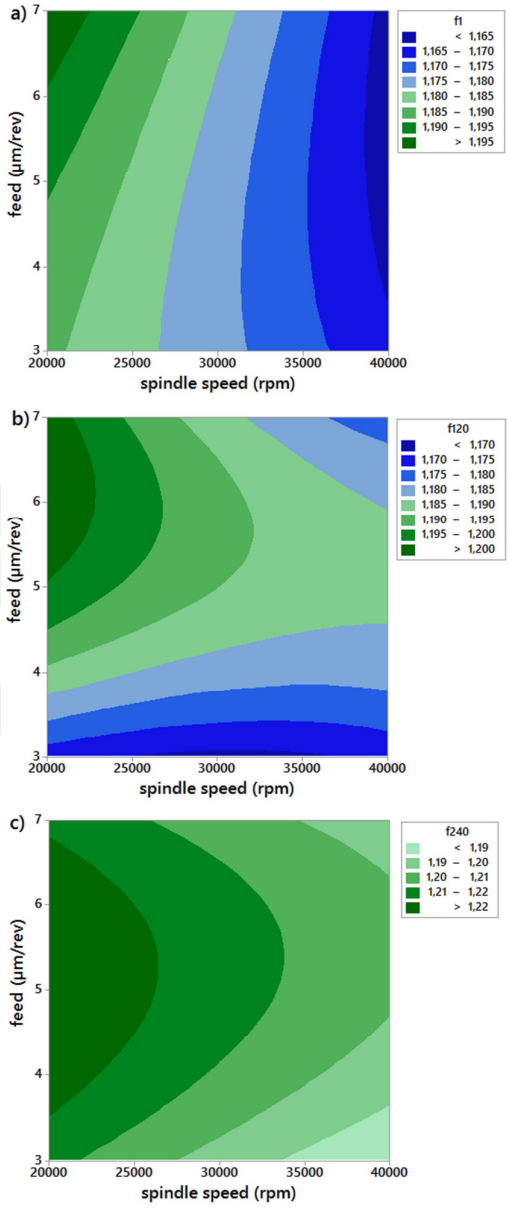

Figure 3.7. Contour plots of the ring shaped cavity damage factors for the entry side in case of aluminum-phenolic support plates. (a - f1:the first holes, b - f120:the middle holes, c - f240:the last holes)

Drilling the metals such as aluminum and brass causes burrs in the entry and exit sides of the workpiece. Exit burrs are usually severe than the entry burrs [92]. It was observed in the experiments that exit burrs of the entry boards caused ring shaped cavity damage to the CFRP laminate. Burrs can be classified using the burr height and burr thickness.

According to the method of derivation of ring shaped cavity damage factors, burr thickness is governing parameter. Burrs can be decreased by proper selection of the cutting parameters but cannot be eliminated completely [93]. It is seen from the contour plots that the spindle speed is more dominant than the feed, and high spindle speed decrease the burr thickness of the aluminum entry board and cause less damage to the CFRP laminate. Increasing the spindle speed increases the resulting feed (mm/min), and tool-workpiece engagement time decreases. Thus, generated heat decreases and exit burrs reduce [94]. Although cutting parameters affect the burr thickness, it is limited to about 3 percent. It can be also concluded that the tool wear has an effect on the ring shaped cavity damage. As micro drill wears, burr thickness increases.

Contour plots of the delamination factors for the exit side are seen in Figure 3.8. Response surface method was used in the same manner to optimize the exit side delamination damage. Optimum values for the exit side delamination are derived as 6.03 µm/rev for feed and 32929 rpm for spindle speed. Delamination factors are obtained as 1.2283 for the first holes, 1.3484 for the middle holes and 1.3771 for the last holes. It is seen that delamination factors settle on intermediate spindle speed and feed. Phenolic backing board increased the delamination factor for the first holes and slightly decreased the delamination factors for the middle and last holes as compared to the exit side delamination factors which were derived for the bare CFRP laminate experiments. Due to the production method of the CFRP laminates which were used in the experiments, rear sides of the CFRP laminates contain the cavities which were formed by flow medium. The cavities may prevent the contact of the backing board to the CFRP laminate. Therefore, sufficient support may not be provided. It is known in conventional drilling of fiber reinforced composite laminates that backing board increases the critical thrust force and therefore reduces the delamination damage [22]. Due to the mentioned effect of the flow medium, it is seen that backing board cannot eliminate the delamination damage.

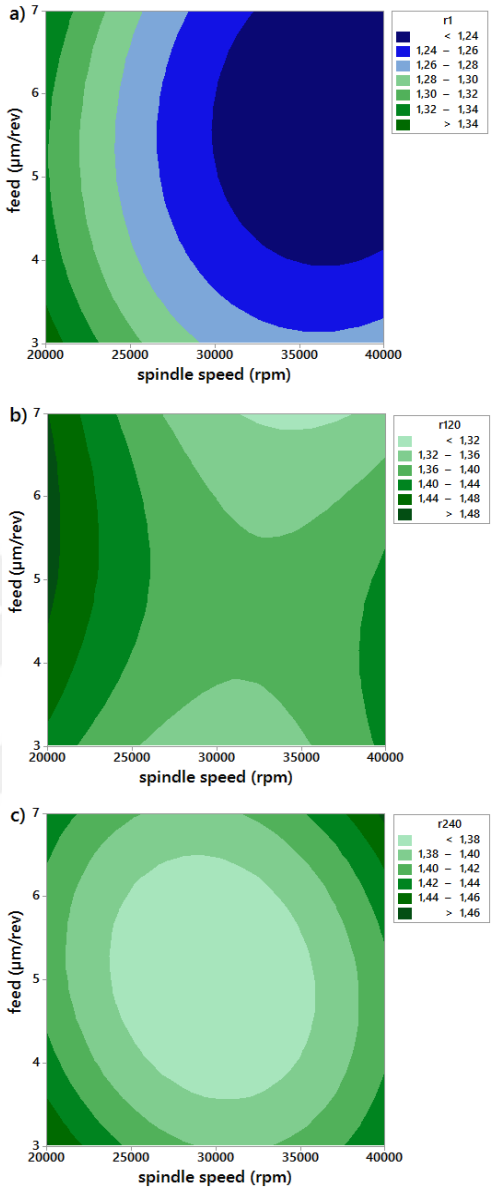

Figure 3.8. Contour plots of the delamination factors for the exit side in case of aluminum-phenolic support plates. (a - r1:the first holes, b - r120:the middle holes, c - r240:the last holes)

Analysis of variance table is shown for the rear side first holes in the case of aluminum-phenolic support plates in Table 3.9. According to the results, p-value of the lack of fit error is equal to 0,834. Therefore, it reveals that full quadratic model fits the data adequately. P-value of the model is 0,163. It indicates that the model can fail. R-sq value indicates that the model accounts for 9,79% of the variability in the model. According to

the results, spindle speed (S.) term is statistically significant due to its p-value which is 0,016.

Table 3.9. Analysis of variance table of response surface regression for the rear side first holes in the case of aluminum-phenolic support plates.

Source	DF	Adj. SS	Adj. MS	F-Value	P-Value
Model	5	0,16271	0,032543	1,63	0,163
Linear	2	0,13143	0,065713	3,29	0,043
S. (rpm)	1	0,12252	0,122522	6,13	0,016
f. (µm/rev)	1	0,00890	0,008904	0,45	0,507
Square	2	0,02963	0,014815	0,74	0,480
S. (rpm)*S. (rpm)	1	0,02047	0,020467	1,02	0,315
f. (µm/rev)*f. (µm/rev)	1	0,00916	0,009164	0,46	0,500
2-Way Interaction	1	0,00166	0,001657	0,08	0,774
S. (rpm)*f. (µm/rev)	1	0,00166	0,001657	0,08	0,774
Error	75	1,49909	0,019988		
Lack-of-Fit	3	0,01773	0,005910	0,29	0,834
Pure Error	72	1,48136	0,020574		
Total	80	1,66180			
S	R-sq		R-sq(adj)	R-sq(pred)	
0,141378	9,79%		3,78%	0,00%	

Analysis of variance table is shown for the rear side middle holes in the case of aluminum-phenolic support plates in Table 3.10. According to the results, p-value of the lack of fit error is equal to 0,941. Therefore, it reveals that full quadratic model fits the data adequately. P-value of the model is 0,050. It indicates that the model is very successful. R-sq value indicates that the model accounts for 13,48% of the variability in the model. According to the results, spindle speed (S.) and spindle speed*spindle speed terms are statistically significant due to their p-values which are 0,050 and 0,031 consecutively.

Table 3.10. Analysis of variance table of response surface regression for the rear side middle holes in the case of aluminum-phenolic support plates.

Source	DF	Adj SS	Adj MS	F-Value	P-Value
Model	5	0,26758	0,053516	2,34	0,050
Linear	2	0,09295	0,046475	2,03	0,139
S. (rpm)	1	0,09124	0,091241	3,98	0,050
f. (µm/rev)	1	0,00171	0,001709	0,07	0,785
Square	2	0,13605	0,068026	2,97	0,057
S. (rpm)*S. (rpm)	1	0,11071	0,110715	4,84	0,031
f. (µm/rev)*f. (µm/rev)	1	0,02534	0,025338	1,11	0,296
2-Way Interaction	1	0,03858	0,038577	1,68	0,198
S. (rpm)*f. (µm/rev)	1	0,03858	0,038577	1,68	0,198
Error	75	1,71726	0,022897		
Lack-of-Fit	3	0,00940	0,003134	0,13	0,941
Pure Error	72	1,70785	0,023720		
Total	80	1,98484			

S	R-sq	R-sq(adj)	R-sq(pred)
0,151317	13,48%	7,71%	0,00

Analysis of variance table is shown for the rear side last holes in the case of aluminum-phenolic support plates in Table 3.11. According to the results, p-value of the lack of fit error is equal to 0,430. Therefore, it reveals that full quadratic model fits the data adequately. P-value of the model is 0,888. It indicates that failure of the model is more probable. R-sq value indicates that the model accounts for 2,21% of the variability in the model. According to the results, spindle speed*spindle speed term has greater adjusted sum of squares values than other terms. It indicates that spindle speed*spindle speed term is more effective on the deviation of delamination damage from the mean.

Table 3.11. Analysis of variance table of response surface regression for the rear side last holes in the case of aluminum-phenolic support plates.

Source	DF	Adj. SS	Adj. MS	F-Value	P-Value
Model	5	0,08166	0,016332	0,34	0,888
Linear	2	0,00022	0,000108	0,00	0,998
S. (rpm)	1	0,00019	0,000188	0,00	0,950
f. (µm/rev)	1	0,00003	0,000028	0,00	0,981
Square	2	0,07517	0,037587	0,78	0,463
S. (rpm)*S. (rpm)	1	0,05106	0,051060	1,06	0,307
f. (µm/rev)*f. (µm/rev)	1	0,02411	0,024114	0,50	0,482
2-Way Interaction	1	0,00627	0,006269	0,13	0,720
S. (rpm)*f. (µm/rev)	1	0,00627	0,006269	0,13	0,720
Error	75	3,62131	0,048284		
Lack-of-Fit	3	0,13539	0,045129	0,93	0,430
Pure Error	72	3,48593	0,048416		
Total	80	3,70297			

S	R-sq	R-sq(adj)	R-sq(pred)
0,219737	2,21%	0,00%	0,00%

As a result, spindle speed is the dominant factor on delamination for the exit side in the case of aluminum-phenol support plates.

3.1.3. Brass-wood support plates experiments

Contrary to the case of aluminum entry board, brass entry board has exhibited the larger damage difference which increases from the first hole to the last hole. Diameter of the ring shaped cavity increases as the number of drilled holes increases. In Table 3.12, entry side damage factors and exit side delamination factors are seen. Shown values are the means of six damage factor for the entry side and the means of six delamination factors for the exit side (2 times repetitions and neighbored 3 holes). Damage factors for the entry side and delamination damage factors for the exit side were also given in Appendix 1-5 and Appendix 1-6.

Table 3.12. Damage factors for CFRP laminate with Brass-Wood support plate micro-drilling experiments.

Spindle speed (rpm)	Feed (µm/rev)	Resulting feed (mm/min)	Front Side Damage Factors			Rear Side Delamination Factors		
			Hole numbers			Hole numbers		
			1-2-3	120-121-122	240-241-242	1-2-3	120-121-122	240-241-242
20000	3	60	1.037	1.196	1.250	1.148	1.412	1.450
30000	3	90	1.036	1.134	1.211	1.219	1.434	1.377
40000	3	120	1.041	1.109	1.218	1.200	1.390	1.436
20000	5	100	1.043	1.150	1.216	1.288	1.371	1.395
30000	5	150	1.032	1.186	1.232	1.272	1.454	1.497
40000	5	200	1.031	1.120	1.176	1.177	1.418	1.552
20000	7	140	1.041	1.151	1.234	1.240	1.419	1.449
30000	7	210	1.065	1.136	1.253	1.225	1.360	1.328
40000	7	280	1.039	1.155	1.180	1.202	1.560	1.633

In Figure 3.9 and Figure 3.10, graphical representations of front side damage and rear side delamination factors for CFRP laminate with Brass-Wood support plates micro-drilling experiments are shown.

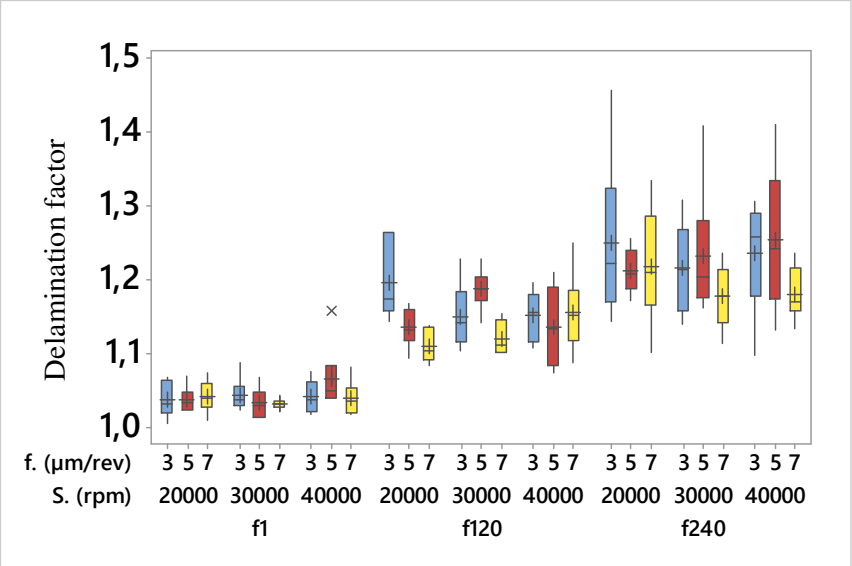

Figure 3.9. Box plots of the front side damage factors for CFRP laminate with Brass-Wood support plates micro-drilling experiments.

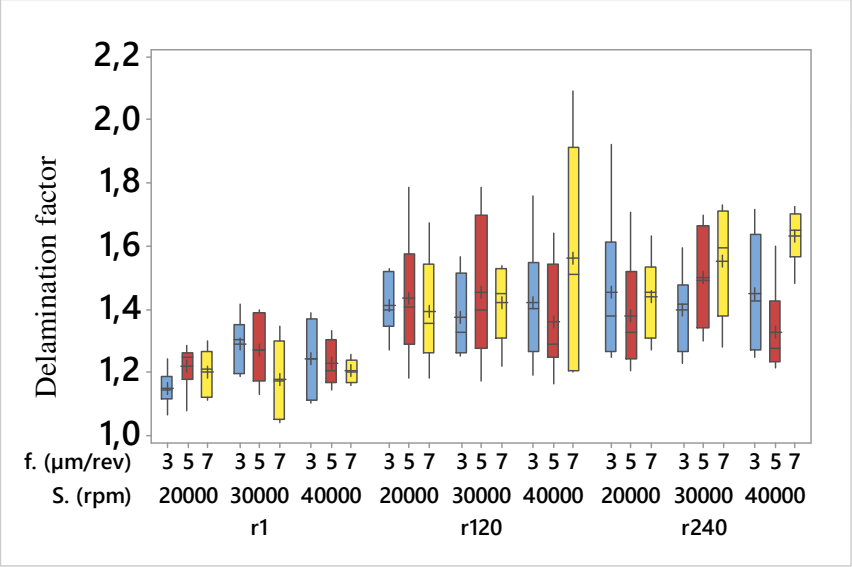

Figure 3.10. Box plots of the rear side delamination factors for CFRP laminate with Brass-Wood support plates micro-drilling experiments.

Using the values of the Table 3.12, response surface method contour plots of the ring shaped cavity damage and delamination damage factors have been constructed. Contour plots are seen for the ring shaped cavity damage in Figure 3.11. It is clearly seen from the contour plots that higher spindle speed and intermediate feed decrease the damages from the first to the last hole. As compared to the aluminum entry board, brass entry

board was much more affected by the tool wear. Burr thickness of the first holes of the brass entry board was very small and caused less damage to the CFRP laminate. However, it increased toward to the last holes. Similar effect of the high spindle speed on decreasing the burr thickness was also seen.

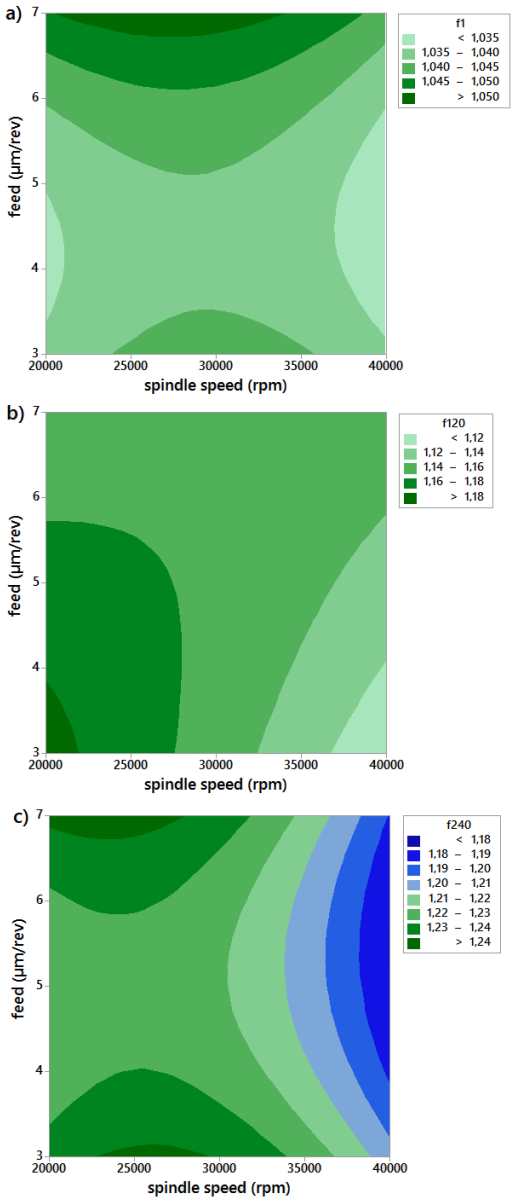

Figure 3.11. Contour plots of the ring shaped cavity damage factors for the entry side in case of brass-wood support plates. (a - r1:the first holes, b - r120:the middle holes, c - r240:the last holes)

In Figure 3.12, contour plots of delamination factors for exit side in case of wood backing board are seen. If it is assumed that ring shaped cavity damage is acceptable, the response surface optimization can be run for the exit side. Optimum values of the spindle speed and feed have been derived as 28283 rpm and 3 µm/rev, and delamination factors have been obtained as 1.2066 for the first holes, 1.4063 for the middle holes and 1.3660 for the last holes.

Compared to the first holes, the delamination damage in the middle and last holes shows contrary trends. This situation, obviously, makes the optimization difficult. In such a case, optimization may be run by leaving out the first holes. Because, highest value of the delamination factor for the first holes cannot exceed the values of the middle and last holes according to the results of the experiments. By using this assumption, optimum values of the spindle speed and feed have been derived as 20347 rpm and 7 µm/rev, and delamination factors have been obtained as 1.2521 for the first holes, 1.3837 for the middle holes and 1.3919 for the last holes. In this case, resulting feed rate is higher, but optimum delamination factors are still not satisfying. Similar to the phenolic backing board, it is seen that wood backing board cannot decrease the delamination as compared to the bare CFRP laminate experiments.

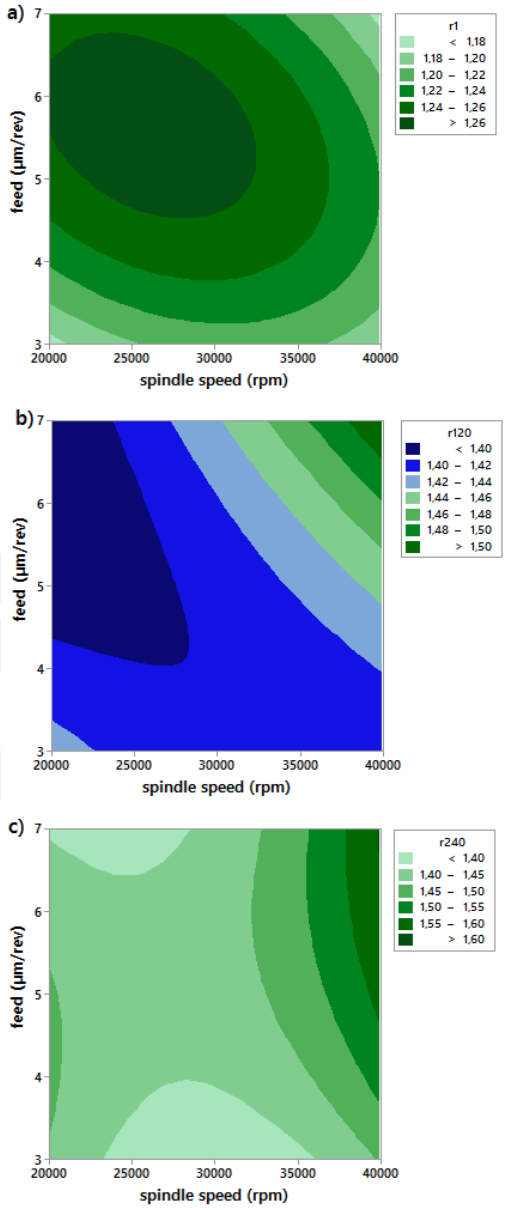

Figure 3.12. Contour plots of the delamination factors for the exit side in case of brass-wood support plates. (a - r1:the first holes, b - r120:the middle holes, c - r240:the last holes)

Analysis of variance table is shown for the rear side first holes in the case of brass-wood support plates in Table 3.13. According to the results, p-value of the lack of fit error is equal to 0,262. Therefore, it reveals that full quadratic model fits the data adequately. P-value of the model is 0,189. It indicates that the model can fail. R-sq value indicates that the model accounts for 14,00% of the variability in the model. According to the results,

spindle speed*spindle speed term has greater adjusted sum of squares values than other terms. It indicates that spindle speed*spindle speed term is more effective on the deviation of delamination damage from the mean.

Table 3.13. Analysis of variance table of response surface regression for the rear side first holes in the case of brass-wood support plates.

Source	DF	Adj. SS	Adj. MS	F-Value	P-Value
Model	5	0,061383	0,012277	1,56	0,189
Linear	2	0,019410	0,009705	1,24	0,300
S. (rpm)	1	0,010020	0,010020	1,28	0,264
f. (µm/rev)	1	0,009390	0,009390	1,20	0,280
Square	2	0,029599	0,014799	1,88	0,163
S. (rpm)*S. (rpm)	1	0,019309	0,019309	2,46	0,123
f. (µm/rev)*f. (µm/rev)	1	0,010290	0,010290	1,31	0,258
2-Way Interaction	1	0,012373	0,012373	1,58	0,216
S. (rpm)*f. (µm/rev)	1	0,012373	0,012373	1,58	0,216
Error	48	0,377057	0,007855		
Lack-of-Fit	3	0,031727	0,010576	1,38	0,262
Pure Error	45	0,345329	0,007674		
Total	53	0,438439			
S	R-sq	R-sq(adj)		R-sq(pred)	
0,0886304	14,00%	5,04%		0,00%	

Analysis of variance table is shown for the rear side middle holes in the case of brass-wood support plates in Table 3.14. According to the results, p-value of the lack of fit error is equal to 0,597. Therefore, it reveals that full quadratic model fits the data adequately. P-value of the model is 0,856. It indicates that failure of the model is more probable. R-sq value indicates that the model accounts for 3,87% of the variability in the model. According to the results, spindle speed (S.)*feed (f.) term has greater adjusted sum of squares values than other terms. It indicates that spindle speed (S.)*feed (f.) term is more effective on the deviation of delamination damage from the mean.

Table 3.14. Analysis of variance table of response surface regression for the rear side middle holes in the case of brass-wood support plates.

Source	DF	Adj. SS	Adj. MS	F-Value	P-Value
Model	5	0,08295	0,016590	0,39	0,856
Linear	2	0,03835	0,019175	0,45	0,642
S. (rpm)	1	0,01072	0,010724	0,25	0,619
f. (µm/rev)	1	0,02763	0,027627	0,64	0,426
Square	2	0,00453	0,002267	0,05	0,949
S. (rpm)*S. (rpm)	1	0,00262	0,002619	0,06	0,806
f. (µm/rev)*f. (µm/rev)	1	0,00192	0,001916	0,04	0,834
2-Way Interaction	1	0,04006	0,040063	0,93	0,339
S. (rpm)*f. (µm/rev)	1	0,04006	0,040063	0,93	0,339
Error	48	2,06004	0,042917		
Lack-of-Fit	3	0,08362	0,027873	0,63	0,597
Pure Error	45	1,97642	0,043920		
Total	53	2,14299			
S	R-sq		R-sq(adj)	R-sq(pred)	
0,207165	3,87%		0,00%	0,00%	

Analysis of variance table is shown for the rear side last holes in the case of brass-wood support plates in Table 3.15. According to the results, p-value of the lack of fit error is equal to 0,247. Therefore, it reveals that full quadratic model fits the data adequately. P-value of the model is 0,106. It indicates that the model can fail. R-sq value indicates that the model accounts for 16,79% of the variability in the model. According to the results, the terms which are related to the feed have greater adjusted sum of squares values than other terms. It indicates that feed related terms are more effective on the deviation of delamination damage from the mean.

Table 3.15. Analysis of variance table of response surface regression for the rear side last holes in the case of brass-wood support plates.

Source	DF	Adj. SS	Adj. MS	F-Value	P-Value
Model	5	0,28951	0,05790	1,94	0,106
Linear	2	0,12822	0,06411	2,14	0,128
S. (rpm)	1	0,02122	0,02122	0,71	0,404
f. (µm/rev)	1	0,10700	0,10700	3,58	0,065
Square	2	0,10261	0,05131	1,72	0,191
S. (rpm)*S. (rpm)	1	0,01567	0,01567	0,52	0,473
f. (µm/rev)*f. (µm/rev)	1	0,08694	0,08694	2,91	0,095
2-Way Interaction	1	0,05868	0,05868	1,96	0,168
S. (rpm)*f. (µm/rev)	1	0,05868	0,05868	1,96	0,168
Error	48	1,43518	0,02990		
Lack-of-Fit	3	0,12468	0,04156	1,43	0,247
Pure Error	45	1,31050	0,02912		
Total	53	1,72469			
S	R-sq	R-sq(adj)		R-sq(pred)	
0,172915	16,79%	8,12%		0,00%	

As a result, a statistically significant term does not take place for the delamination damage in the case of brass-wood support plates from the first to the last hole. However, spindle speed*spindle speed term for the first holes, spindle speed*feed term for the middle holes and feed term for the last holes is more effective on the deviation of results from the mean.

3.1.4. Comparison of the supported and unsupported cases

According to the experimental results, it was found that entry boards eliminated the entry side delamination damage completely. On the other hand, effects of backing boards on exit side delamination damage are more complicated. Percentage variations of rear side delamination factors of supported CFRP laminate experiments as compared to those of bare CFRP laminate experiments are given in Table 3.16. Each value is the cells corresponds to the percentage variation and calculated as the ratio of the difference between the delamination damage of supported case and delamination damage of unsupported case to the delamination damage of unsupported case. According to the results, the effect of phenolic backing board on the delamination damage is between the -3% and 9% for the first holes, -10% and 12% for the middle holes, and -7% and 11% for the last holes, and effect of wood backing board on the delamination damage is between the -15% and 8% for the first holes, -7% and 19% for the middle holes, and -5% and

21% for the last holes with respect to the bare CFRP experiments. Due to the fact that different cutting conditions cannot be selected for the first, the middle and the last holes, arithmetic mean of the percentage variations of delamination damages were used to make a comparison. According to the arithmetic means, phenolic backing board can decrease the rear side mean delamination damage as 5% and can increase the rear side mean delamination damage as 7%, and wood backing board can decrease the rear side mean delamination damage as 7% and can increase the rear side mean delamination as 16% with respect to the bare CFRP experiments depending on the cutting conditions.

Table 3.16. Percentage variations of rear side delamination factors of supported CFRP laminate experiments as compared to bare CFRP laminate experiments.

			Phenolic backing board				Wood backing board			
Spindle Speed (rpm)	Feed (µm/rev)	Feed Rate (mm/min)	The first three holes (%)	The middle three holes (%)	The last three holes (%)	Arithmetic mean (%)	The first three holes (%)	The middle three holes (%)	The last three holes (%)	Arithmetic mean (%)
20000	3	60	1	1	-5	-1	-15	-1	-4	-7
30000	3	90	-3	-4	-1	-3	-6	3	-5	-3
40000	3	120	6	6	7	6	0	5	8	4
20000	5	100	8	12	-4	6	7	5	-4	3
30000	5	150	8	-7	-7	-2	8	-2	-1	2
40000	5	200	2	1	-4	0	-2	1	8	2
20000	7	140	4	5	1	3	-4	0	-1	-2
30000	7	210	2	-10	-6	-5	0	-7	-5	-4
40000	7	280	9	1	11	7	7	19	21	16
The best			-3	-10	-7	-5	-15	-7	-5	-7
The worst			9	12	11	7	8	19	21	16

Derived results from the Section 3.1 which concern the evaluation of delamination damage were also given in reference [95].

3.2. Hole Form Quality

3.2.1. Diameter

In Table 3.17, mean values of the hole diameters are seen. Each value in the cells corresponds to the mean of nine values with three trials and consecutive three holes for the first and the second setups. It corresponds to the mean of six values with two trials and consecutive three holes for the third setup. Hole diameters were also given in Appendix 2.

Table 3.17. Mean values of the hole diameters.

			Front Side Diameters (µm)			Rear Side Diameters (µm)		
	Spindle Speed (rpm)	Feed (µm/rev)	Mean of 1-2-3	Mean of 120-121-122	Mean of 240-241-242	Mean of 1-2-3	Mean of 120-121-122	Mean of 240-241-242
1. setup Bare CFRP	20000	3	503,4	494,3	495,7	492,4	483,3	485,2
	20000	5	504,9	505,0	506,1	498,2	484,5	484,2
	20000	7	503,9	495,7	500,0	499,1	489,0	485,4
	30000	3	502,9	500,7	499,0	492,3	479,8	479,3
	30000	5	506,7	498,0	496,9	492,6	480,8	481,4
	30000	7	502,1	497,0	499,2	495,5	486,6	487,6
	40000	3	500,9	495,9	490,6	493,7	480,9	484,7
	40000	5	501,8	497,9	496,5	495,0	488,3	483,1
	40000	7	502,5	497,5	491,2	487,7	481,8	485,5
2. setup Aluminum-CFRP-Phenolic	20000	3	512,4	509,5	506,7	505,9	486,8	489,0
	20000	5	505,5	502,7	506,6	493,1	497,0	495,4
	20000	7	513,2	503,3	504,6	496,3	491,7	492,3
	30000	3	505,8	502,2	505,0	496,7	489,8	486,3
	30000	5	508,0	506,3	506,6	492,6	492,8	489,7
	30000	7	512,6	510,8	505,1	496,2	492,0	491,1
	40000	3	506,1	502,1	505,4	494,9	490,7	485,9
	40000	5	507,2	504,5	506,0	496,1	492,4	484,8
	40000	7	511,6	502,7	505,9	497,3	489,7	489,8
3. setup Brass-CFRP-Fir wood	20000	3	496,9	495,0	495,1	492,3	479,8	486,3
	20000	5	499,5	494,3	496,5	504,5	491,4	486,5
	20000	7	501,6	496,8	503,6	497,2	490,9	485,5
	30000	3	501,0	500,0	497,5	497,3	481,0	479,1
	30000	5	501,3	498,7	495,4	497,8	491,8	485,8
	30000	7	500,1	503,5	499,3	498,7	490,5	488,1
	40000	3	500,2	496,8	492,0	498,5	490,0	476,0
	40000	5	499,3	496,7	497,5	493,6	481,2	481,7
	40000	7	503,4	507,7	506,3	497,8	491,5	488,8

Graphical representations of variations of hole diameters are shown in Figure 3.13 for front side the first holes, in Figure 3.14 for front side the middle holes, in Figure 3.15 for front side the last holes, in Figure 3.16 for rear side the first holes, in Figure 3.17 for rear side the middle holes, and in Figure 3.18 for rear side the last holes (Bare CFRP in blue, Aluminum-CFRP-Phenolic in red, and Brass-CFRP-Fir wood in yellow). In the plots, horizontal lines indicate the median values, plus signs indicate the mean values, multiplication signs indicate the outliers, and boxes indicate the interquartile ranges. Whiskers extend to the highest and lowest values within the limits. Upper limit equals to Q_3+1,5(Q_3-Q_1) and lower limit equals to Q_1-1.5 (Q_3 - Q_1).

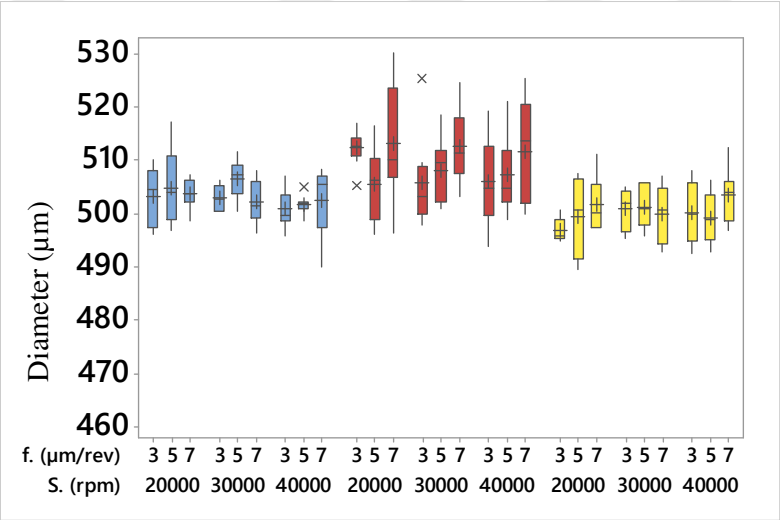

Figure 3.13. Front side the first holes diameters.

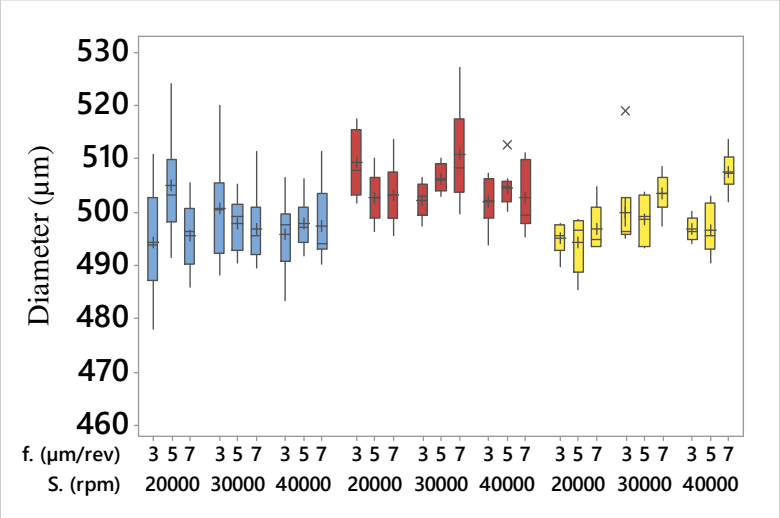

Figure 3.14. Front side the middle holes diameters.

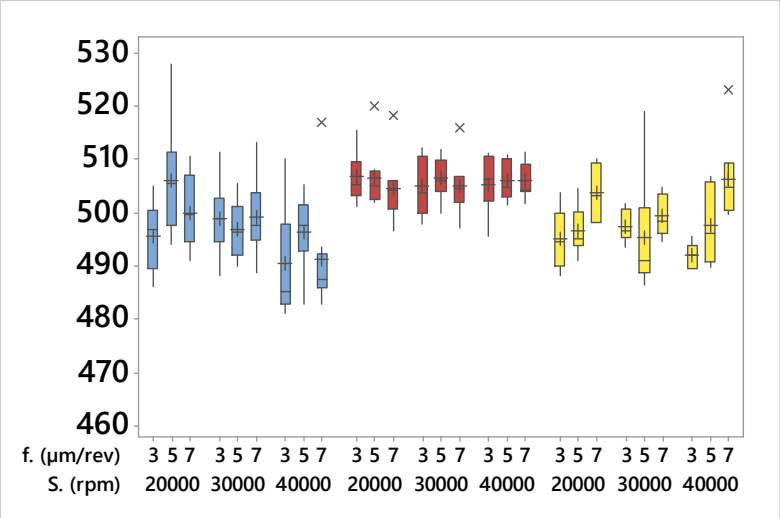

Figure 3.15. Front side the last holes diameters.

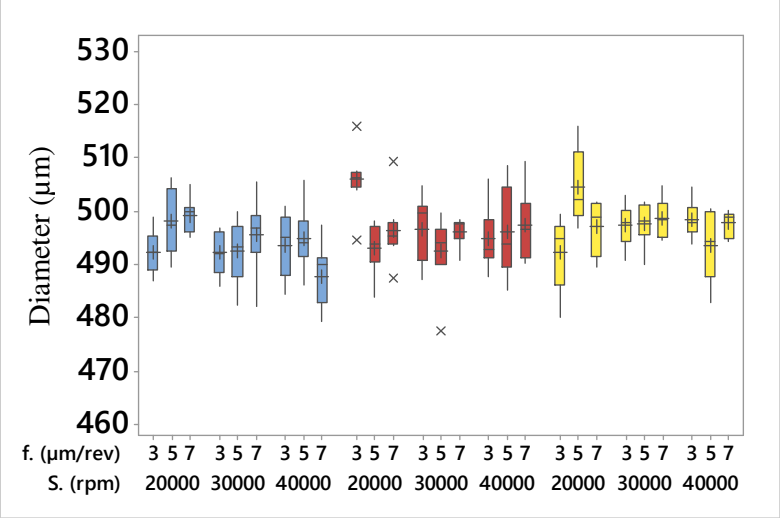

Figure 3.16. Rear side the first holes diameters.

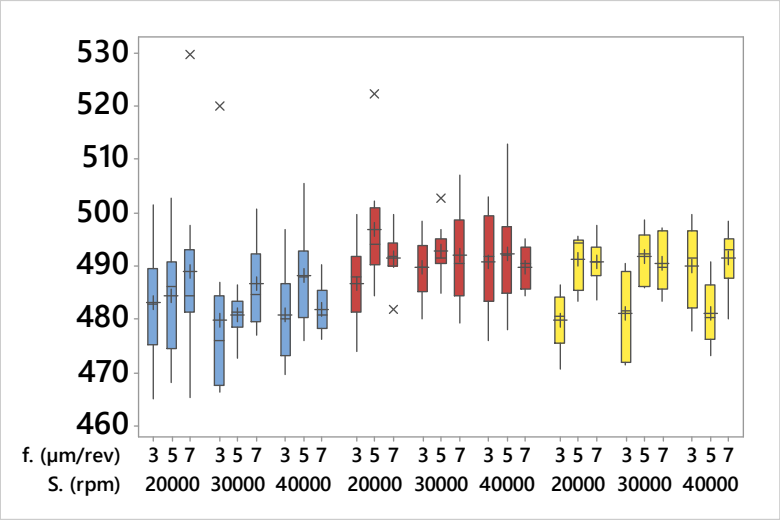

Figure 3.17. Rear side the middle holes diameters.

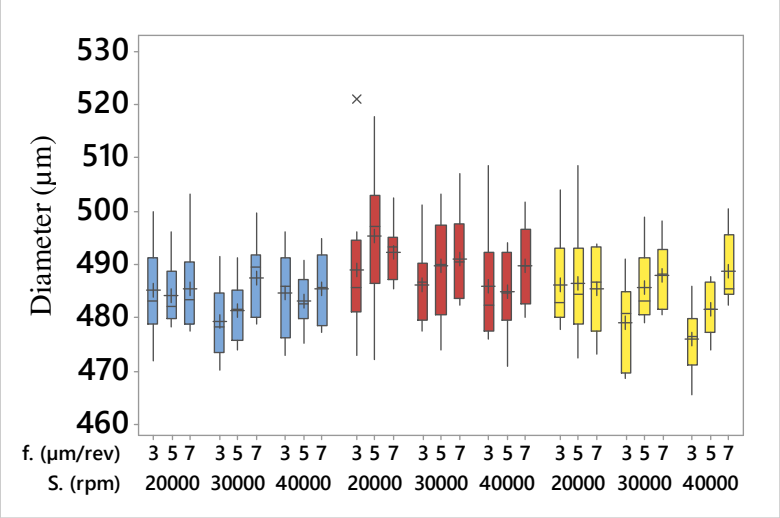

Figure 3.18. Rear side the last holes diameters.

By using Minitab 17, main effects plots of the hole diameters of the front and rear sides were derived similarly for each setup. For a proper comparison, the range of the vertical axes in the plots was kept constant for each raw. Plots in each column present an individual setup.

In Figure 3.19, main effects plots are shown for the front side hole diameters. By using the plots, following results can be derived for each setup. Effect of the spindle speed on the mean hole diameter variation is similar from the first to the last hole for the bare CFRP laminate experiments, and it is also valid for the feed. For an individual experiment, only parameter which affects the variations of the process outputs from the

first hole to the last hole is deterioration of the micro drill. In Figure 3.20, the flank face pictures which indicate the reduction of the micro drill are shown for both unused drill and worn drill. Therefore, the variations of the CFRP laminate's hole diameter, roundness error, and fiber overlap can be attributed to the tool wear. For the bare CFRP laminate experiments, effects of the variables increase as tool wears. Mean hole diameter decreases as spindle speed increases and increases as feed increases to an intermediate value, then decreases with further increasing the feed. Increasing the spindle speed increases the thermal gradient around the hole [77], and may cause the decrease in the hole diameter due to matrix softening. Increase of the hole diameter at intermediate feed may not be related to the tool wear due to the similar trends from the first to the last hole. Effect of the feed on the hole diameter can be explained such that the hole diameter decreases as feed increases due to the decrease in the engage time which prevent the matrix softening as a general trend but decreases again due to the ploughing effect at the feed of 3 µm/rev which corresponds to the uncut chip thickness of 1.5 µm which equals to the cutting edge radius. Rahamathullah and Shunmugam [2] carried out an experimental study by using peck drilling with close values of cutting parameters to the this study and stated that spindle speed did not affect the hole diameter, and low feed (starting from 5 µm/rev) increased the hole diameter. Mean diameters of the first holes are greater than the mean diameters of the middle and the last holes. Mean hole diameters are close to the drill diameter. Variation of the mean hole diameter from the first to the last hole indicates the tool wear effect. As micro drill wears, mean diameter decreases.

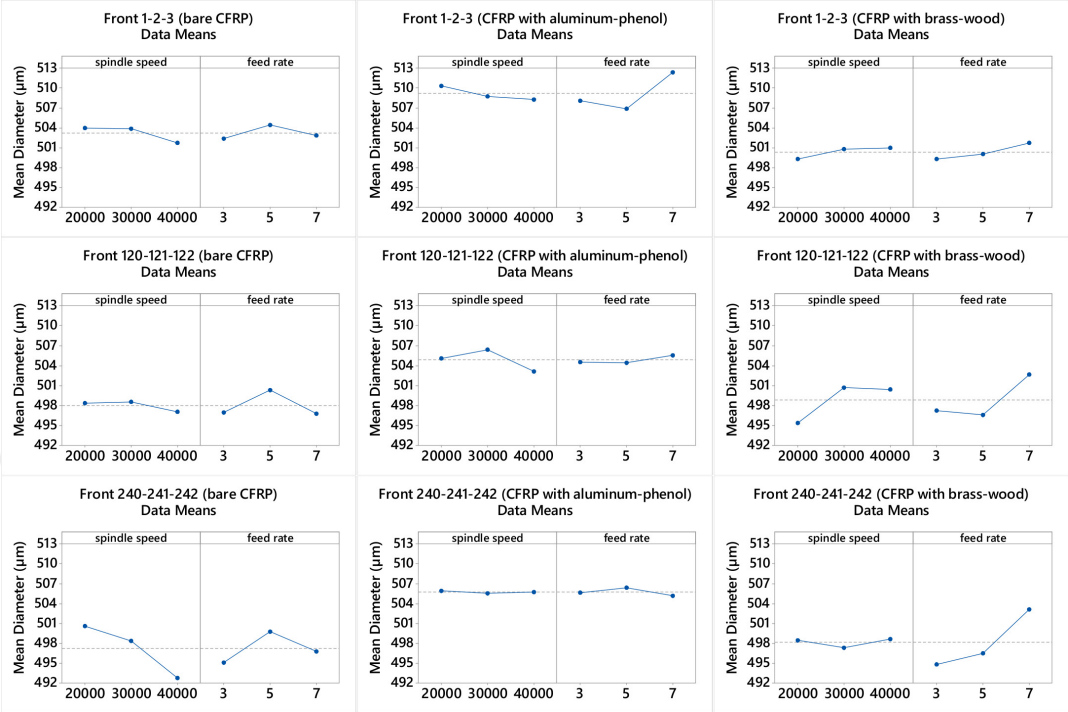

Figure 3.19. Main effects plots for the front side hole diameters.

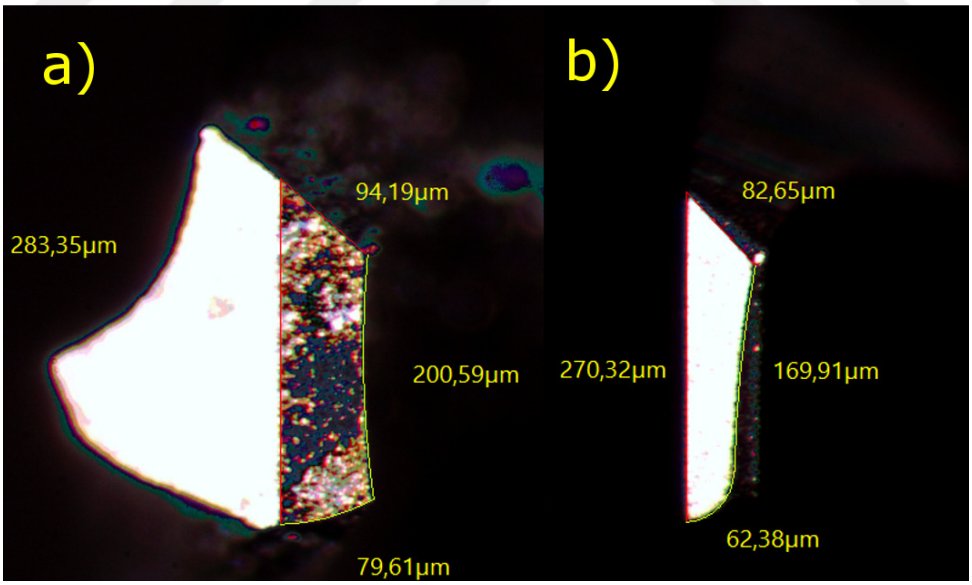

Figure 3.20. Wear of the micro drill: (a) unused drill, (b) worn drill at 242nd hole (40000 rpm, 5 µm/rev)

For the case of aluminum entry board, spindle speed and feed do not affect the mean hole diameters significantly except the effects of feed for the first holes and spindle speed for the middle holes. The aluminum entry board has greatly enlarged the mean hole diameter

for the first holes. Even though the following mean hole diameters are slightly smaller, they are larger than the drill diameters. Increase in the hole diameter can be attribute to the exit burrs of the entry board. During the process, micro-drill cuts the entry board first, and exit burrs of the entry board are formed but cannot extend due to the workpiece of CFRP laminate which blocks the burrs and expand the burrs outside the hole. Thus, hole diameter increases. It is thought that exit burrs of the entry board are governing parameter which affects the hole diameter. Mean hole diameter decreases approximately 5 microns as tool wears. For the case of brass entry board, mean hole diameter increases as feed increases. Spindle speed does not affect the mean hole diameter for the last holes. However, mean hole diameter increases as spindle speed increases for the first and the middle three holes. Mean hole diameters in the case of brass entry board are very stable and close to the drill diameter from the first to the last hole. Burr size of the brass entry board is less than the burr size of the aluminum entry board in comparison. Typical exit burrs of the entry boards are seen in Figure 3.21. By using the mean hole diameter plots and the inspections, it can be concluded that increase in the feed and spindle speed increases the burr size of the entry board and the hole diameter, and tool wear does not affect the mean hole diameter significantly.

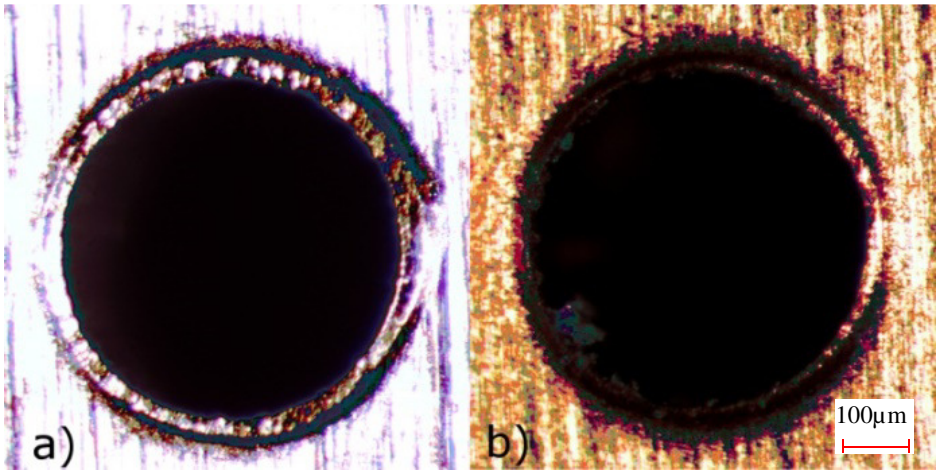

Figure 3.21. Typical exit burrs of the entry boards: (a) aluminum entry board (b) brass entry board.

In Figure 3.22, main effects plots are seen for the rear side hole diameters. Generally, it is seen from the plots that the rear side mean hole diameter decreases as spindle speed increases and feed decreases for all setups. Similar to the front side hole diameter,

increasing the spindle speed increases the thermal gradient around the hole [77]. Thus, hole diameter decreases. Increasing the feed increases the thrust force. Rising thrust force may cause the hole diameter to increase. Phenolic backing board provides less mean hole diameter variation from the first to the last hole among the setups. Wood backing board is the worst to sustain the mean hole diameter stability. Mean diameters of the holes are under the drill diameter. Mean hole diameter in case of phenolic backing board is close to the drill diameter. It is followed by the wood backing board. Structural resemblance of the phenolic backing board to the CFRP laminate may play a role in providing a hole diameter close to the drill diameter as compared to the wood backing board due to the fact that it provides the continuity between the CFRP laminate and backing board. Using backing board eliminates the push out effect of the micro drill. Thus, efficient cutting is provided. It can be noted that the mean hole diameter usually decreases from the first to the last hole. This is an evidence of the tool wear effect on the hole diameter.

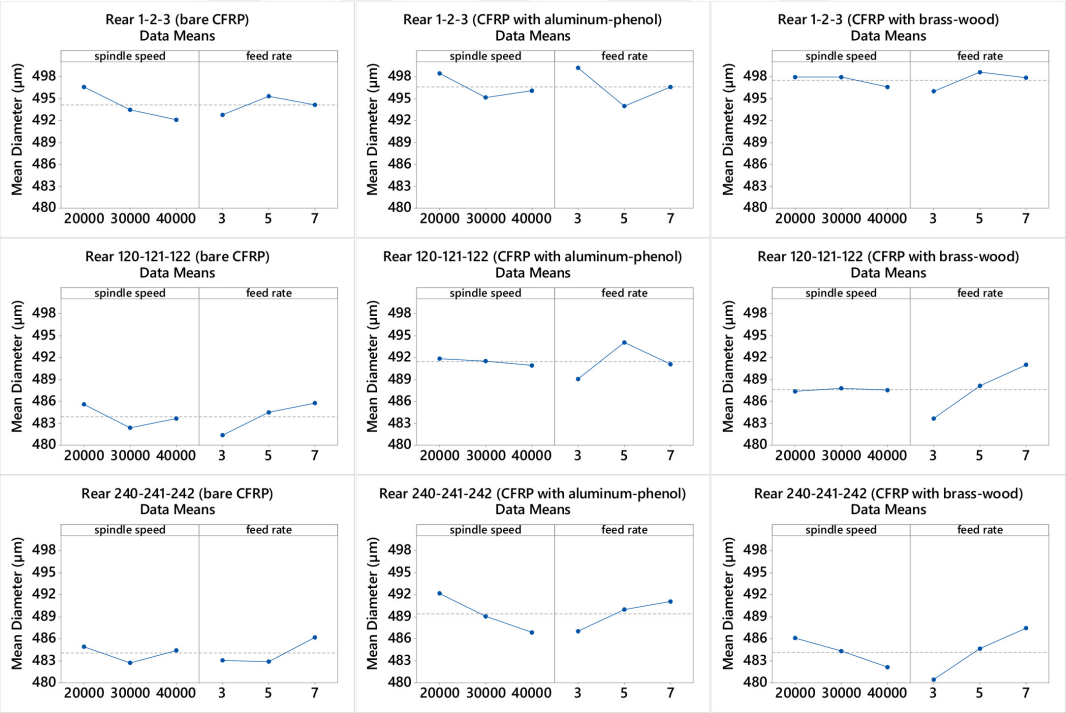

Figure 3.22. Main effects plots for the rear side hole diameters.

In Table 3.18, percentage deviations of front side hole diameters from the nominal hole diameter are shown. Each value is the cells corresponds to the percentage deviation and calculated as the ratio of the difference between the hole diameter of supported case and

nominal hole diameter to the nominal hole diameter. According to the results, the deviation of front side hole diameter from the nominal hole diameter for the bare CFRP laminate experiments is between the 0,2% and 1,3% for the first holes, 0,1% and -1,1% for the middle holes, and 0,0% and -1,9% for the last holes, and the deviation of front side hole diameter from the nominal hole diameter for the CFRP laminate with aluminum entry board experiments is between the 1,1% and 2,6% for the first holes, 0,4% and 2,2% for the middle holes, and 0,9% and 1,3% for the last holes, and the deviation of front side hole diameter from the nominal hole diameter for the CFRP laminate with brass entry board experiments is between the 0,0% and 0,7% for the first holes, 0,0% and 1,5% for the middle holes, and -0,1% and -1,6% for the last holes. Although it can be thought that these variations are very small, it must be taken into consideration that 1% deviation corresponds to 5 µm. Due to the fact that different cutting conditions cannot be selected for the first, the middle and the last holes, Root Mean Square (RMS) values of the percentage deviations of diameters from the nominal hole diameter were used to make a comparison. According to the RMS values, front side RMS hole diameter varies between the 0,4% and 1,2% for the bare CFRP laminate experiments, front side RMS hole diameter varies between the 0,9% and 2% for the CFRP laminate with aluminum entry board, and front side RMS hole diameter varies between the 0,3% and 1,2% for the CFRP laminate with brass entry board depending on the cutting conditions. By using these results, it can be concluded that minimum front side RMS hole diameter variation can be derived with supported case with brass entry board (0,3%), it is followed by unsupported case (0,4%) and supported case with aluminum entry board (0,9%). On the other hand, the variation of hole diameters from the first hole to the last hole is an important parameter for drilling operations, and it is desired to minimize the hole diameter variation. Therefore, minimum and maximum hole diameter differences from the first to the last hole were also indicated in Table 3.18. According to the results, minimum and maximum percentage differences for front side diameters are 0,2% and 2,3% for bare CFRP laminate experiments, 0,3% and 1,9% for the CFRP laminate with aluminum entry board, and 0,4% and 1,6% for the CFRP laminate with brass entry board depending on the cutting conditions. By using these results, it can be concluded that minimum deviation from the first to the last hole for the front side can be derived with unsupported case (0,2%), it is followed by supported case

with aluminum entry board (0,3%) and supported case with brass entry board (0,4%).

Table 3.18. Percentage deviations of front side hole diameters from the nominal diameter.

			Bare CFRP					Aluminum entry board					Brass entry board				
Spindle Speed (rpm)	Feed (µm/rev)	Feed Rate (mm/min)	The first holes (%)	The middle holes (%)	The last holes (%)	RMS (%)	The max - min (%)	The first holes (%)	The middle holes (%)	The last holes (%)	RMS (%)	The max - min (%)	The first holes (%)	The middle holes (%)	The last holes (%)	RMS (%)	The max - min (%)
20000	3	60	0,7	-1,1	-0,9	0,9	1,8	2,5	1,9	1,3	2,0	1,2	-0,6	-1,0	-1,0	0,9	0,4
20000	5	100	1,0	1,0	1,2	1,1	0,2	1,1	0,5	1,3	1,0	0,8	-0,1	-1,1	-0,7	0,8	1,0
20000	7	140	0,8	-0,9	0,0	0,7	1,7	2,6	0,7	0,9	1,6	1,9	0,3	-0,6	0,7	0,6	1,3
30000	3	90	0,6	0,1	-0,2	0,4	0,8	1,2	0,4	1,0	0,9	0,8	0,2	0,0	-0,5	0,3	0,7
30000	5	150	1,3	-0,4	-0,6	0,9	1,9	1,6	1,3	1,3	1,4	0,3	0,3	-0,3	-0,9	0,6	1,2
30000	7	210	0,4	-0,6	-0,2	0,4	1,0	2,5	2,2	1,0	2,0	1,5	0,0	0,7	-0,1	0,4	0,8
40000	3	120	0,2	-0,8	-1,9	1,2	2,1	1,2	0,4	1,1	1,0	0,8	0,0	-0,6	-1,6	1,0	1,6
40000	5	200	0,4	-0,4	-0,7	0,5	1,1	1,5	0,9	1,2	1,2	0,6	-0,2	-0,7	-0,5	0,5	0,5
40000	7	280	0,5	-0,5	-1,8	1,1	2,3	2,3	0,5	1,2	1,5	1,8	0,7	1,5	1,3	1,2	0,8
The best			0,2	0,1	0,0	0,4	0,2	1,1	0,4	0,9	0,9	0,3	0,0	0,0	-0,1	0,3	0,4
The worst			1,3	-1,1	-1,9	1,2	2,3	2,6	2,2	1,3	2,0	1,9	0,7	1,5	-1,6	1,2	1,6

In Table 3.19, percentage deviations of rear side hole diameters from the nominal hole diameter are shown. According to the results, the deviation of rear side hole diameter from the nominal hole diameter for the bare CFRP laminate experiments is between the -0,2% and -2,5% for the first holes, -2,2% and -4,0% for the middle holes, and -2,5% and -4,2% for the last holes, and the deviation of rear side hole diameter from the nominal hole diameter for the CFRP laminate with phenolic backing board experiments is between the -0,5% and -1,5% for the first holes, -0,6% and -2,6% for the middle holes, and -0,9% and -3,0% for the last holes, and the deviation of rear side hole diameter from the nominal hole diameter for the CFRP laminate with wood backing board experiments is between the -0,3% and -1,5% for the first holes, -1,6% and -4,0% for the middle holes, and -2,3% and -4,8% for the last holes. According to the RMS values, rear side RMS hole diameter varies between the 2,1% and 3,5% for the bare CFRP laminate experiments, rear side RMS hole diameter varies between the 1,0% and 2,1% for the CFRP laminate with phenolic backing board, and rear side RMS hole diameter varies between the 1,7% and 3,3% for the CFRP laminate with wood backing board depending

on the cutting conditions. By using these results, it can be concluded that minimum RMS rear side hole diameter variation can be derived with supported case with phenolic backing board (1,0%), it is followed by supported case with wood backing board (1,7%) and unsupported case (2,1%). According to the results, minimum and maximum percentage differences for rear side diameters are 1,1% and 2,8% for bare CFRP laminate experiments, 0,6% and 3,8% for the CFRP laminate with phenolic backing board, and 1,9% and 4,5% for the CFRP laminate with wood backing board depending on the cutting conditions. By using these results, it can be concluded that minimum deviation from the first to the last hole for the front side can be derived with supported case with phenolic backing board (0,6%), it is followed by unsupported case (1,1%) and supported case with wood backing board (1,9%).

Table 3.19. Percentage deviations of rear side hole diameters from the nominal diameter.

			Bare CFRP					Aluminum entry board					Brass entry board				
Spindle Speed (rpm)	Feed (µm/rev)	Feed Rate (mm/min)	The first holes (%)	The middle holes (%)	The last holes (%)	RMS (%)	The max - min (%)	The first holes (%)	The middle holes (%)	The last holes (%)	RMS (%)	The max - min (%)	The first holes (%)	The middle holes (%)	The last holes (%)	RMS (%)	The max - min (%)
20000	3	60	-1,5	-3,4	-3,0	2,8	1,9	1,2	-2,6	-2,2	2,1	3,8	-1,5	-4,0	-2,7	2,9	2,5
20000	5	100	-0,4	-3,1	-3,2	2,6	2,8	-1,4	-0,6	-0,9	1,0	0,8	0,9	-1,7	-2,7	1,9	3,6
20000	7	140	-0,2	-2,2	-2,9	2,1	2,7	-0,7	-1,7	-1,5	1,4	1,0	-0,6	-1,8	-2,9	2,0	2,3
30000	3	90	-1,5	-4,0	-4,2	3,5	2,7	-0,7	-2,1	-2,7	2,0	2,0	-0,5	-3,8	-4,2	3,3	3,7
30000	5	150	-1,5	-3,9	-3,7	3,2	2,4	-1,5	-1,5	-2,1	1,7	0,6	-0,5	-1,6	-2,9	1,9	2,4
30000	7	210	-0,9	-2,7	-2,5	2,2	1,8	-0,8	-1,6	-1,8	1,5	1,0	-0,3	-1,9	-2,4	1,8	2,1
40000	3	120	-1,3	-3,8	-3,1	2,9	2,5	-1,0	-1,9	-2,8	2,0	1,8	-0,3	-2,0	-4,8	3,0	4,5
40000	5	200	-1,0	-2,4	-3,4	2,5	2,4	-0,8	-1,5	-3,0	2,0	2,2	-1,3	-3,8	-3,7	3,2	2,5
40000	7	280	-2,5	-3,6	-2,9	3,0	1,1	-0,5	-2,1	-2,0	1,7	1,6	-0,4	-1,7	-2,3	1,7	1,9
The best			-0,2	-2,2	-2,5	2,1	1,1	-0,5	-0,6	-0,9	1,0	0,6	-0,3	-1,6	-2,3	1,7	1,9
The worst			-2,5	-4,0	-4,2	3,5	2,8	-1,5	-2,6	-3,0	2,1	3,8	-1,5	-4,0	-4,8	3,3	4,5

3.2.2. Roundness error

In Table 3.20, mean values of the roundness errors are seen. Each value in the cells corresponds to the mean of nine values with three trials and consecutive three holes for the first and the second setups. It corresponds to the mean of six values with two trials and consecutive three holes for the third setup. Roundness errors were also given in

Appendix 3.

Table 3.20. Mean values of the roundness errors.

			Front Side Roundness Error (µm)			Rear Side Roundness Error (µm)		
	Spindle Speed (rpm)	Feed (µm/rev)	Mean of 1-2-3	Mean of 120-121-122	Mean of 240-241-242	Mean of 1-2-3	Mean of 120-121-122	Mean of 240-241-242
1. setup Bare CFRP	20000	3	4,4	10,1	17,5	10,6	16,5	13,4
	20000	5	6,1	10,2	11,3	9,0	14,4	15,3
	20000	7	4,5	13,8	13,3	10,4	13,4	18,2
	30000	3	6,2	12,3	13,0	11,8	20,7	17,3
	30000	5	6,3	10,2	15,8	9,1	12,2	19,6
	30000	7	6,0	12,5	9,6	9,1	11,7	11,7
	40000	3	6,9	12,7	12,6	9,0	19,8	18,6
	40000	5	5,3	8,8	12,2	8,7	9,8	17,1
	40000	7	6,3	13,8	13,2	12,2	14,7	13,5
2. setup Aluminum-CFRP-Phenolic	20000	3	4,8	6,6	5,8	11,5	21,5	28,5
	20000	5	6,0	3,4	7,0	11,2	15,7	21,2
	20000	7	6,5	4,9	5,2	13,9	21,3	18,4
	30000	3	4,8	5,6	5,5	10,7	16,6	20,3
	30000	5	5,3	4,9	7,2	16,4	26,0	18,3
	30000	7	4,9	4,2	3,8	9,3	17,5	18,0
	40000	3	5,1	6,4	5,4	9,3	18,0	17,4
	40000	5	5,1	4,5	4,8	13,0	16,8	21,3
	40000	7	4,9	4,9	5,0	9,7	16,0	14,8
3. setup Brass-CFRP-Fir wood	20000	3	5,0	7,0	7,1	8,8	19,0	21,9
	20000	5	5,3	6,9	5,6	10,4	13,2	19,7
	20000	7	4,6	4,8	8,3	9,4	15,5	17,4
	30000	3	6,1	7,2	6,1	8,9	16,0	21,9
	30000	5	6,4	8,0	9,0	8,7	16,4	20,8
	30000	7	6,0	5,7	6,9	8,7	19,1	19,7
	40000	3	7,1	7,2	5,9	7,8	18,3	18,7
	40000	5	5,9	3,5	9,9	10,2	20,7	18,0
	40000	7	4,9	6,1	6,7	6,8	15,9	13,9

Graphical representations of variations of roundness errors are shown in Figure 3.23 for front side the first holes, in Figure 3.24 for front side the middle holes, in Figure 3.25 for front side the last holes, in Figure 3.26 for rear side the first holes, in Figure 3.27 for rear side the middle holes, and in Figure 3.28 for rear side the last holes (Bare CFRP in blue, Aluminum-CFRP-Phenolic in red, and Brass-CFRP-Fir wood in yellow). In the plots, horizontal lines indicate the median values, plus signs indicate the mean values,

multiplication signs indicate the outliers, and boxes indicate the interquartile ranges. Whiskers extend to the highest and lowest values within the limits. Upper limit equals to Q_3+1,5(Q_3-Q_1) and lower limit equals to Q_1-1.5 (Q_3 - Q_1).

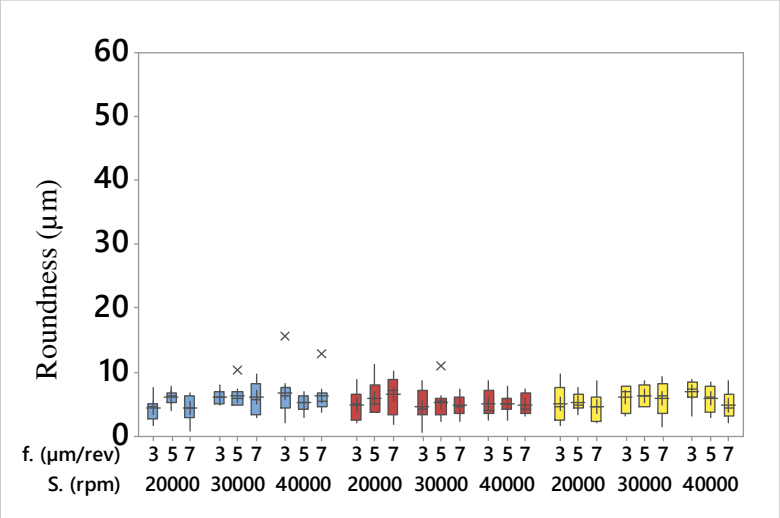

Figure 3.23. Front side the first holes roundness errors.

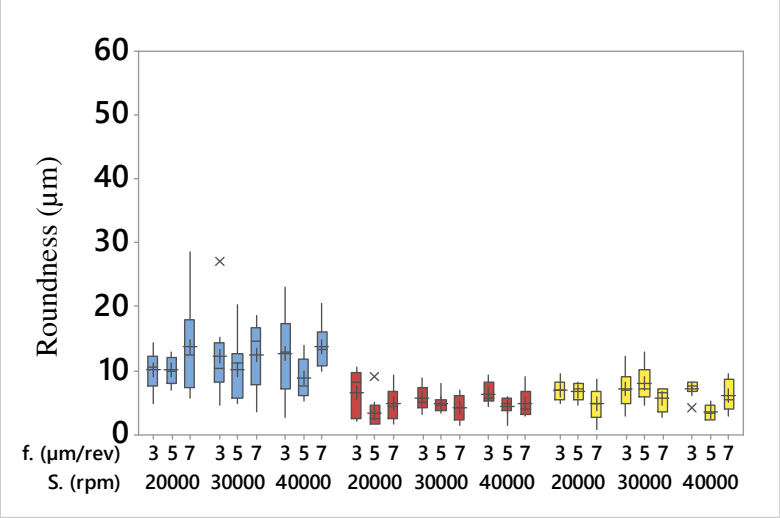

Figure 3.24. Front side the middle holes roundness errors.

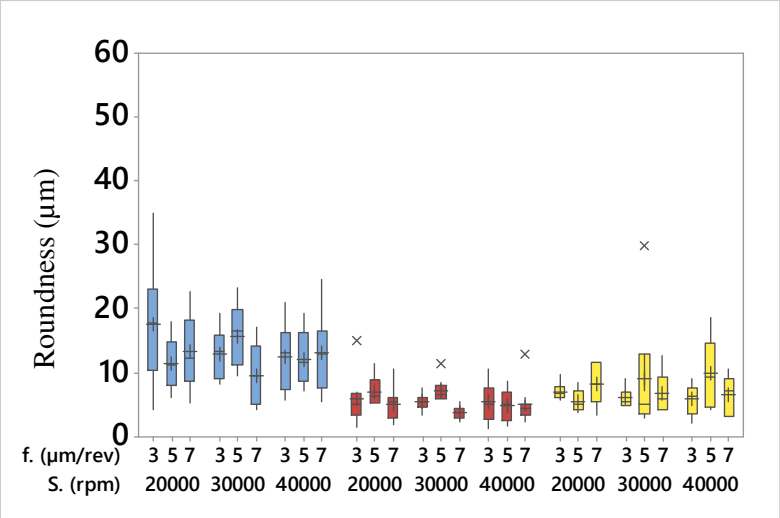

Figure 3.25. Front side the last holes roundness errors.

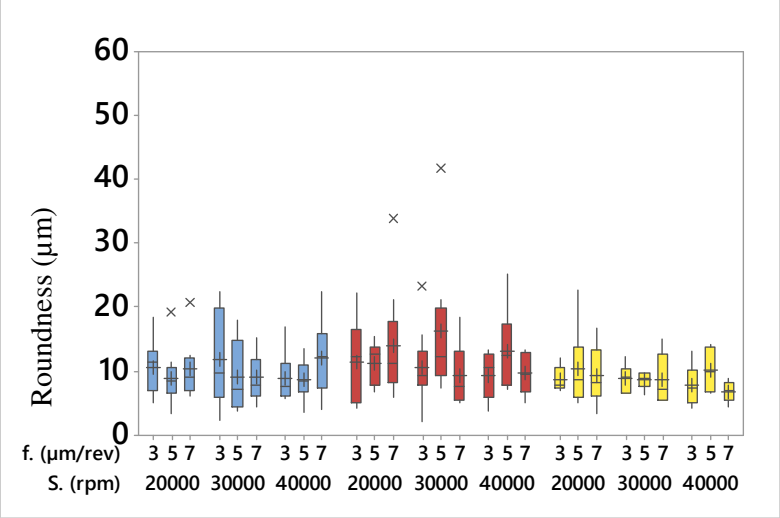

Figure 3.26. Rear side the first holes roundness errors.

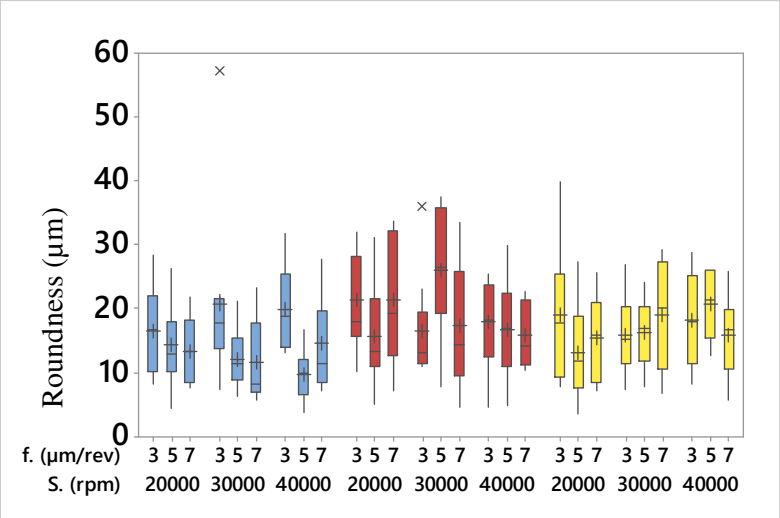

Figure 3.27. Rear side the middle holes roundness errors.

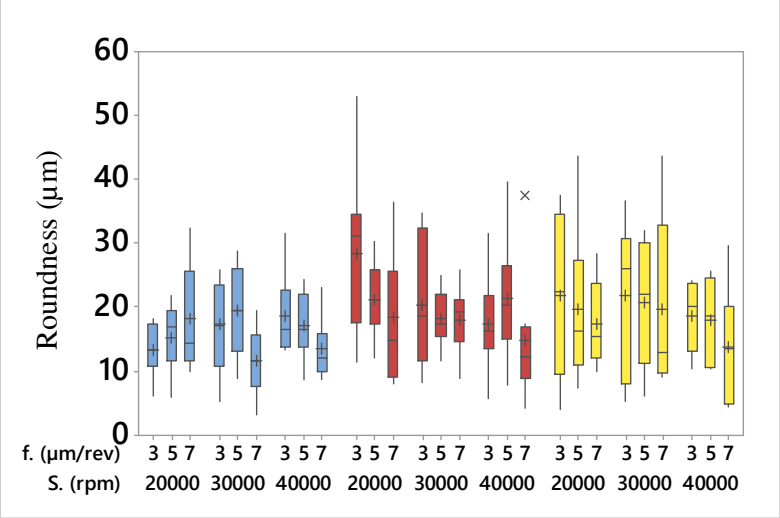

Figure 3.28. Rear side the last holes roundness errors.

In Figure 3.29, main effects plots for the front side roundness error are shown. Among the three different setups, aluminum entry board provides the least mean roundness error values from the first to the last hole. It is followed by brass entry board. It is seen from the plots that process variables do not affect the roundness significantly for the aluminum and brass entry boards, and mean roundness error values are similar from the first to the last hole. It is an evident that tool wear does not affect the roundness for the aluminum and brass entry boards. One of the advantages using the entry board is that it provides the effective centering of the micro drill during the initial entrance thanks to its less anisotropic structure as compared to the CFRP laminate which is highly anisotropic.

Watanabe et al. [96] carried out an experimental study to investigate the effect of radial run-out on hole quality, and stated that entry board effectively reduced the deviation of hole position by means of enhancing centripetal action. Thus, misalignment of the micro drill is prevented. Otherwise, micro drill deflects and deviates with propagation, and drill margin increases the roundness error. It is seen from the bare CFRP plots that mean roundness error increases drastically from the first to the last hole. As the micro drill wears, centering of the micro drill becomes more difficult due to the blunt drill point, chisel edge, and cutting edge. Thus, roundness error increases. Although variations of the roundness error values due to the variable cutting conditions in the case of bare CFRP are greater than the other cases, the variations are limited to 4 µm. According to the presented data for conventional drilling of CFRP laminates by Krishnaraj et al. [97], roundness error increased with increasing spindle speed and decreased with increasing feed. Similar trends are shown for the first holes of the bare CFRP experiments.

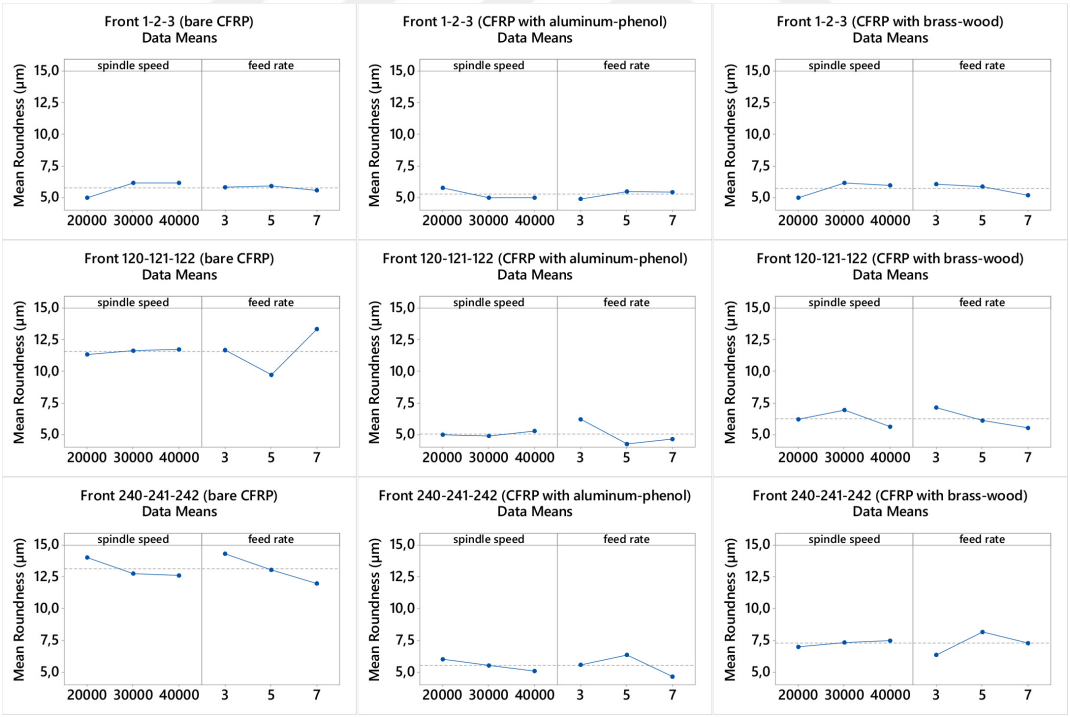

Figure 3.29. Main effects plots for the front side roundness error.

In Figure 3.30, main effects plots for the rear side roundness error are shown. It is clearly seen that the rear side roundness error is more severe than the front side roundness error. For the unsupported case, spindle speed does not affect the mean roundness error.

However, mean roundness error decreases as feed increases to an intermediate value then increases with further increasing the feed for the first and the middle three holes and vice versa for the last three holes. For the phenolic backing board, mean roundness error decreases as spindle speed increases and feed increases for the last holes. Feed does not affect the mean roundness error significantly for the middle holes. Mean roundness error increases first and then decreases with increasing feed for the first holes. Feed effect is similar for the wood backing board. For the wood backing board, mean roundness error decreases as spindle speed increases for the first and the last holes, and vice versa for the middle holes. The case of bare CFRP is the most desirable condition to decrease the rear side roundness error due to the fact that it provides less roundness error values as compared to the other cases, and it is free from the spindle speed effect. It can be concluded that backing boards deteriorate the roundness. Possible reason may be explained as follows. Rear side of the CFRP laminate which corresponds to the drill exit surface contains resin-rich regions due to the production method of resin infusion and also contains the cavities which were formed by flow medium. By inspecting the rear side hole pictures which are shown in Figure 3.31, it is seen that resin burrs which cannot be separated from the CFRP laminate as chips due to their ductile structure cover the hole edge due to the blocking effect of the backing boards. Thus, roundness error increases because of non-uniformed coverage of the burrs. As compared to the phenolic backing board, wood backing board provides less roundness error values. It may be attributed to the filling capability of the wood backing board to the cavities of the CFRP laminate. Thus, it prevents the coverage of the burrs. Same mechanism cannot be considered for the phenolic backing board due to its harder surface. Spindle speed and feed can be thought as the governing parameters which affect the magnitude of the coverage of the resin burrs. It must be also noted that the tool wear increases the mean roundness error value similar to the front side.

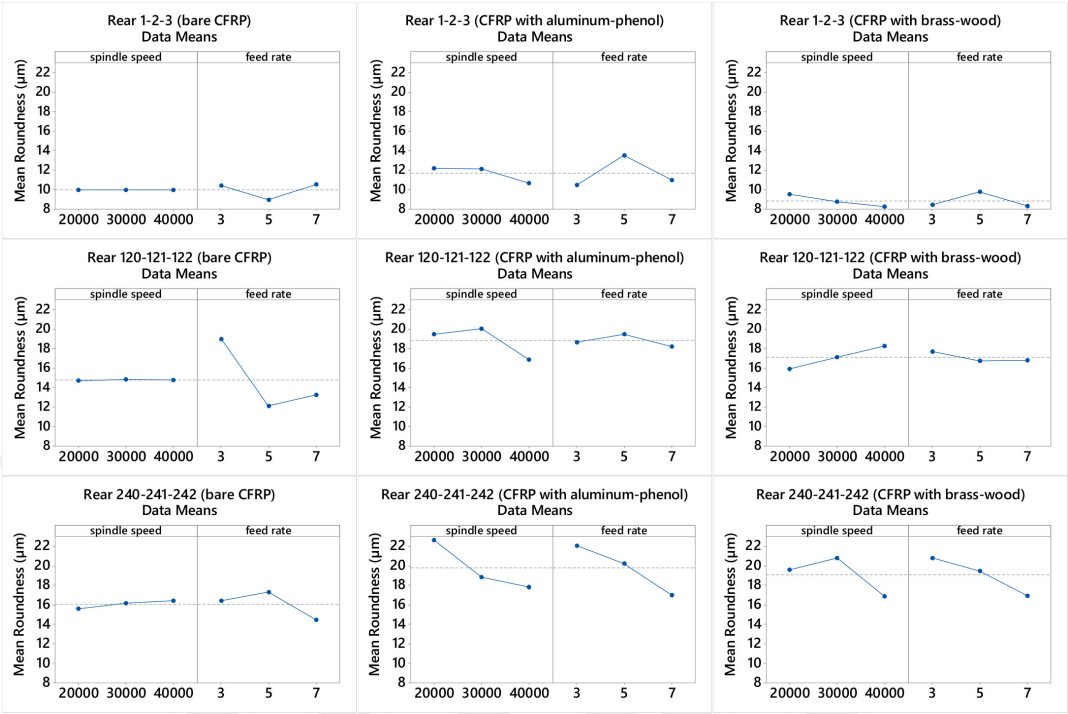

Figure 3.30. Main effects plots for the rear side roundness error.

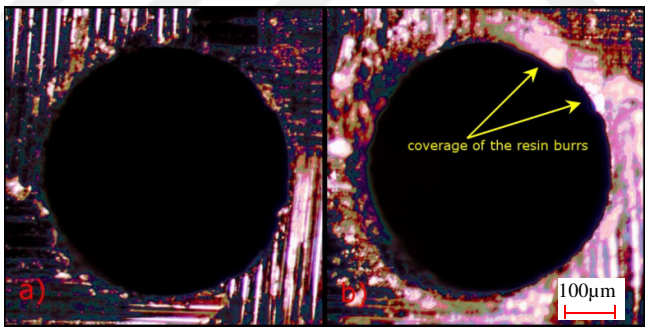

Figure 3.31. Typical rear side first hole pictures: a) bare CFRP experiment, b) aluminum-phenol support plates experiment. (S20000 rpm, f7 µm/rev)

In Table 3.21, percentage variations of front side roundness errors of supported CFRP laminate experiments as compared to those of bare CFRP laminate experiments are shown. Each value is the cells corresponds to the percentage variation and calculated as the ratio of the difference between the roundness error of supported case and roundness error of unsupported case to the roundness error of unsupported case. According to the results, the effect of aluminum entry board on the roundness error is between the -26% and 46% for the first holes, -67% and -35% for the middle holes, and -67% and -38% for the last holes, and effect of brass entry board on the roundness error is between the -

22% and 15% for the first holes, -65% and -22% for the middle holes, and -60% and -18% for the last holes with respect to the bare CFRP experiments. Due to the fact that different cutting conditions cannot be selected for the first, the middle and the last holes, arithmetic mean of the percentage variations of roundness errors were used to make a comparison. According to the arithmetic means, aluminum entry board can decrease the front side mean roundness error up to 50%, and brass entry board can decrease the front side mean roundness error up to 42% with respect to the bare CFRP experiments depending on the cutting conditions.

Table 3.21. Percentage variations of front side roundness errors of supported CFRP laminate experiments as compared to those of bare CFRP laminate experiments.

			Aluminum entry board				Brass entry board			
Spindle Speed (rpm)	Feed (µm/rev)	Feed Rate (mm/min)	The first three holes (%)	The middle three holes (%)	The last three holes (%)	Arithmetic mean (%)	The first three holes (%)	The middle three holes (%)	The last three holes (%)	Arithmetic mean (%)
20000	3	60	9	-35	-67	-31	15	-31	-60	-25
20000	5	100	-3	-66	-38	-36	-13	-33	-51	-32
20000	7	140	46	-65	-61	-27	3	-65	-38	-33
30000	3	90	-23	-54	-58	-45	-2	-42	-53	-32
30000	5	150	-16	-52	-54	-41	1	-22	-43	-21
30000	7	210	-19	-67	-60	-49	0	-54	-28	-28
40000	3	120	-26	-49	-57	-44	3	-43	-54	-31
40000	5	200	-4	-49	-60	-38	12	-60	-18	-22
40000	7	280	-22	-64	-62	-50	-22	-56	-49	-42
The best			-26	-67	-67	-50	-22	-65	-60	-42
The worst			46	-35	-38	-27	15	-22	-18	-21

In Table 3.22, percentage variations of rear side roundness errors of supported CFRP laminate experiments as compared to those of bare CFRP laminate experiments are shown. According to the results, the effect of phenolic backing board on the roundness error is between the -20% and 80% for the first holes, -20% and 114% for the middle holes, and -7% and 113% for the last holes, and effect of wood backing board on the roundness error is between the -44% and 17% for the first holes, -23% and 112% for the

middle holes, and -5% and 69% for the last holes with respect to the bare CFRP experiments. Due to the fact that different cutting conditions cannot be selected for the first, the middle and the last holes, arithmetic mean of the percentage variations of roundness errors were used to make a comparison. According to the arithmetic means, phenolic backing board can decrease the rear side mean roundness error as 4% and can increase the rear side mean roundness error as 62%, and wood backing board can decrease the rear side mean roundness error as 11% and can increase the rear side mean roundness error as 45% with respect to the bare CFRP experiments depending on the cutting conditions.

Table 3.22. Percentage variations of rear side roundness errors of supported CFRP laminate experiments as compared to those of bare CFRP laminate experiments.

			Aluminum entry board				Brass entry board			
Spindle Speed (rpm)	Feed (µm/rev)	Feed Rate (mm/min)	The first three holes (%)	The middle three holes (%)	The last three holes (%)	Arithmetic mean (%)	The first three holes (%)	The middle three holes (%)	The last three holes (%)	Arithmetic mean (%)
20000	3	60	9	30	113	51	-17	15	63	20
20000	5	100	25	10	38	24	16	-8	28	12
20000	7	140	34	59	1	31	-10	16	-5	1
30000	3	90	-9	-20	17	-4	-25	-23	27	-7
30000	5	150	80	114	-7	62	-5	34	6	12
30000	7	210	2	49	55	35	-5	63	69	42
40000	3	120	3	-9	-6	-4	-14	-8	1	-7
40000	5	200	51	72	25	49	17	112	5	45
40000	7	280	-20	9	9	-1	-44	8	2	-11
The best			-20	-20	-7	-4	-44	-23	-5	-11
The worst			80	114	113	62	17	112	69	45

3.2.3. Fiber overlap

In Table 3.23, mean values of the percentage fiber overlap are seen. Each value in the cells corresponds to the mean of nine values with three trials and consecutive three holes for the first and the second setups. It corresponds to the mean of six values with two

trials and consecutive three holes for the third setup. Fiber overlap areas were also given in Appendix 4.

Table 3.23. Mean values of the percentage fiber overlap.

			Front Side Percentage Fiber Overlap (%)			Rear Side Percentage Fiber Overlap (%)		
	Spindle Speed (rpm)	Feed (µm/rev)	Mean of 1-2-3	Mean of 120-121-122	Mean of 240-241-242	Mean of 1-2-3	Mean of 120-121-122	Mean of 240-241-242
1. setup Bare CFRP	20000	3	2,8	3,5	5,5	10,8	25,7	26,6
	20000	5	3,1	5,4	5,5	6,6	12,7	29,7
	20000	7	3,2	5,6	8,7	9,7	14,6	35,5
	30000	3	3,2	3,7	5,6	4,6	24,7	31,9
	30000	5	1,9	3,8	5,6	18,8	27,6	15,8
	30000	7	2,6	4,2	4,3	4,7	17,5	21,2
	40000	3	2,2	2,5	2,5	4,3	25,5	37,9
	40000	5	2,6	3,6	5,8	15,4	21,3	28,6
	40000	7	2,1	4,6	5,7	3,7	18,5	29,7
2. setup Aluminum-CFRP-Phenolic	20000	3	3,2	4,5	4,5	8,8	10,3	20,4
	20000	5	3,5	4,3	4,4	6,0	17,4	12,1
	20000	7	4,3	4,1	3,7	6,0	12,3	8,4
	30000	3	2,9	4,1	4,2	6,7	11,0	19,5
	30000	5	4,2	3,4	3,8	7,3	15,6	12,5
	30000	7	3,0	3,6	4,1	5,9	11,6	8,6
	40000	3	4,0	4,1	4,3	5,9	22,7	14,3
	40000	5	2,8	4,1	3,6	6,4	13,8	15,7
	40000	7	4,8	3,2	5,1	5,6	12,0	14,6
3. setup Brass-CFRP-Fir wood	20000	3	3,1	3,7	4,1	6,4	16,0	25,6
	20000	5	4,3	4,0	4,2	10,8	9,7	14,9
	20000	7	3,9	2,5	4,5	5,4	10,9	10,8
	30000	3	1,5	3,4	3,8	4,4	15,6	22,8
	30000	5	3,4	3,3	4,4	7,4	11,6	22,2
	30000	7	2,5	3,4	3,3	5,4	16,2	14,7
	40000	3	5,0	3,5	5,1	6,3	13,7	17,0
	40000	5	4,4	3,1	2,7	5,7	13,7	14,4
	40000	7	3,3	3,0	3,4	7,0	17,8	19,5

Graphical representations of variations of percentage fiber overlaps are shown in Figure 3.32 for front side the first holes, in Figure 3.33 for front side the middle holes, in Figure

3.34 for front side the last holes, in Figure 3.35 for rear side the first holes, in Figure 3.36 for rear side the middle holes, and in Figure 3.37 for rear side the last holes (Bare CFRP in blue, Aluminum-CFRP-Phenolic in red, and Brass-CFRP-Fir wood in yellow). In the plots, horizontal lines indicate the median values, plus signs indicate the mean values, multiplication signs indicate the outliers, and boxes indicate the interquartile ranges. Whiskers extend to the highest and lowest values within the limits. Upper limit equals to Q_3+1,5(Q_3-Q_1) and lower limit equals to Q_1-1.5 (Q_3 - Q_1).

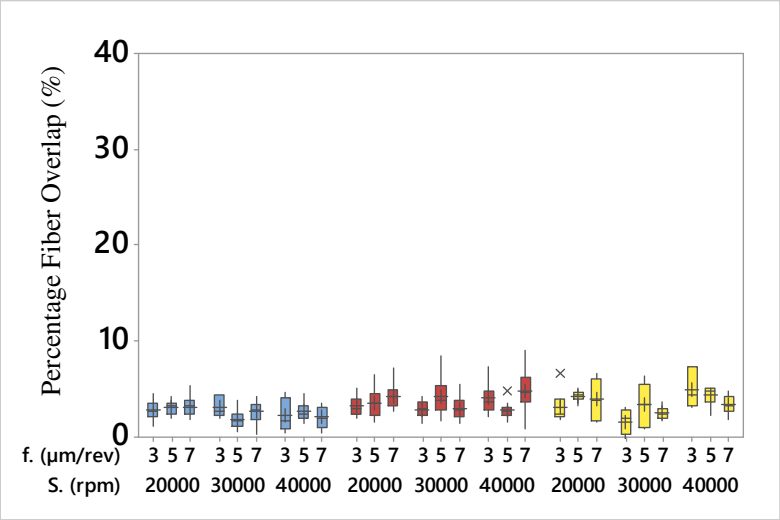

Figure 3.32. Front side the first holes percentage fiber overlaps.

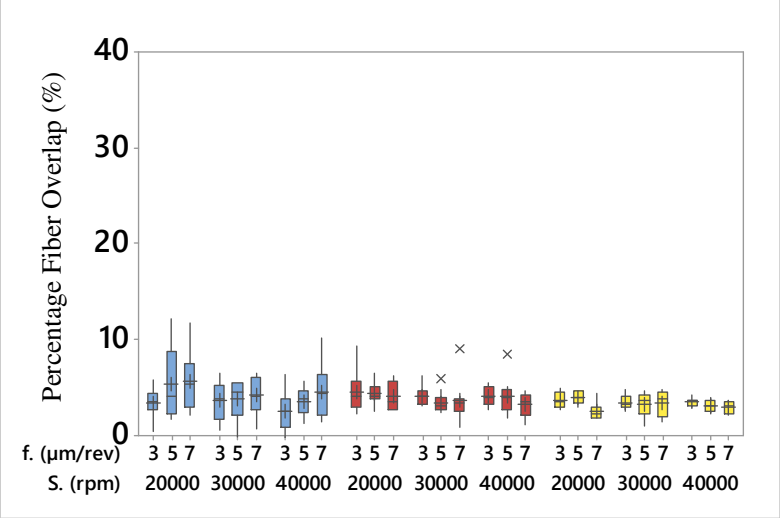

Figure 3.33. Front side the middle holes percentage fiber overlaps.

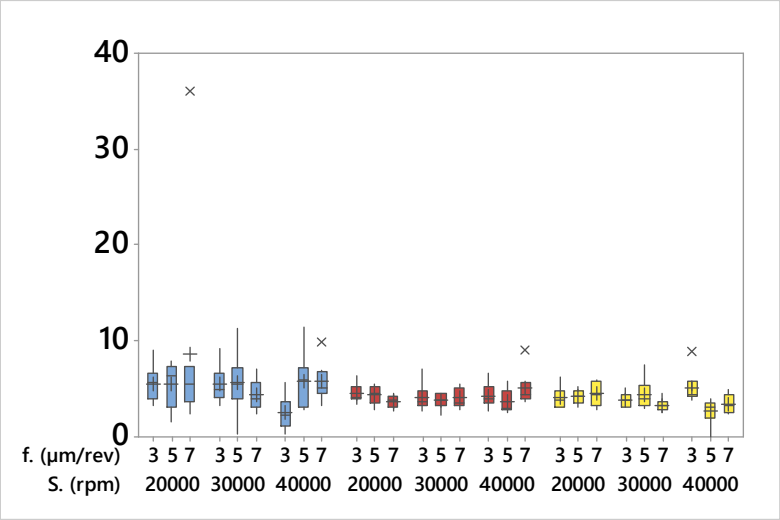

Figure 3.34. Front side the last holes percentage fiber overlaps.

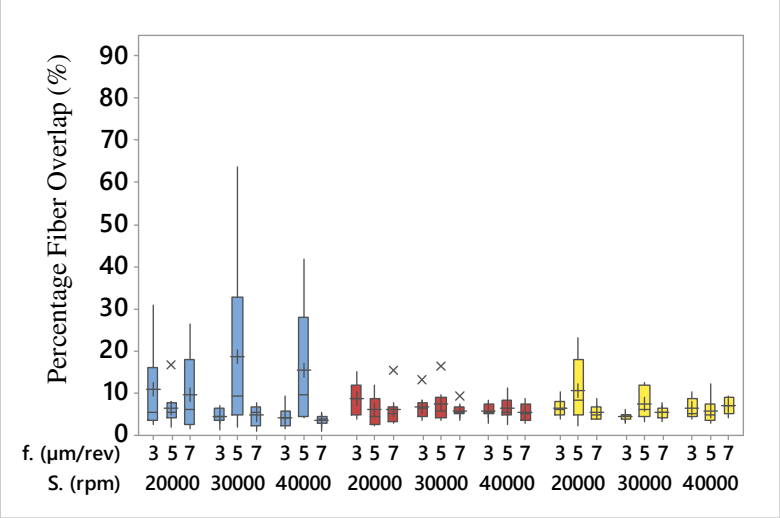

Figure 3.35. Rear side the first holes percentage fiber overlaps.

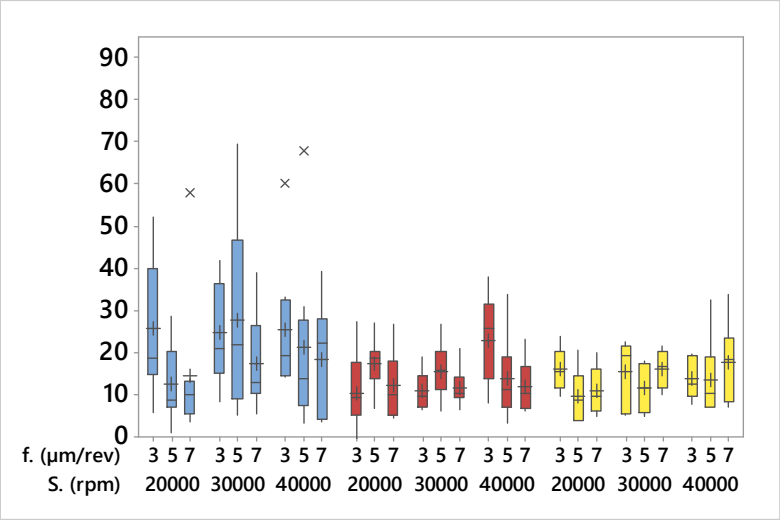

Figure 3.36. Rear side the middle holes percentage fiber overlaps.

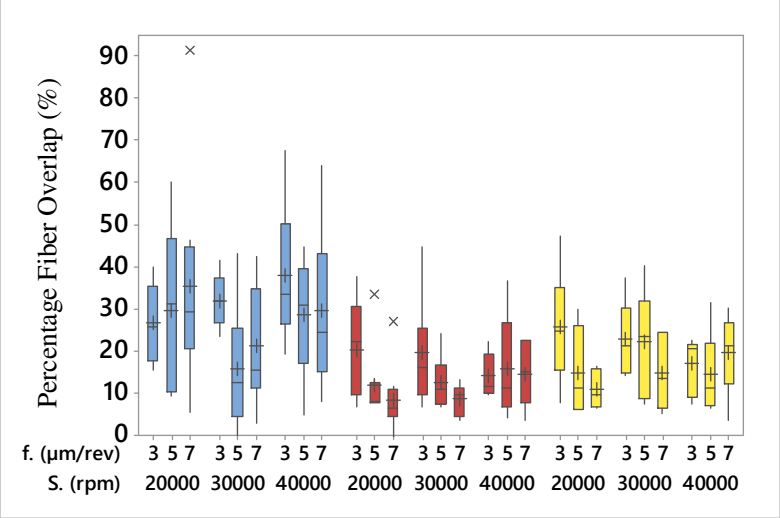

Figure 3.37. Rear side the last holes percentage fiber overlaps.

Main effects plots of the front side fiber overlap are shown in Figure 3.38. As seen from the plots, mean percentage fiber overlap increases slightly from the first to the last hole due to the tool wear. In cases of support plates, spindle speed and feed do not affect the mean percentage fiber overlap significantly for the middle and last holes. Intermediate value of the spindle speed decreases the mean percentage fiber overlap significantly for the first holes in case of brass entry board. Mean percentage fiber overlap decreases as spindle speed increases and feed decreases in case of bare CFRP laminate experiments except that feed does not affect the mean percentage fiber overlap for the first holes. Although cutting conditions have effects on the fiber overlap, their effects are limited to

about 6 percent for the worst case. Effects of the cutting conditions on the fiber overlap can be explained as follows. It is going to be validated in Chapter 3.5 that cutting temperature increases as spindle speed increases and feed decreases. Elevated temperature causes the matrix softening. Rubio et al. [77] stated that probable reason of less delamination damage at high speed was the matrix softening. It is also going to be validated in Chapter 3.6 that the highest torque and thrust force values occur for low spindle speed and high feed. Therefore, both low temperature and high cutting forces cause higher deformation to the epoxy boundary of the hole entry, and percentage fiber overlap increases. For the first holes, mean percentage fiber overlap in case of bare CFRP laminate is the least. For the middle and the last holes, brass entry board provides the least mean percentage fiber overlap. It is seen from the results that support plates tend to keep the front side fiber overlap close to a constant value regardless of the spindle speed, feed, and tool wear which are more effective for the unsupported case.

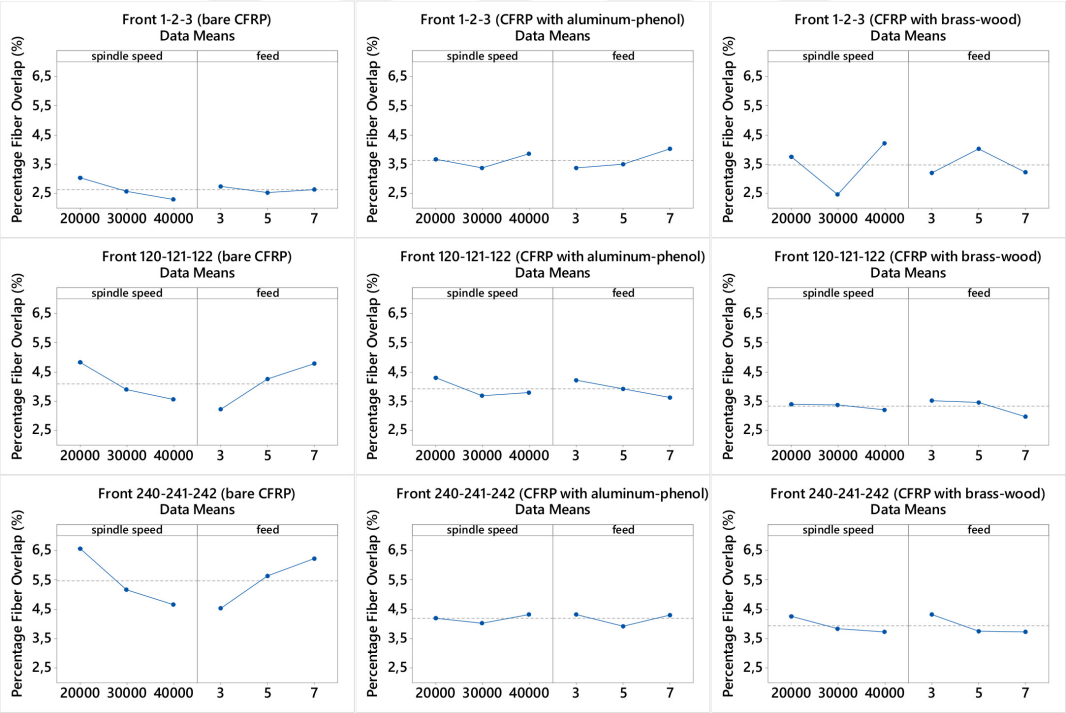

Figure 3.38. Main effects plots for the front side fiber overlap.

In Figure 3.39, main effects plots are shown for the rear side fiber overlap. If the plots are inspected, it is seen that the support plates decrease the mean percentage fiber overlap distinctively from the first to the last hole. Mean percentage fiber overlaps are

close to the each other for the first and the middle holes for the supported cases. However, phenolic backing board provides less mean percentage fiber overlap area for the last holes as compared to the wood backing board. High feed and intermediate spindle speed are the best choice for the phenolic backing board to decrease the rear side fiber overlap. For each setup, it is clearly seen that fiber overlap increases from the first to the last hole. A general tendency is not seen for the changes of the spindle speed and feed as tool wears in any setup, but variation of the mean percentage fiber overlap is less in the cases of support plates. The fibers on the hole which remain after the drilling operation may be attributed to two probable mechanisms. One of them is that the fibers may be the extensions of the delaminated fibers. As fibers delaminate, they resist to be cut due to the bending of them. Bonnet et al. [98] have pointed out that fiber orientation has a significant effect on the rear side delamination damage, and they have described the delamination zones with respect to the fiber orientation. Similar to their study, it can be concluded that fiber orientation also affects the formation of the occupational fibers which are the extensions of the delaminated fibers. In Figure 3.40a, occupational fibers which have formed in accordance to the fiber orientation are seen. Another mechanism (Figure 3.40b) is that even though the fibers are cut, they may not separate as the corner of the micro drill exits the laminate due to the resin-rich rear side of the CFRP laminate. As tool wears, corner radius of the micro-drill also increases, and in this case, this mechanism works more efficiently which increases the fiber overlap.

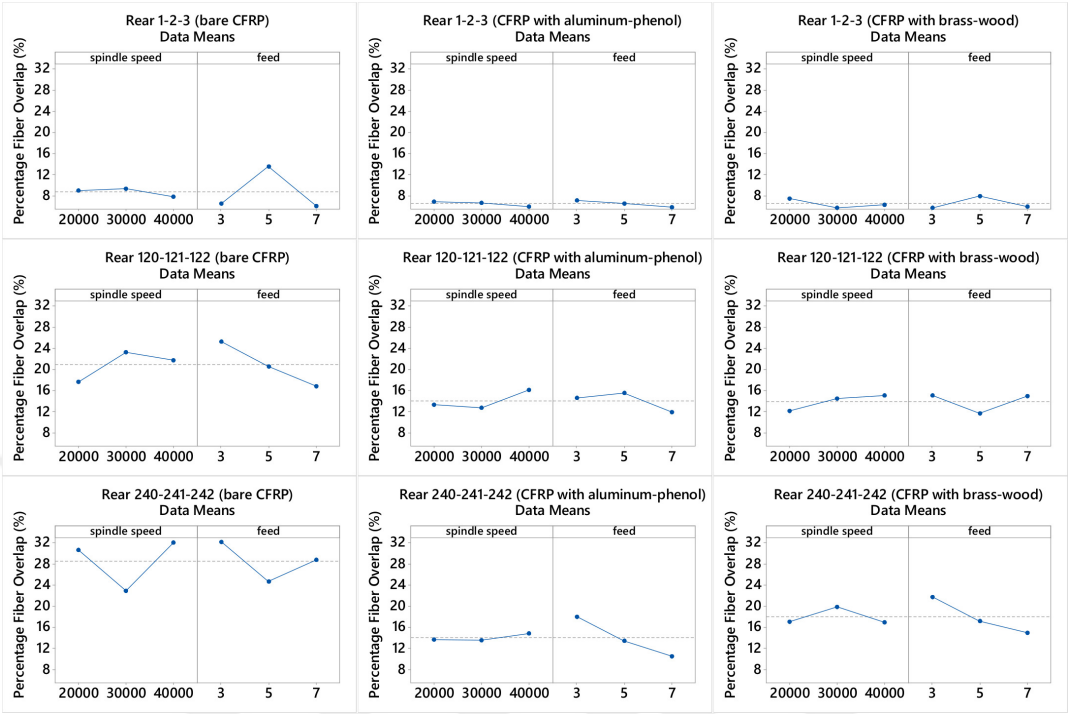

Figure 3.39. Main effects plots for the rear side fiber overlap.

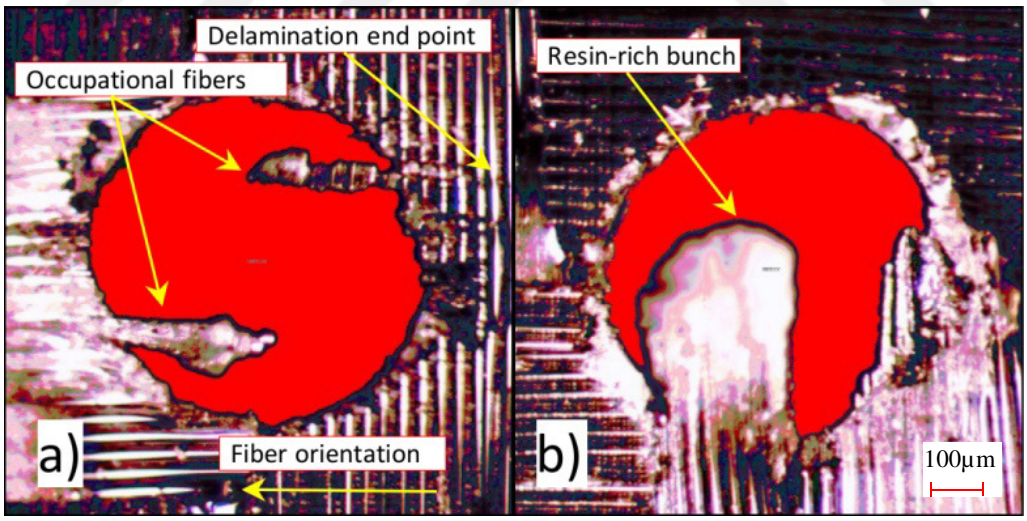

Figure 3.40. Mechanisms of the fiber overlap: a) extension of the delamination, b) resin-rich bunch.

In Table 3.24, percentage variations of front side fiber overlaps of supported CFRP laminate experiments as compared to those of bare CFRP laminate experiments are shown. Each value is the cells corresponds to the percentage variation and calculated as the ratio of the difference between the percentage fiber overlap of supported case and

percentage fiber overlap of unsupported case to the percentage fiber overlap of unsupported case. According to the results, the effect of aluminum entry board on the fiber overlap is between the -9% and 131% for the first holes, -29% and 63% for the middle holes, and -58% and 73% for the last holes, and effect of brass entry board on the fiber overlap is between the -51% and 122% for the first holes, -55% and 37% for the middle holes, and -54% and 106% for the last holes with respect to the bare CFRP experiments. Due to the fact that different cutting conditions cannot be selected for the first, the middle and the last holes, arithmetic mean of the percentage variations of fiber overlaps were used to make a comparison. According to the arithmetic means, aluminum entry board can decrease the front side mean fiber overlap as 17% and can increase the front side mean fiber overlap as 72%, and brass entry board can decrease the front side mean fiber overlap as 30% and can increase the front side mean fiber overlap as 88% with respect to the bare CFRP experiments depending on the cutting conditions.

Table 3.24. Percentage variations of front side fiber overlaps of supported CFRP laminate experiments as compared to those of bare CFRP laminate experiments.

			Aluminum entry board				Brass entry board			
Spindle Speed (rpm)	Feed (µm/rev)	Feed Rate (mm/min)	The first three holes (%)	The middle three holes (%)	The last three holes (%)	Arithmetic mean (%)	The first three holes (%)	The middle three holes (%)	The last three holes (%)	Arithmetic mean (%)
20000	3	60	15	31	-17	10	10	6	-26	-3
20000	5	100	14	-19	-20	-9	37	-26	-23	-4
20000	7	140	35	-27	-58	-17	24	-55	-48	-27
30000	3	90	-9	12	-25	-7	-51	-6	-31	-30
30000	5	150	125	-9	-33	28	78	-13	-21	15
30000	7	210	16	-14	-6	-2	-4	-18	-24	-15
40000	3	120	80	63	73	72	122	37	106	88
40000	5	200	6	15	-38	-6	67	-12	-54	0
40000	7	280	131	-29	-12	30	59	-34	-40	-5
The best			-9	-29	-58	-17	-51	-55	-54	-30
The worst			131	63	73	72	122	37	106	88

In Table 3.25, percentage variations of rear side fiber overlaps of supported CFRP laminate experiments as compared to those of bare CFRP laminate experiments are shown. According to the results, the effect of phenolic backing board on the fiber overlap is between the -61% and 52% for the first holes, -60% and 38% for the middle holes, and -76% and -21%, and effect of wood backing board on the fiber overlap is between the -63% and 89% for the first holes, -58% and -4% for the middle holes, and -70% and 40% with respect to the bare CFRP experiments. Due to the fact that different cutting conditions cannot be selected for the first, the middle and the last holes, arithmetic mean of the percentage variations of fiber overlaps were used to make a comparison. According to the arithmetic means, phenolic backing board can decrease the rear side mean fiber overlap up to 46%, and wood backing board can decrease the rear side mean fiber overlap as 50% and can increase the rear side mean fiber overlap as 17% with respect to the bare CFRP experiments depending on the cutting conditions.

Table 3.25. Percentage variation of rear side fiber overlap of supported CFRP laminate experiments as compared to those of bare CFRP laminate experiments.

			Phenolic backing board				Wood backing board			
Spindle Speed (rpm)	Feed (µm/rev)	Feed Rate (mm/min)	The first three holes (%)	The middle three holes (%)	The last three holes (%)	Arithmetic mean (%)	The first three holes (%)	The middle three holes (%)	The last three holes (%)	Arithmetic mean (%)
20000	3	60	-18	-60	-23	-34	-40	-38	-4	-27
20000	5	100	-9	38	-59	-10	63	-24	-50	-3
20000	7	140	-38	-16	-76	-43	-44	-26	-70	-47
30000	3	90	44	-55	-39	-17	-5	-37	-28	-23
30000	5	150	-61	-44	-21	-42	-61	-58	40	-26
30000	7	210	27	-34	-60	-22	15	-7	-31	-8
40000	3	120	36	-11	-62	-13	45	-46	-55	-19
40000	5	200	-58	-35	-45	-46	-63	-36	-50	-50
40000	7	280	52	-35	-51	-11	89	-4	-34	17
The best			-61	-60	-76	-46	-63	-58	-70	-50
The worst			52	38	-21	-10	89	-4	40	17

3.3. Tool Wear

Through all experiments, flank wear was found as the severest wear mode. The amount of wear increases from the drill point to the drill corner as seen in the Figure 3.41. Drill corner radius also increases as the tool wears. Chisel edge wear is smaller than the main cutting edge wear. It may be attributed to the negative rake angle of the chisel edge and low cutting speed due to the radial closeness to the drill center. In Table 3.26, remaining flank face area and corresponding percentage flank wear values are shown. Percentage flank wear was calculated as the ratio of the flank wear area to the entire flank area. According to the raw data, percentage flank wear varies between 36.2% and 49.4% for the bare CFRP laminate experiments (1st setup), 33.2% and 53.1% for the experiments of the CFRP laminate with aluminum-phenolic support plates (2nd setup), and 34.3% and 61.0% for the experiments of the CFRP laminate with brass-wood support plates (3rd setup). The interval of the percentage flank wear is the least for the 1st setup with the value of 13.2% and followed by 2nd setup with the value of 19.9% and 3rd setup with the value of 26.7%. Therefore, it reveals that the cutting parameters are more effective on tool wear when the support plates are used. Support plates decreased the flank wear as compared to the unsupported case for some cutting conditions and raised the flank wear drastically under some cutting conditions especially for low feeds.

Table 3.26. Remaining flank face area and corresponding percentage flank wear.

		Remaining Flank Face Area (μm²) and Percentage Flank Wear				
Spindle Speed (rpm)	**Feed (μm/rev)**	**1. setup Bare CFRP**				
		1.trial	**2.trial**	**3.trial**	**mean**	**%**
20000	3	8064	9219	9829	9037	47.1
20000	5	7017	9535	9387	8646	49.4
20000	7	11047	9812	10311	10390	39.2
30000	3	8303	10481	10060	9615	43.7
30000	5	11407	10460	10836	10901	36.2
30000	7	9410	10344	9983	9912	41.9
40000	3	8520	9128	9933	9194	46.2
40000	5	10695	11351	9230	10425	38.9
40000	7	8623	12186	10544	10451	38.8
Spindle Speed (rpm)	**Feed (μm/rev)**	**2. setup Aluminum-CFRP-Phenolic**				
		1.trial	**2.trial**	**3.trial**	**mean**	**%**
20000	3	6726	7809	9488	8008	53.1
20000	5	10559	10488	6946	9331	45.4
20000	7	10375	10840	11439	10885	36.3
30000	3	7843	8063	8635	8180	52.1
30000	5	9205	9921	10195	9774	42.8
30000	7	10302	9663	10297	10087	40.9
40000	3	9019	8017	10602	9213	46.0
40000	5	11145	9786	10185	10372	39.3
40000	7	11696	12171	10341	11403	33.2
Spindle Speed (rpm)	**Feed (μm/rev)**	**3. setup Brass-CFRP-Wood**				
		1.trial	**2.trial**	**mean**	**%**	
20000	3	8219	6947	7583	55.6	
20000	5	8592	7783	8188	52.0	
20000	7	11396	10470	10933	36.0	
30000	3	10566	9374	9970	41.6	
30000	5	10748	8247	9498	44.4	
30000	7	9227	9573	9400	44.9	
40000	3	7896	5438	6667	61.0	
40000	5	8771	7825	8298	51.4	
40000	7	11645	10807	11226	34.3	
Unused tool						17075

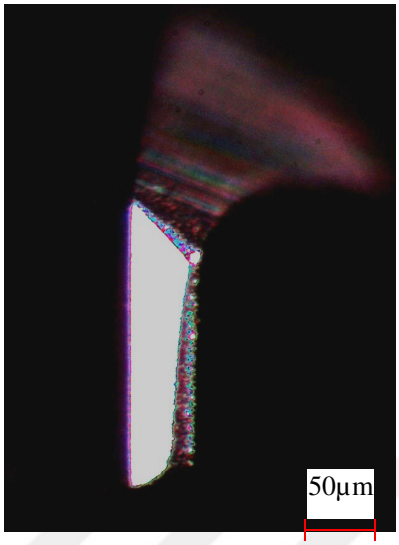

Figure 3.41. Flank face of worn micro drill.

Surface plots (Figure 3.42) and main effects plots (Figure 3.43) were constructed to comprehend the general trends easily. As seen in main effects plots, the flank wear decreases as feed increases in all setups. Shyha et al. [23] stated that higher feeds lower the contact time between the cutting tool and workpiece, and thus, tool wear and cutting temperature decrease. However, although higher spindle speeds can also decrease the contact time between the cutting tool and workpiece, similar effect of the spindle speed on decreasing the tool wear is not observed. Therefore, the real factor which decreases the tool wear as feed increases must be defined as the required number of turns of the micro drill to cut the material which has a specific thickness. Because, contact time is a dependent factor which is determined by the both spindle speed and feed. Increasing the feed decreases the required number of turns of the micro drill, thus micro drill travels less distance on the workpiece. When the workpiece is highly abrasive, higher feeds can reduce the tool wear by means of the explained manner. However, this mechanism is limited due to the fact that further increasing the feed eventually causes the sudden breakage of the micro drill because of the generated stress state. Although a general trend is not seen for the first setup, minimum flank wear occurs for 30000 rpm and 5 µm/rev, and higher feeds and spindle speeds can be count in the same level. For the second setup, flank wear decreases as feed and spindle speed increase. For the third setup, flank wear does not change significantly in any feed for 30000 rpm and decreases as feed increases for 20000 rpm and 40000 rpm. Minimum flank wear is derived with 40000 rpm and 7

µm/rev for the second and third setups. Contrary to the obtained results, it has been reported for the conventional drilling of graphite/bismaleimide and titanium stacks that increasing feed rate increased the tool wear [99,100].

For the conventional drilling of CFRP laminates, it has been reported that increasing spindle speed increases the tool wear according to the experimental studies [58, 61], and it is also valid for graphite/bismaleimide and titanium stacks [99,100]. However, derived experimental results have shown that a general wear trend does not occur as spindle speed changes. Similar effect of the spindle speed on flank wear was just observed for the feed of 7 µm/rev in all setups. For this level of feed, flank wear increases as spindle speed increases to the intermediate value, then decreases with further increase in the spindle speed. At low feed values, obviously wear mechanism is more complex due to the ploughing. When the depth of cut is comparable to the cutting edge radius, cutting mechanism changes to ploughing and efficient shearing cannot take place [101]. Ploughing causes higher flank wear [68]. Therefore excessive flank wear in the cases of support plates can be attributed to the ploughing at low feeds.

Material effect of the support plates on tool wear can also be detected. Backing boards are not assumed to contribute to the tool wear due to their limited drilling depth and non-abrasive structures. Variation of the flank wear can be attributed to the material effect of the entry boards. Brass entry board caused higher flank wear as compared to the aluminum entry board under any cutting parameters. The reason may be explained that micro drill cuts the entry board first, and drilling the aluminum at low cutting speeds causes the built-up edges which are formed on the rake face of the cutting tool and act such as cutting edge [73]. Then, micro drill exits the entry board and enters the CFRP laminate. During the initial stage of drilling CFRP laminate, abrasive carbon fibers brush the built-up edges [60]. Thus, cutting edges of the micro drill are exposed to less abrasive wear. Addition of 3% lead which is a toxic material increases the machinability of the brass [102]. However, lead free brass was used in the experiments. Therefore, occurrence of higher flank wear for the case of brass entry board as compared to the case of aluminum entry board is predictable.

Using wear map provides the eligible cutting parameters for the drilling process when a general trend does not occur for the tool wear. This kind of map is obviously limited to

the boundaries of the experiments. Regression curves may be used to estimate the tool wear when the selected cutting parameters exceed the boundaries of the experiments, but the precision is not reliable due to the lack of tendency. In Figure 3.42, contour plots which correspond to the wear maps for each setup are shown.

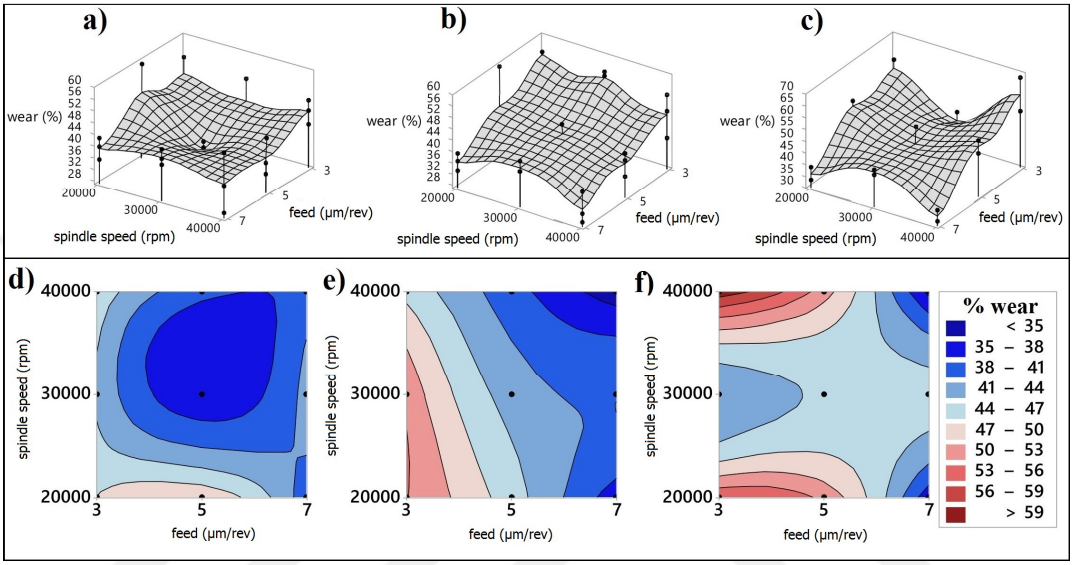

Figure 3.42. Surface plots: (a) bare CFRP, (b) CFRP with aluminum-phenolic, (c) CFRP with brass-wood, and Contour plots: (d) bare CFRP, (e) CFRP with aluminum-phenolic, (f) CFRP with brass-wood.

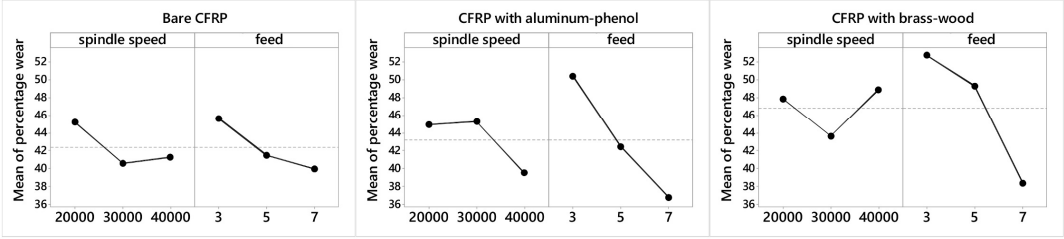

Figure 3.43. Main effects plots.

Minitab 17 was used to evaluate the experimental results statistically. Three terms which are spindle speed, feed, and product of spindle speed and feed were used to model the flank wear behavior. In Table 3.27, percentage contributions of the variables and p-values are shown. P-value which is less than 0.05 points out statistically significant variable. According to the p-values of each setup, feed is statistically significant variable for the supported cases, and product of the spindle speed and feed is statistically significant for the case of CFRP laminate with brass-wood support plates. For the case of

bare CFRP laminate, a statistically significant variable was not observed.

Table 3.27. Percentage contribution of spindle speed and feed on the flank wear.

Terms	1. setup (Bare CFRP)		
	Degree of freedom	Percentage contribution	P-value
Spindle Speed	2	9.5	0.256
Feed	2	13.4	0.155
Spindle Speed * Feed	4	18.7	0.260
Error	18	58.3	
Terms	2. setup (Aluminum-CFRP-Phenolic)		
	Degree of freedom	Percentage contribution	P-value
Spindle Speed	2	10.5	0.118
Feed	2	47.5	0.001
Spindle Speed * Feed	4	2.6	0.872
Error	18	39.3	
Terms	3. setup (Brass-CFRP-Wood)		
	Degree of freedom	Percentage contribution	P-value
Spindle Speed	2	5.8	0.318
Feed	2	42.1	0.006
Spindle Speed * Feed	4	32.1	0.051
Error	9	20.0	

3.4. Chip Morphology

In this section, it is aimed to present the types of the chips which have been formed during drilling the CFRP laminates under variable drilling conditions for each setup. Chips of the CFRP laminate (Figure 3.44a) came up with powders of brittle fractured fibers and tangled epoxy. Generally, it was observed that the support type was the most influencing parameter on the chip morphology. Spindle speed and feed rate did not affect the chip types of the CFRP laminate significantly. Conglomerated chips of the CFRP laminate usually occurred in the setups of support plates. This indicates the poor chip evacuation in these cases. If the efficient evacuation is not performed, several detrimental effects occur such as poor surface roughness of the hole wall [73] and sudden breakage of the drill [103]. Chips of the aluminum entry board (Figure 3.44c) were formed as long ribbon shape. The maximum observed length of the aluminum chips was around 8 mm.

For the brass entry board, the chips (Figure 3.44d) were usually created as long conical helical shape. The maximum observed length of the brass chips was around 6 mm. Combined long ribbon shape and long conical helical chips were also rarely observed with the cutting conditions of 30000 rpm - 5 µm/rev, 20000 rpm - 5 µm/rev and 20000 rpm - 7 µm/rev. It is considered that the short conical helical shape is the most suitable case for drilling operations [104]. But, chips of the support plates were not observed as short conical helical shape for any condition.

Helical shape of the conglomerated chips (Figure 3.44b) which have occurred for the supported cases gives some information about their formation. It is understood that chips of the CFRP laminate get stuck in the flute of the micro drill and formed conglomerated chips because of the entry board which causes poor chip evacuation.

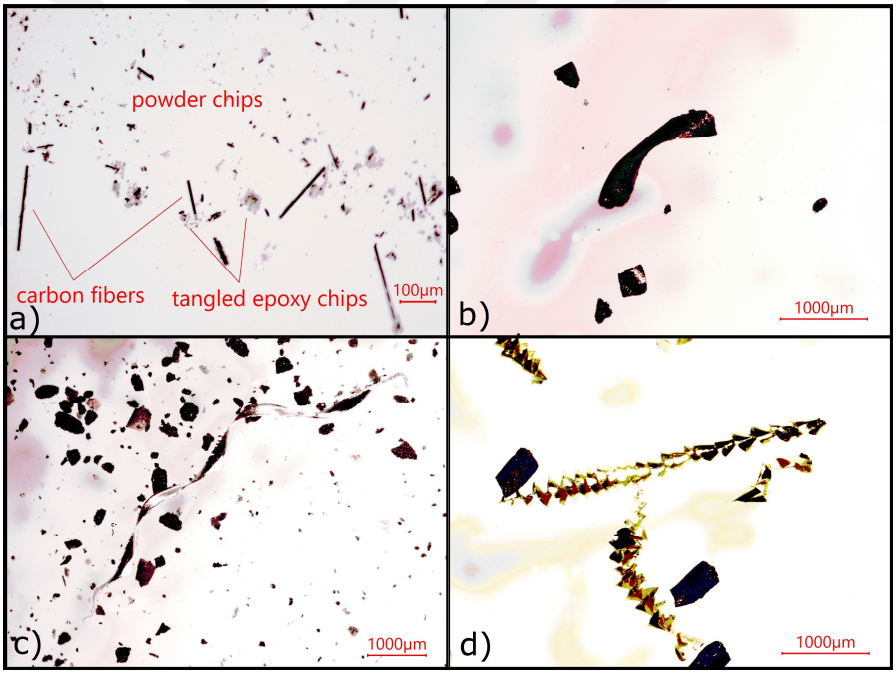

Figure 3.44. Typical chip morphologies: (a) CFRP chips in unsupported case; (b) conglomerated chip; (c) aluminum entry board chip; (d) brass entry board chip.

3.5. Cutting Temperature

Measured highest temperatures with the thermocouple in Figure 3.45 and infrared thermography in Figure 3.46 are shown. Each bar corresponds to mean of 4 repeats.

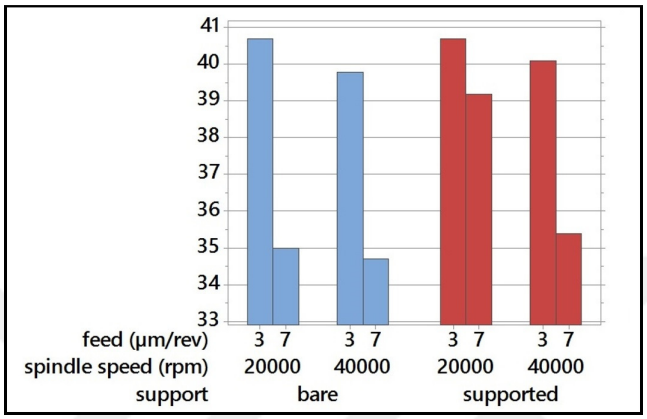

Figure 3.45. Graphical representation of thermocouple measurements.

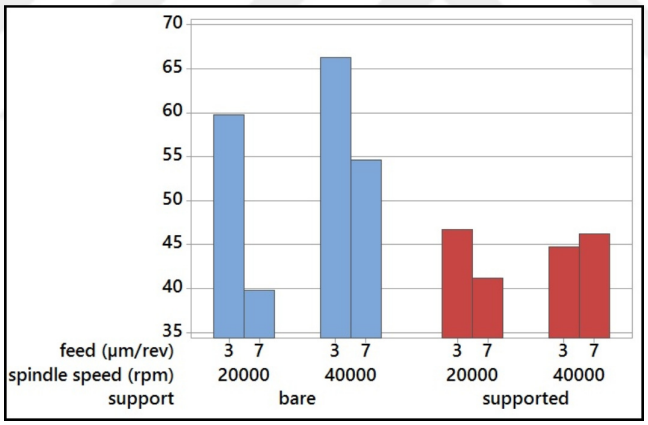

Figure 3.46. Graphical representation of infrared thermography measurements.

Primary results have shown that generated maximum temperatures in micro-drilling of CFRP laminates are well below the glass transition temperature under the selected ranges of cutting conditions. Although this result cannot be drawn by considering the thermocouple measurements due to the fact that the highest temperature occurs on the tool tip which is far from measurement point, infrared thermography measurements which detect the highest temperature around the cutting zone are below the glass transition temperature too.

3.5.1. Effects of support plates, spindle speed, and feed

3.5.1.1. Bare CFRP laminate experiments

For the bare CFRP laminate experiments, it is seen that generated maximum temperature decreases as feed increases. This result can be validated by both thermocouple and infrared thermography measurements. Similar results in conventional drilling of CFRP laminates have been already stated in several experimental studies. Chen [62] and Sorrentino et al. [75] stated that high feed reduces the cutting time, and therefore, flank surface temperature decreases. The cutting time can also be reduced with high spindle speed, but contrary behavior is observed. At high feeds, required number of turns of the micro drill is less for a specific thickness of workpiece. Thus, heat generation decreases due to the less frictional travel between the micro drill and workpiece. It is seen in Fig.3.45 that generated temperature decreases as spindle speed increases according to the thermocouple measurement, but it is seen in Fig.3.46 that generated temperature increases as spindle speed increases according to the infrared thermography measurement. At high spindle speed, process time is low. Because, feed rate (mm/min) is a function of both spindle speed and feed. Maximum measured temperatures in all experiments have occurred after process ends as mentioned before for the thermocouple method. By considering the both process time and delay due to the heat conduction in the CFRP laminate, it can be concluded that results of the infrared thermography method are more reliable to decide the relationship between the spindle speed and generated temperature. As a result, higher temperatures occur as spindle speed increases. Similar results in conventional drilling of CFRP laminates verify the findings [62, 69, 71, 75]. It can be also derived that feed is more effective on the generated temperature than the spindle speed according to the experimental results.

3.5.1.2. Supported CFRP laminate experiments

According to the measured temperatures in Fig.3.45 and Fig.3.46, it can be derived that variation of temperatures are less in the supported CFRP laminate experiments for various cutting conditions. Infrared thermography measurements (Fig.3.46) show that generated temperatures in the supported case are also less than those of the bare CFRP laminate experiments. It reveals the fact that aluminum entry board which has a better

thermal conductivity than the CFRP laminate dissipates the generated heat effectively. Thus, cutting temperature reduces. It is seen that generated temperature decreases as feed increases at low cutting speed as similar to the bare CFRP experiments and does not change significantly at high cutting speed. Thermocouple measurements at high cutting speed may be misleading due to the mentioned phenomena in the bare CFRP experiments. The generated temperature did not change at all as spindle speed varies at low feed and increased slightly for the high feed according to the infrared thermography measurements.

Cutting mechanism differs in machining of CFRP laminates due to the chip formation which occurs as fracture of carbon fibers [105,106]. It was observed that chips of the CFRP laminate (Figure 3.47) came up with the powders of brittle fractured fibers and tangled epoxy, and cutting parameters did not affect the chip types significantly. By using this observation, it can be derived that machining of CFRP laminates requires less plastic deformation, and chip length is also small. Small chip length produces less frictional force in the secondary deformation zone [62]. Therefore, generated temperature is less as compared to the metal cutting. Cutting mechanism in machining of aluminum occurs on the shear plane which causes high plastic deformation. Therefore, generated temperatures are higher in metal cutting. It is seen that heat generation in the aluminum entry board at high feeds contributes significantly to the resulting temperature on the CFRP laminate. This result can be derived by comparing the generated maximum temperatures for the bare and supported cases at spindle speed of 20000 rpm in Figure 3.45. It is seen that although generated maximum temperature is the same for the bare and supported cases at the feed value of 3 μm/rev, it is higher for the supported case at the feed value of 7 μm/rev.

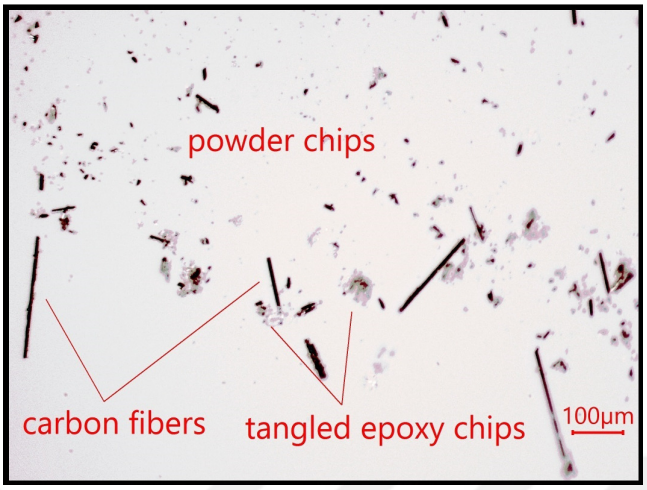

Figure 3.47. Chips of the CFRP laminate.

3.5.2. Effect of tool wear

This experiment was carried out with the low spindle speed and feed values of 20000 rpm and 3µm/rev due to the advantage of low resulting feed rate which causes higher process time. Thus, it was aimed that misleading results in thermocouple measurements by means of low process time at high spindle speed and delay due to the poor thermal conductivity of the CFRP laminate may be prevented. In this experiment, it was intended to find out the severity of the generated temperature as micro drill wears. Totally 250 holes were drilled on the bare CFRP laminate with the same micro drill and averages of the first and the last 4 holes' maximum temperatures were derived with the thermocouple method. Before the each temperature measurement, sufficient time was allowed to the workpiece and micro drill to cool down. It revealed that generated temperature increased from 40,7 °C to 49,4 °C as micro drill wears. This result shows that tool wear has a significant effect on the generated temperature. In Figure 3.48, heavy flank wear on the micro drill's chisel and primary cutting edge is shown. Due to the abrasive nature of the carbon fibers [46], micro drill wears rapidly. Thus, micro drill experiences high frictional forces which increase the generated temperature in the process.

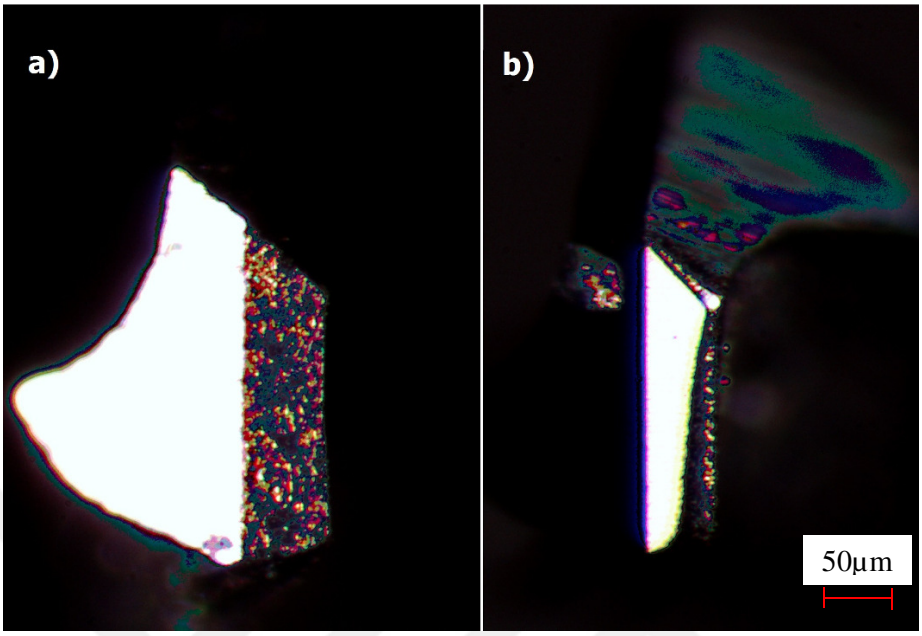

Figure 3.48. Comparison of the new (a) and used micro drill (b).

3.5.3. Effect of drill margin friction

To inspect the heat generation due to the friction between the drill margin and workpiece, an experiment was organized for the drilling conditions of 20000 rpm and 3µm/rev. Hence, it was aimed to find out whether a heat generation occurs between the micro-drill margin and drilled hole wall. For comparison, a hole was drilled until cutting edge corner of the micro drill reaches the back side of the CFRP laminate for the first case and then another hole was drilled 0,5 mm deeper than the previous hole for the second case. Thus, it was provided that micro drill does not cut any material for the last 0,5 mm depth, but friction between the drill margin and drilled hole wall continues, and only friction between the drill margin and drilled hole wall contributes to the heat generation which is expected to cause higher resulting temperature at the end of the process. In Figure 3.49, graphical representation of heat generation sources are shown as micro drill travels through the workpiece. Temperature measurements were made by thermocouple method, and experiments were repeated 4 times for each case. It revealed that generated temperature increased from 40,7 °C to 42,4 °C due to the drill margin friction. This result shows the significance of drill margin friction as a source of heat generation.

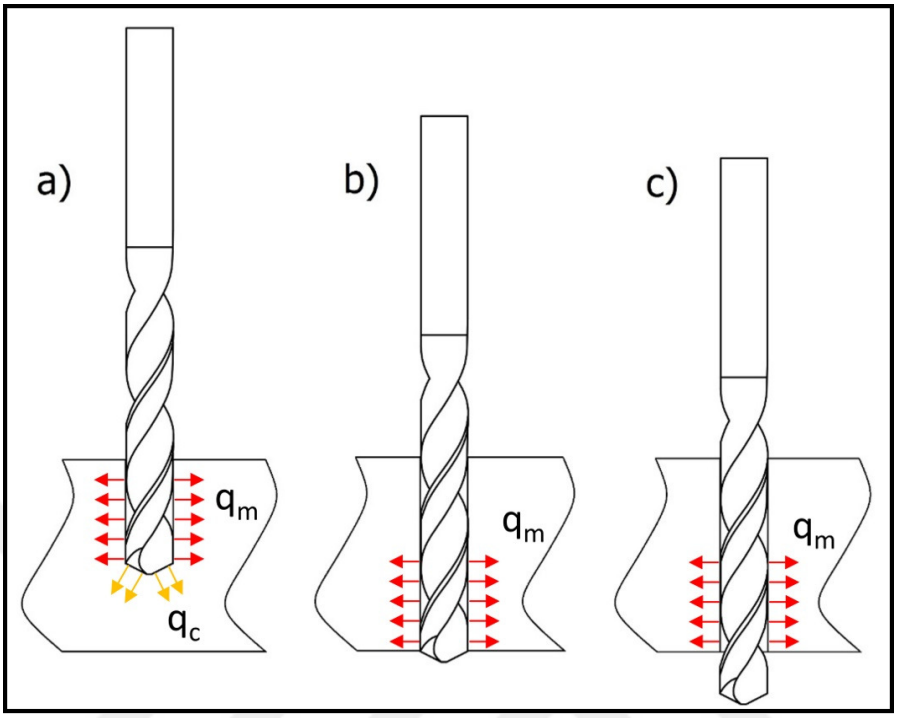

Figure 3.49. (a) Heat generation due to cutting (q_c) and drill margin friction (q_m), (b) End of heat generation due to cutting, and (c) Heat generation due to drill margin friction.

3.6. Cutting Forces

In Figure 3.50, typical thrust force and torque diagrams are shown for bare CFRP laminate. Diagrams were divided into the segments to indicate the drill position through the workpiece. It is seen that the force and torque diagrams were composed of local peaks and valleys due to the structure of the CFRP laminate which contains the carbon fiber and epoxy layers. In carbon fiber layers, required thrust force is higher as expected. When drill exits the carbon fiber layer and enters the epoxy layer, thrust force decreases. This fluctuation repeats 8 times for the bare CFRP laminate. Because the workpiece consists of 8 carbon fiber plies. For the specific cutting conditions of 20000 rpm and 3 µm/rev, the highest thrust force and torque values are 2.59 N and 5.67 Nmm. It is also seen in the diagram that thrust force and torque values for each ply are not equally spaced. It may be attributed to the warp-fill arrangement of each carbon fiber fabric. Slope of the thrust force decreases while micro drill exits the workpiece. It may be attributed to the probable start of the exit delamination.

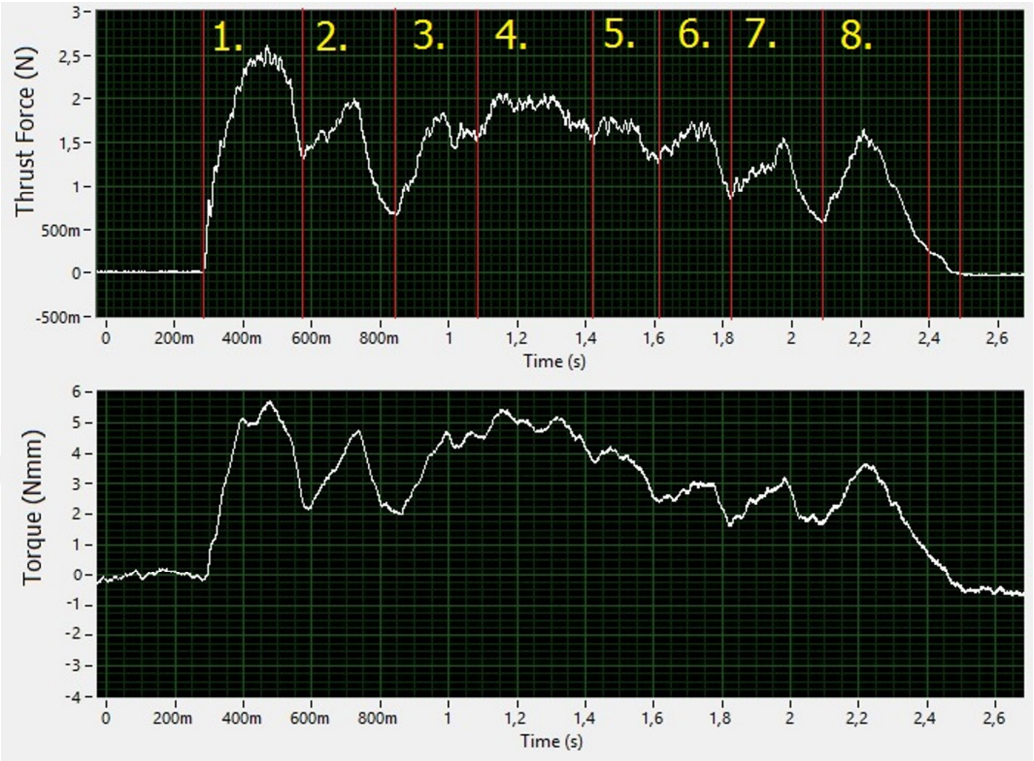

Figure 3.50. Thrust force and torque diagrams for the cutting conditions of 20000 rpm and 3 µm/rev in case of bare CFRP laminate.

In Figure 3.51, typical thrust force and torque diagrams are shown for supported CFRP laminate. The drilling sequence consists of 0.5 mm thick aluminum entry board, 2 mm thick CFRP laminate, and 4 mm thick phenolic plate. Phenolic plate was drilled with a drilling depth of 0.5 mm for each supported case. As similar to the bare CFRP laminate diagrams, it seen from the thrust force diagram that thrust force has local peaks and valleys. But, fluctuation repeats 10 times because of the entry board and backing board. It is seen that the highest thrust force occurs when micro drill cuts the aluminum entry board but the highest drilling torque occurs when micro drill reaches the end point. In Table 3.28, the highest trust force and torque values are shown for each experiment.

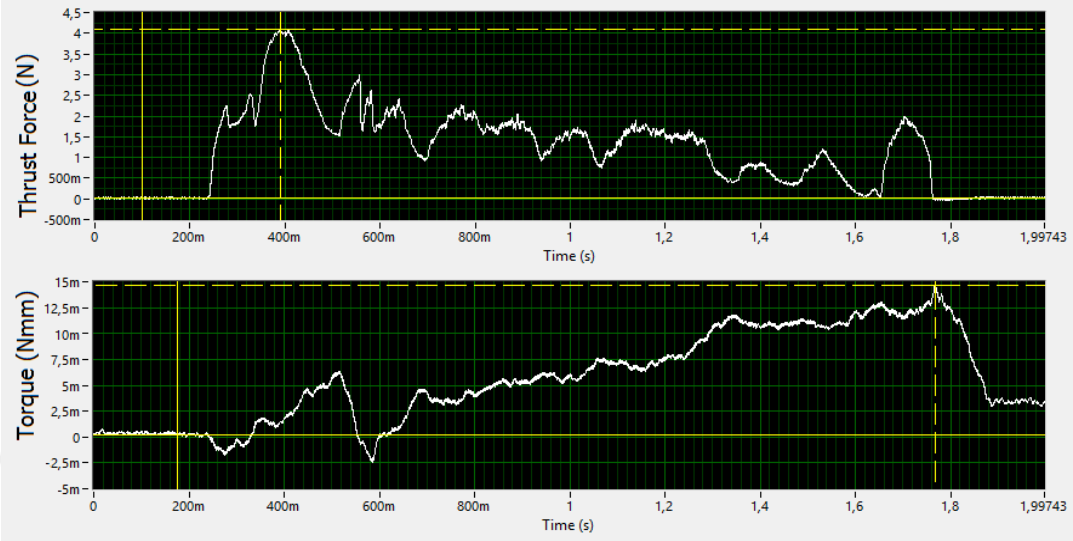

Figure 3.51. Thrust force and torque diagrams for the cutting conditions of 40000 rpm and 3 µm/rev in case of supported CFRP laminate.

Table 3.28. Maximum thrust force and torque values.

			Bare CFRP laminate experiments		Supported CFRP laminate experiments	
Spindle Speed (rpm)	Feed (µm/rev)		Thrust force (N)	Torque (Nmm)	Thrust force (N)	Torque (Nmm)
20000	3	1st trial	1.90	2.53	4.34	14.80
		2nd trial	2.59	5.67	6.19	18.13
		3rd trial	2.61	7.89	4.31	12.02
		mean	2.37	5.36	4.95	14.98
20000	7	1st trial	2.29	13.78	4.61	9.80
		2nd trial	2.57	10.50	5.28	8.16
		3rd trial	3.34	7.22	6.93	6.41
		mean	2.73	10.50	5.61	8.12
40000	3	1st trial	1.85	6.31	6.05	8.54
		2nd trial	2.25	7.17	3.94	9.31
		3rd trial	1.93	10.83	4.08	14.48
		mean	2.01	8.10	4.69	10.78
40000	7	1st trial	1.97	10.87	4.52	3.72
		2nd trial	2.46	5.73	4.43	7.54
		3rd trial	2.70	4.98	4.25	16.93
		mean	2.38	7.19	4.40	9.40

In Figure 3.52, variations of thrust force and torque values according to the spindle speed and feed are shown for the bare CFRP laminate experiments. It is clearly seen that thrust force decreases as spindle speed increases and feed decreases. It was validated by infrared thermography measurements that generated temperature increases as spindle speed increases. Elevated temperature may cause the matrix softening. Thus, thrust force decreases. Chip load increases as feed increases. Thus, higher thrust force is required. It is seen that torque increases as spindle speed increases at the low feed and vice versa for the high feed.

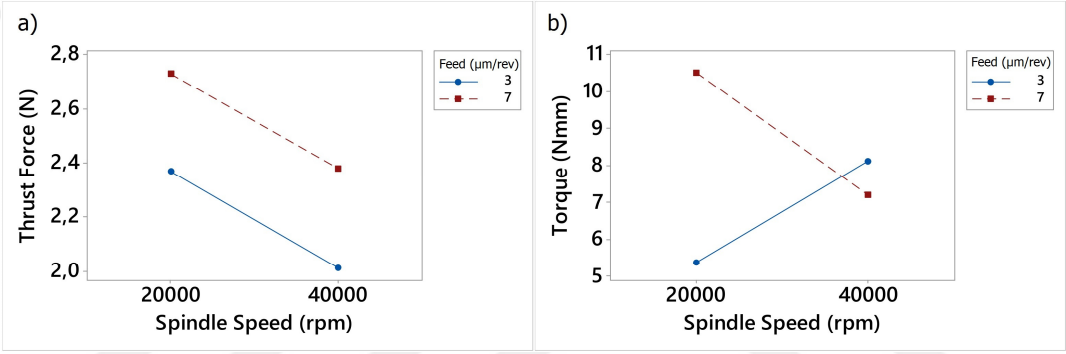

Figure 3.52. Effects of spindle speed and feed on the thrust force (a) and torque (b) in the case of bare CFRP laminate.

It was validated in Chapter 3.1 that spindle speed is more effective on the delamination damage and delamination decreases as spindle speed increases for the exit side. It is clearly seen in Figure 3.52(a) that thrust force also decreases as spindle speed increases. Therefore, it can be derived that decrease in exit side delamination damage is related to the decrease in thrust force as spindle speed increases. There is also an interaction between the thrust force and cutting temperature. If the thrust force graphic in Figure 3.52(a) and cutting temperature graphic in Figure 3.53 are compared, contrary trend is observed between the cutting temperature and thrust force, that is, thrust force decreases as cutting temperature increases. This relation clearly reflects the effect of cutting temperature on the thrust force by means of matrix softening.

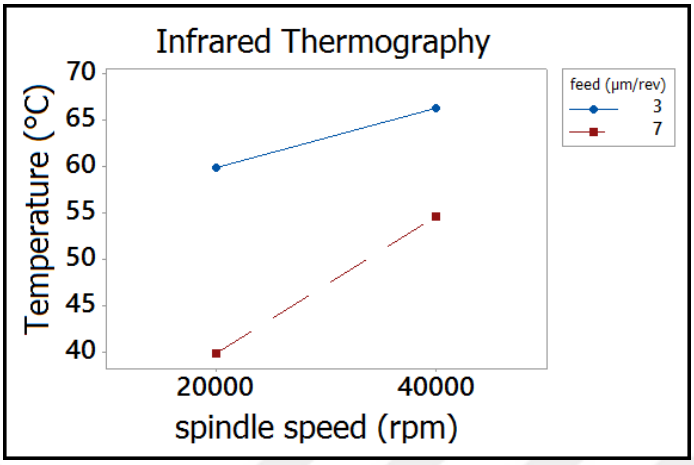

Figure 3.53. Variation of cutting temperature in the case of bare CFRP laminate experiments according to the infrared thermography method.

In Figure 3.54, variations of thrust force and torque values according to the spindle speed and feed are shown for the supported CFRP laminate experiments. It is seen that thrust force and torque values are higher for the supported case as compared to the bare CFRP laminate experiments. Similar trends for the thrust force are seen. Thrust force decreases as spindle speed increases and feed decreases. Contrary to the bare CFRP laminate experiments, torque increases as spindle speed increases at the high feed and vice versa for the low feed. It is seen that higher torque is required for the low feed. It may be related to the ploughing at the low feed value.

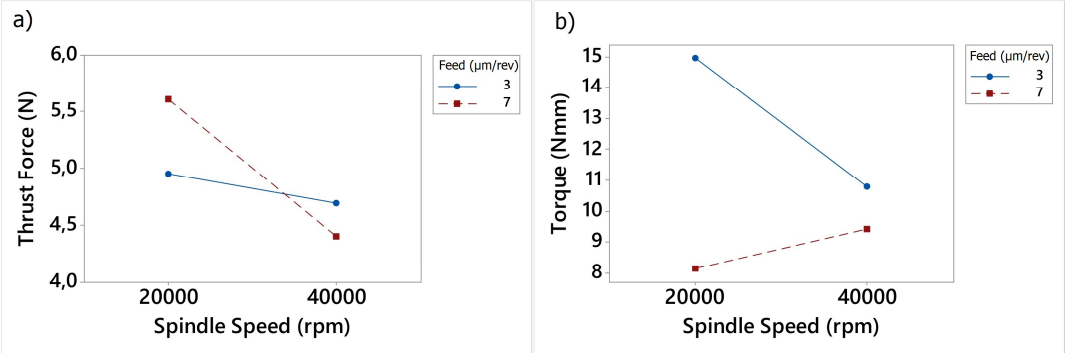

Figure 3.54. Effects of spindle speed and feed on the thrust force (a) and torque (b) in the case of supported CFRP laminate.

6. CONCLUSIONS

In this dissertation, effects of support plates on delamination damage, hole form quality, and tool wear in micro-drilling of CFRP laminates were investigated experimentally under various cutting conditions of spindle speed and feed. Additionally, cutting temperature and cutting forces were investigated for both bare and supported CFRP laminates. Following conclusions can be drawn.

6.1. Delamination

For the entry side delamination, it is clear that the delamination factors for the first holes in bare CFRP experiments are extremely satisfying, but deteriorating toward the last holes. Entry support plates prevent the delamination, but bring another kind of damage to the surface of the workpiece. Acceptance of this damage as opposed to the delamination is an argument. If the burrs of the entry board which occur during drilling are avoided, ring shaped cavity damage can be eliminated. By using the results of the optimization process, followings can be drawn. Intermediate feed rate and low spindle speed in the selected ranges provided the least delamination damages for the entry side in case of bare CFRP laminate, and feed rate is more effective than the spindle speed.

As for the exit side delamination, it is concluded that backing boards (phenolic and wooden) in two cases increased the delamination for the first holes. Phenolic backing board slightly decreased the delamination for the middle and last holes, and wood backing board slightly decreased the delamination for the last holes. According to the arithmetic mean of the first, the middle and the last holes with same cutting conditions, rear side mean delamination damage varies between -5% and 7% for the phenolic backing board and -7% and 16% for the wood backing board with respect to the bare CFRP experiments depending on the cutting conditions. It should not be forgotten that CFRP laminates were produced by vacuum resin infusion method, and vacuum bag side of the CFRP laminate was placed downwards on the fixture through the all experiments. Different production methods of the CFRP laminate may cause the distinctive delamination damages. According to the results of the optimization, intermediate feed rate and high spindle speed in the selected ranges provided the least delamination damages for the rear side in case of bare CFRP laminate. For the case of phenolic

backing board, it is found as intermediate feed rate and intermediate spindle speed. Optimum values of spindle speed and feed rate are determined as high feed rate and low spindle speed for the case of wood backing board. It is concluded that spindle speed is the dominant factor for the rear side delamination.

For an individual experiment, delamination behavior changes drastically from the first to the last hole. This behavior is clearly related to the tool wear. As micro drill wears, cutting edge radius increases, and the ratio of the uncut chip thickness to the cutting edge radius changes. Therefore, the variation of delamination behavior can be attributed to the size effect.

6.2. Hole Form Quality

Aluminum entry board increased the front side hole diameters. Front side RMS hole diameter varies between the 0,9% and 2,0%, and variation of the mean hole diameter from the first to the last hole was high (0,3% and 1,9%). Probably, it was caused by the exit burrs of the aluminum entry board. Diameters of the holes in the cases of bare CFRP and brass entry board were close to the drill diameter. Front side RMS hole diameter varies between the 0,4% and 1,2% for the bare CFRP laminate experiments and varies between the 0,3% and 1,2% for the CFRP laminate with brass entry board depending on the cutting conditions. Minimum and maximum percentage differences for front side hole diameters are 0,2% and 2,3% for bare CFRP laminate experiments and 0,4% and 1,6% for the CFRP laminate with brass entry board depending on the cutting conditions. Rear side hole diameters were smaller than the front side hole diameters. Phenolic backing board provided close values of the hole diameters to the drill diameter for the rear side. Rear side RMS hole diameter varies between the 2,1% and 3,5% for the bare CFRP laminate experiments, 1,0% and 2,1% for the CFRP laminate with phenolic backing board, 1,7% and 3,3% for the CFRP laminate with wood backing board depending on the cutting conditions. It was attributed to the structural resemblance of phenolic backing board to the CFRP laminate. Thus, the continuity was ensured. The least variation of the rear side mean hole diameter from the first to the last hole was derived with phenolic backing board. Minimum and maximum percentage differences for rear side diameters are 1,1% and 2,8% for bare CFRP laminate experiments, 0,6% and 3,8% for the CFRP laminate with phenolic backing board, and 1,9% and 4,5% for

the CFRP laminate with wood backing board depending on the cutting conditions.

Roundness in the case of bare CFRP was the worst for the front side. It was followed by the brass entry board. The best roundness was derived with the aluminum entry board. Aluminum entry board can decrease the front side mean roundness error up to 50%, and brass entry board can decrease the front side mean roundness error up to 42% with respect to the bare CFRP experiments depending on the cutting conditions. It was concluded that entry boards improved the centering capability of the micro drill. Bare CFRP experiments provided the best roundness for the rear side. Also, spindle speed did not affect the roundness from the first to the last hole. It was followed by the wood backing board. The worst rear side roundness was derived with the phenolic backing board. Phenolic backing board can increase the rear side mean roundness error up to 62% and wood backing board can increase the rear side mean roundness error up to 45% with respect to the bare CFRP experiments depending on the cutting conditions. Deterioration of the rear side roundness was attributed to the production method of the CFRP laminates which produced resin rich zones.

Variation of the front side fiber overlap for the cases of support plates was smaller than that of bare CFRP experiments. The smallest fiber overlap was derived with the first holes of the bare CFRP experiments, but it increased toward to the last holes. Also, cutting parameters strongly affected the fiber overlap. According to the arithmetic means, aluminum entry board can decrease the front side mean fiber overlap as 17% and can increase the front side mean fiber overlap as 72%, and brass entry board can decrease the front side mean fiber overlap as 30% and can increase the front side mean fiber overlap as 88% with respect to the bare CFRP experiments depending on the cutting conditions. The phenolic backing board was found the best to decrease the rear side fiber overlap. The wood backing board provided close values to the phenolic backing board. Cutting parameters had little effects on the rear side fiber overlap for the support cases. The worst rear side fiber overlap occurred in the bare CFRP experiments. According to the arithmetic means, phenolic backing board can decrease the rear side mean fiber overlap up to 46%, and wood backing board can decrease the rear side mean fiber overlap as 10% and can increase the rear side mean fiber overlap as 17% with respect to the bare CFRP experiments depending on the cutting conditions.

As a result, support plates improved the hole form quality and made the process outputs less sensitive to the change of the spindle speed, feed, and tool wear. Materials of the support plates have influences on the process outputs. For some of the process outputs, support plates deteriorated the situation, e.g. increased the front side hole diameter in the aluminum entry board case, increased the rear side roundness error in the cases of the phenolic and wood backing boards, and increased the fiber overlap for the first holes in the cases of the aluminum and brass entry boards.

6.3. Tool Wear

The following conclusions can be drawn;

- Drilling the bare CFRP laminate causes the least flank wear variation.

- For some of the cutting conditions, support plates provided less flank wear as compared to the bare CFRP experiments, especially for the cutting conditions of 20000 rpm – 7 µm/rev and 40000 rpm – 7 µm/rev.

- Support plates caused higher flank wear for the low feeds.

- Using the support plates is beneficial for less flank wear, if appropriate spindle speed and feed are chosen by using the wear map.

- Higher feeds provide less flank wear for the supported cases.

- Materials of the support plates affect the flank wear. Aluminum-phenol support plates are better than brass-wood support plates in decreasing flank wear.

- Cutting parameters are more effective on flank wear for the supported cases.

- It is shown by the statistical analysis that feed is the most influential variable on the flank wear for the supported cases, and a statistically significant variable does not occur for the unsupported case.

6.4. Cutting Temperature

Effects of process variables as spindle speed, feed, and support plates on the heat generation in micro-drilling of CFRP laminates has been investigated experimentally. Furthermore, effects of tool wear and drill margin friction on the generated temperatures have been investigated for a specific case, and following findings can be drawn.

- It was observed that generated temperatures are well below the glass transition temperature for the selected ranges of the process variables.

- It turned out that temperature measurements must be done with more than one method to verify the findings. Measurements with the thermocouple method may be misleading due to the very small process time. The highest temperatures measured by the thermocouple method occurred after the end of the process for all experiments. Transient heat conduction, poor thermal conductivity of the CFRP, and very small process time bring difficulties to the thermocouple method in temperature measurement.

- Feed is more effective on the generated temperature than the spindle speed.

- Generated temperature increases as feed decreases and spindle speed increases.

- Supported CFRP laminate with the aluminum entry board made the generated temperature less sensitive to the process variables of spindle speed and feed. It was observed in the infrared thermography measurements that aluminum entry board reduced the cutting temperature in the CFRP laminate with heat dissipation thanks to its better thermal conductivity.

- Tool wear has a significant effect on the generated temperature. Micro drill deteriorates rapidly due to the abrasive carbon fibers. Visual inspection of the micro drill reveals the heavy flank wear which elevates the generated temperature by means of increased frictional forces.

- It was found that friction between the drill margin and drilled hole wall was a source of heat generation.

6.5. Cutting Forces

- It was derived that thrust force decreases as spindle speed increases and feed decreases.

- It was found that thrust force and torque values are higher for the supported case than those for the bare CFRP laminate experiments.

- Comparison of the thrust force and cutting temperature graphics revealed that thrust force decreases as cutting temperature increases.

6.6. Recommendations for Future Work

In this dissertation, tool wear was investigated for the full range of cutting conditions, but cutting forces were investigated with the unused drill for two levels of spindle speed and feed. Therefore, effects of tool wear and wide range of cutting parameters on the cutting forces in micro-drilling of CFRP laminates can be investigated in the future work. Other methods can be applied to investigate the cutting temperature. Due to the small size of the drill, cutting edge temperature could not be measured with the infrared thermography and thermocouple methods. Heat sensitive paints or tool-workpiece coupling method may be used for comprehensive investigation. Primary challenges in micro-drilling of CFRP laminates are delamination and rapid tool wear. In this study, application of the support plates as a preventive method to decrease the delamination damage has been used. Other methods can be investigated to decrease the drilling induced delamination, for instance, special micro drills. Tool coatings or PCD tools can be used to decrease the tool wear, and their effects can be inspected. It was mentioned that entry boards caused the ring shaped cavity damage to the hole entry due to the exit burrs of the entry boards. Burr formation mechanism can be investigated to decrease the size of the burrs. Although support plates have positive effects on the micro-drilling process, they are wasted after the process and increase the cost of production. Active support systems without using the supplementary materials must be developed due to environmental and economic reasons.

REFERENCES

[1] Dornfeld, D., Min, S., and Takeuchi, Y. (2006) Recent advances in mechanical micromachining. CIRP Annals - Manufacturing Technology, 55(2), 745-768.

[2] Rahamathullah, I., Shunmugam, M.S. (2012) Analyses of forces and hole quality in micro-drilling of carbon fabric laminate composites. Journal of Composite Materials, 47(9), 1129-1140.

[3] Alpha Omega Swiss, https://www.alphaomegaswiss.com/swiss-machining/micro machining, 16.10.2017.

[4] Phadnis, V.A., Makhdum, F., Roy, A., Silberschmidt, V.V. (2013) Drilling in carbon/epoxy composites: Experimental investigations and finite element implementation. Composites: Part A, 47, 41-51.

[5] Karpat, Y., Bahtiyar, O., Değer, B., Kaftanoğlu, B. (2014) A mechanistic approach to investigate drilling of UD-CFRP laminates with PCD drills. CIRP Annals - Manufacturing Technology, 63, 81-84.

[6] Samejima, S., Ozaki, T., Inoue, A., Suzuki, K., Osuga, H., Sato, S., Matsui, K. (2008) Low thermal expansion and high heat dissipation printed wiring boards. 41st International Symposium on Microelectronics, 2-6 November, Providence, Rhode Island, USA.

[7] Ogawa, K., Nakagawa, H., Hirogaki, T., Aoyama, E. (2015) Effects of diamond coated tools in micro-drilling of CFRP plates using a high-speed spindle. Advances in Materials and Processing Technologies, 1, 192-200.

[8] Cheong, M.S., Cho, D.W., Ehmann, K.F. (1999) Identification and control for micro-drilling productivity enhancement. International Journal of Machine Tools and Manufacture, 39, 1539-1561.

[9] Teti, R. (2002) Machining of composite materials. CIRP Annals-Manufacturing Technology, 51(2), 611-634.

[10] Zitoune, R., Krishnaraj, V., Almabouacif, B. S., Collombet, F., Sima, M., Jolin, A. (2012) Influence of machining parameters and new nano-coated tool on drilling performance of CFRP/Aluminium sandwich. Composites Part B: Engineering, 43(3), 1480-1488.

[11] Persson, E., Eriksson, I., Zackrisson, L. (1997) Effects of hole machining defects on strength and fatigue life of composite laminates. Composites Part A: Applied Science and Manufacturing, 28, 141-151.

[12] Ogawa, K., Nakagawa, H., Hirogaki, T., Aoyama, E. (2012) Micro-drilling of CFRP plates using a high-speed spindle. Key Engineering Materials, 523-524, 1035-1040.

[13] Coombs Jr, C. F., (1995) Printed Circuits Handbook, 4th edition, (McGraw-Hill)

[14] Kudla, L.A. (2011) Fracture phenomena of microdrills in static and dynamic conditions. Engineering Fracture Mechanics, 78, 1-12.

[15] Langella, A., Nele, L., Maio, A. (2005) A torque and thrust prediction model for drilling of composite materials. Composites Part A: Applied Science and Manufacturing, 36, 83-93.

[16] Won, M.S., Dharan, C.K.H. (2002) Chisel edge and pilot hole effects in drilling composite laminates. Journal of Manufacturing Science and Engineering, 124(2), 242-247.

[17] Ramos, A.C., Autenrieth, H., Strauß, T., Deuchert, M., Hoffmeister, J., Schulze, V. (2012) Characterization of the transition from ploughing to cutting in micro machining and evaluation of the minimum thickness of cut. Journal of Materials Processing Technology, 212(3), 594-600

[18] Woon, K.S., Rahman, M., Fang, F.Z., Neo, K.S., Liu, K. (2008) Investigations of tool edge radius effect in micromachining: a FEM simulation approach. Journal of Materials Processing Technology, 195, 204-211.

[19] Jin, X., Altintas, Y. (2011) Slip-line field model of micro-cutting process with round tool edge effect. Journal of Materials Processing Technology, 211, 339-355.

[20] Su, Y., Jia, Z., Niu, B., Bi, G. (2017) Size effect of depth of cut on chip formation mechanism in machining of CFRP. Composite Structures, 164, 316-327.

[21] Liu, D., Tang, Y., Cong, W.L. (2012) A review of mechanical drilling for composite laminates. Composite Structures, 94, 1265-1279.

[22] Hocheng, H., Tsao, C.C. (2005) The path towards delamination-free drilling of composite materials. Journal of Materials Processing Technology, 167, 251-264.

[23] Shyha, I.S., Aspinwall, D.K., Soo, S.L., Bradley, S. (2009) Drill geometry and operating effects when cutting small diameter holes in CFRP. International Journal of Machine Tools and Manufacture, 49, 1008-1014.

[24] Isbilir, O., Ghassemieh, E. (2013) Numerical investigation of the effects of drill geometry on drilling induced delamination of carbon fiber reinforced composites. Composite Structures, 105,126-133.

[25] Hocheng, H., Tsao, C.C. (2006) Effects of special drill bits on drilling-induced delamination of composite materials. International Journal of Machine Tools and Manufacture, 46, 1403-1416.

[26] Tsao, C.C., Hocheng, H. (2003) The effect of chisel length and associated pilot hole on delamination when drilling composite materials. International Journal of Machine Tools and Manufacture, 43, 1087-1092.

[27] Tsao, C. C., Hocheng, H. (2007) Effect of tool wear on delamination in drilling composite materials. International journal of mechanical sciences, 49(8), 983-988.

[28] Khashaba, U. A., El-Sonbaty, I. A., Selmy, A. I., Megahed, A. A. (2010) Machinability analysis in drilling woven GFR/epoxy composites: Part II–Effect of drill wear. Composites Part A: Applied Science and Manufacturing, 41(9), 1130-1137.

[29] Ertunc, H. M., Oysu, C. (2004) Drill wear monitoring using cutting force signals. Mechatronics, 14(5), 533-548.

[30] Patra, K., Jha, A. K., Szalay, T., Ranjan, J., Monostori, L. (2017) Artificial neural network based tool condition monitoring in micro mechanical peck drilling using thrust force signals. Precision Engineering, 48, 279-291.

[31] Kim, H. Y., Ahn, J. H., Kim, S. H., Takata, S. (2002) Real-time drill wear estimation based on spindle motor power. Journal of Materials Processing Technology, 124(3), 267-273.

[32] König, W., Kutzner, K., Schehl, U. (1992) Tool monitoring of small drills with acoustic emission. International Journal of Machine Tools and Manufacture, 32(4), 487-493.

[33] El-Wardany, T. I., Gao, D., Elbestawi, M. A. (1996) Tool condition monitoring in drilling using vibration signature analysis. International Journal of Machine Tools and Manufacture, 36(6), 687-711.

[34] König, W., Wulf, C.H., Graß, P.H., Willerscheid, H. (1985) Machining of fibre reinforced plastics. CIRP Annals - Manufacturing Technology, 34(2), 537-548.

[35] Hocheng, H., Dharan, C.K.H. (1990) Delamination during drilling in composite laminates. Journal of Manufacturing Science and Technology, 112(3), 236-239.

[36] Tsao, C.C., Hocheng, H. (2005) Effects of exit back-up on delamination in drilling composite materials using a saw drill and core drill. International Journal of Machine Tools and Manufacture, 45, 1261-1270.

[37] Capello, E. (2004) Workpiece damping and its effect on delamination damage in drilling thin composite laminates. Journal of Materials Processing Technology, 148, 186-195.

[38] El-Sonbaty, I., Khashaba, U. A., Machaly, T. (2004) Factors affecting the machinability of GFR/epoxy composites. Composite structures, 63(3), 329-338.

[39] Velayudham, A., Krishnamurthy, R., Soundarapandian, T. (2005) Evaluation of drilling characteristics of high volume fraction fibre glass reinforced polymeric composite. International Journal of Machine Tools and Manufacture, 45(4), 399-406.

[40] Singh, I., Bhatnagar, N., Viswanath, P. (2008) Drilling of uni-directional glass fiber reinforced plastics: experimental and finite element study. Materials Design, 29(2), 546-553.

[41] Abrao, A. M., Rubio, J. C., Faria, P. E., Davim, J. P. (2008) The effect of cutting tool geometry on thrust force and delamination when drilling glass fibre reinforced plastic composite. Materials Design, 29(2), 508-513.

[42] Hocheng, H., Tsao, C. C. (2003) Comprehensive analysis of delamination in drilling of composite materials with various drill bits. Journal of Materials Processing Technology, 140(1), 335-339.

[43] Mohan, N. S., Ramachandra, A., Kulkarni, S. M. (2005) Influence of process parameters on cutting force and torque during drilling of glass - fiber polyester reinforced composites. Composite structures, 71(3), 407-413.

[44] Davim, J. P., Reis, P., Antonio, C. C. (2004) Experimental study of drilling glass fiber reinforced plastics (GFRP) manufactured by hand lay-up. Composites Science and Technology, 64(2), 289-297.

[45] Davim, J. P., Reis, P. (2003) Drilling carbon fiber reinforced plastics manufactured by autoclave - experimental and statistical study. Materials design, 24(5), 315-324.

[46] Davim, J. P., Reis, P. (2003) Study of delamination in drilling carbon fiber reinforced plastics (CFRP) using design experiments. Composite structures, 59(4), 481-487.

[47] Sardinas, R. Q., Reis, P., Davim, J. P. (2006) Multi-objective optimization of cutting parameters for drilling laminate composite materials by using genetic algorithms. Composites Science and Technology, 66(15), 3083-3088.

[48] Kilickap, E. (2010) Optimization of cutting parameters on delamination based on Taguchi method during drilling of GFRP composite. Expert Systems with Applications, 37(8), 6116-6122.

[49] Khashaba, U. A. (2004) Delamination in drilling GFR-thermoset composites. Composite Structures, 63(3), 313-327.

[50] Gaitonde, V. N., Karnik, S. R., Rubio, J. C., Correia, A. E., Abrao, A. M., Davim, J. P. (2008) Analysis of parametric influence on delamination in high-speed drilling of carbon fiber reinforced plastic composites. Journal of Materials Processing Technology, 203(1), 431-438.

[51] Karnik, S. R., Gaitonde, V. N., Rubio, J. C., Correia, A. E., Abrão, A. M., Davim, J. P. (2008) Delamination analysis in high speed drilling of carbon fiber reinforced plastics (CFRP) using artificial neural network model. Materials & Design, 29(9), 1768-1776.

[52] Rubio, J. C., Abrao, A. M., Faria, P. E., Correia, A. E., Davim, J. P. (2008) Effects of high speed in the drilling of glass fibre reinforced plastic: evaluation of the delamination factor. International Journal of Machine Tools and Manufacture, 48(6), 715-720.

[53] Rawat, S., Attia, H. (2009) Characterization of the dry high speed drilling process of woven composites using Machinability Maps approach. CIRP Annals-Manufacturing Technology, 58(1), 105-108.

[54] Tsao, C. C., Hocheng, H. (2005) Computerized tomography and C-Scan for measuring delamination in the drilling of composite materials using various drills. International Journal of Machine Tools and Manufacture, 45(11), 1282-1287.

[55] Anand, R.S., Patra, K., Steiner, M. (2014) Size effects in micro drilling of carbon fiber reinforced plastic composite. Production Engineering, 8(3), 301-307.

[56] Anand, R. S., Patra, K. (2016) Mechanistic cutting force modelling for micro-drilling of CFRP composite laminates. CIRP Journal of Manufacturing Science and Technology, 16, 55-63.

[57] Wang, X., Kwon, P. Y., Sturtevant, C., Lantrip, J. (2013) Tool wear of coated drills in drilling CFRP. Journal of Manufacturing Processes, 15(1), 127-135.

[58] Rawat, S., Attia, H. (2009) Wear mechanisms and tool life management of WC–Co drills during dry high speed drilling of woven carbon fibre composites. Wear, 267(5), 1022-1030.

[59] Zheng, L. J., Wang, C. Y., Fu, L. Y., Yang, L. P., Qu, Y. P., Song, Y. X. (2012) Wear mechanisms of micro-drills during dry high speed drilling of PCB. Journal of Materials Processing Technology, 212(10), 1989-1997.

[60] Wang, X., Kwon, P. Y., Sturtevant, C., Lantrip, J. (2014) Comparative tool wear study based on drilling experiments on CFRP/Ti stack and its individual layers. Wear, 317(1), 265-276.

[61] Lin, S. C., Chen, I. K. (1996) Drilling carbon fiber-reinforced composite material at high speed. Wear, 194(1-2), 156-162.

[62] Chen, W. C. (1997) Some experimental investigations in the drilling of carbon fiber-reinforced plastic (CFRP) composite laminates. International Journal of Machine Tools and Manufacture, 37(8), 1097-1108.

[63] Zitoune, R., El Mansori, M., Krishnaraj, V. (2013) Tribo-functional design of double cone drill implications in tool wear during drilling of copper mesh/CFRP/woven ply. Wear, 302(1), 1560-1567.

[64] Faraz, A., Biermann, D., Weinert, K. (2009) Cutting edge rounding: An innovative tool wear criterion in drilling CFRP composite laminates. International Journal of Machine Tools and Manufacture, 49(15), 1185-1196.

[65] Samuel Raj, D., Karunamoorthy, L. (2017) Cutting edge - flatting and roughness measurement—to monitor blunting and chipping of the drill cutting edge when drilling CFRP. The International Journal of Advanced Manufacturing Technology, 92, 953-968.

[66] Liu, T. I. (1990) A computer vision approach for drill wear measurements. Journal of Materials Shaping Technology, 8(1), 11-16.

[67] Su, J. C., Huang, C. K., Tarng, Y. S. (2006) An automated flank wear measurement of microdrills using machine vision. Journal of Materials Processing Technology, 180(1), 328-335.

[68] Imran, M., Mativenga, P. T., Withers, P. J. (2012) Assessment of machining performance using the wear map approach in micro-drilling. The International Journal of Advanced Manufacturing Technology, 59(1-4), 119-126.

[69] Brinksmeier, E., Fangmann, S., Rentsch, R. (2011) Drilling of composites and resulting surface integrity. CIRP Annals-Manufacturing Technology, 60(1), 57-60.

[70] Yashiro, T., Ogawa, T., Sasahara, H. (2013) Temperature measurement of cutting tool and machined surface layer in milling of CFRP. International Journal of Machine Tools and Manufacture, 70, 63-69.

[71] Wang, H., Sun, J., Li, J., Lu, L., Li, N. (2016) Evaluation of cutting force and cutting temperature in milling carbon fiber-reinforced polymer composites. International Journal of Advanced Manufacturing Technology, 82, 1517-1525.

[72] Pinho, L. V., Carou, D., Davim, J. P. (2016) Comparative study of the performance of diamond-coated drills on the delamination in drilling of carbon fiber reinforced plastics: assessing the influence of the temperature of the drill. Journal of Composite Materials, 50(2), 179-189.

[73] Zitoune, R., Krishnaraj, V., Collombet, F. (2010) Study of drilling of composite material and aluminium stack. Composite Structures, 92(5), 1246-1255.

[74] Ghafarizadeh, S., Lebrun, G., Chatelain, J. F. (2016) Experimental investigation of the cutting temperature and surface quality during milling of unidirectional carbon fiber reinforced plastic. Journal of Composite Materials, 50(8), 1059-1071.

[75] Sorrentino, L., Turchetta, S., Bellini, C. (2017) In process monitoring of cutting temperature during the drilling of FRP laminate. Composite Structures, 168, 549-561.

[76] Wang, C. Y., Chen, Y. H., An, Q. L., Cai, X. J., Ming, W. W., Chen, M. (2015) Drilling temperature and hole quality in drilling of CFRP/aluminum stacks using diamond coated drill. International Journal of Precision Engineering and Manufacturing, 16(8), 1689-1697.

[77] Merino-Pérez, J. L., Royer, R., Ayvar-Soberanis, S., Merson, E., Hodzic, A. (2015) On the temperatures developed in CFRP drilling using uncoated WC-Co tools Part I: Workpiece constituents, cutting speed and heat dissipation. Composite Structures, 123, 161-168.

[78] Zheng, L., Wang, C., Yang, L., Song, Y., Fu, L. (2012) Characteristics of chip formation in the micro-drilling of multi-material sheets. International Journal of Machine Tools and Manufacture, 52, 40-49.

[79] Davim, J.P., Rubio, J.C., Abrao, A.M. (2007) A novel approach based on digital image analysis to evaluate the delamination factor after drilling composite laminates. Composite Science and Technology, 67, 1939-1945.

[80] Gaugel, S., Sripathy, P., Haeger, A., Meinhard, D., Bernthaler, T., Lissek, F., Kaufeld, M., Knoblauch, V., Schneider, G., 2016. A comparative study on tool wear and laminate damage in drilling of carbon-fiber reinforced polymers (CFRP) Composite Structures, 155, 173-183.

[81] Chae, J., Park, S.S., Freiheit, T. (2006) Investigation of micro-cutting operations. International Journal of Machine Tools and Manufacture, 46, 313-332.

[82] Altintas, Y., Weck, M. (2004) Chatter stability of metal cutting and grinding. CIRP Annals – Manufacturing Technology, 53, 619-642.

[83] Komanduri, R., Hou, Z. B. (2001) A review of the experimental techniques for the measurement of heat and temperatures generated in some manufacturing processes and tribology. Tribology International, 34(10), 653-682.

[84] Davies, M. A., Ueda, T., M'saoubi, R., Mullany, B., Cooke, A. L. (2007) On the measurement of temperature in material removal processes. CIRP Annals-Manufacturing Technology, 56(2), 581-604.

[85] Abukhshim, N. A., Mativenga, P. T., Sheikh, M. A. (2006) Heat generation and temperature prediction in metal cutting: A review and implications for high speed machining. International Journal of Machine Tools and Manufacture, 46(7), 782-800.

[86] Lazoglu, I., Altintas, Y. (2002) Prediction of tool and chip temperature in continuous and interrupted machining. International Journal of Machine Tools and Manufacture, 42(9), 1011-1022.

[87] Sala, G. (2000) Composite degradation due to fluid absorption. Composites Part B: Engineering, 31(5), 357-373.

[88] Weinert, K., Kempmann, C. (2004) Cutting temperatures and their effects on the machining behaviour in drilling reinforced plastic composites. Advanced Engineering Materials, 6(8), 684-689.

[89] Nakagawa, H., Ogawa, K., Kihara, A., Hirogaki, T. (2007) Improvement of micro-drilled hole quality for printed wiring boards. Journal of Materials Processing Technology, 191(1), 293-296.

[90] Seif, M.A., Khashaba, U.A., Rojas-Oviedo, R. (2007) Measuring delamination in carbon/epoxy composites using a shadow moire laser based imaging technique. Composite Structures, 79, 113-118.

[91] Hocheng, H., Tsao, C.C., Chen, H.T. (2016) Utilizing internal icing force to reduce delamination in drilling composite tubes. Composite Structures, 139, 36-41.

[92] Bhandari, B., Hong, Y-S., Yoon, H-S., Moon, J-S., Pham, M-Q., Lee, G-B., Huang, Y., Linke, B.S., Dornfeld, D.A., Ahn, S. (2014) Development of a micro-drilling burr-control chart for PCB drilling. Precision Engineering, 38, 221-229.

[93] Giasin, K., Ayvar-Soberanis, S. (2017) An investigation of burrs, chip formation, hole size, circularity and delamination during drilling operation of GLARE using ANOVA. Composite Structures, 159, 745-760.

[94] Xu, J., Mkaddem, A., Mansori, M.E. (2016) Recent advances in drilling FRP/Ti composite: A state-of-the-art review. Composite Structures, 135, 316-338.

[95] Dogrusadik, A., Kentli, A. (2017) Comparative assessment of support plates' influences on delamination damage in micro-drilling of CFRP laminates. Composite Structures, 173, 156-167.

[96] Watanabe, H., Tsuzaka, H., Masuda, M. (2008) Microdrilling for printed circuit boards (PCBs) - influence of radial run-out of microdrills on hole quality. Precision Engineering, 32(4), 329-335.

[97] Krishnaraj, V., Zitoune, R., Davim, J. P. (2013) Drilling of polymer-matrix composites. Heidelberg: Springer.

[98] Bonnet, C., Poulachon, G., Rech, J., Girard, Y., Costes, J.P., 2015. CFRP drilling: Fundamental study of local feed force and consequences on hole exit damage. International Journal of Machine Tools and Manufacture, 94, 57-64.

[99] Ramulu, M., Branson, T., Kim, D. (2001) A study on the drilling of composite and titanium stacks. Composite Structures, 54(1), 67-77.

[100] Kim, D., Ramulu, M. (2004) Drilling process optimization for graphite/bismaleimide–titanium alloy stacks. Composite structures, 63(1), 101-114.

[101] Lee, K., Dornfeld, D. A. (2005) Micro-burr formation and minimization through process control. Precision Engineering, 29(2), 246-252.

[102] Schultheiss, F., Johansson, D., Bushlya, V., Zhou, J., Nilsson, K., Ståhl, J. E. (2017) Comparative study on the machinability of lead-free brass. Journal of Cleaner Production, 149, 366-377.

[103] Mellinger, J.C., Ozdoganlar, O.B., Devor, R.E., Kapoor, S.G. (2002) Modelling chip-evcuation forces and prediction of chip-clogging in drilling. Journal of Manufacturing Science and Engineering, 124(3), 605-614.

[104] Bakkal, M., Shih, A.J., McSpadden, S.B., Liu, C.T., Scttergood, R.O. (2005) Light emission, chip morphology, and burr formation in drilling the bulk metallic glass. International Journal of Machine Tools and Manufacture, 45, 741-752.

[105] Wang, D. H., Ramulu, M., Arola, D. (1995) Orthogonal cutting mechanisms of graphite/epoxy composite. Part I: unidirectional laminate. International Journal of Machine Tools and Manufacture, 35(12), 1623-1638.

[106] Arola, D., Ramulu, M., Wang, D. H. (1996) Chip formation in orthogonal trimming of graphite/epoxy composite. Composites Part A: applied science and manufacturing, 27(2), 121-133.

APPENDICES

Appendix 1-1. Front side delamination factors for bare CFRP laminate micro-drilling experiments.

Run Order	Spindle Speed (rpm)	Feed (µm/rev)	Feed Rate (mm/min)	Front delamination factor 1	Front delamination factor 2	Front delamination factor 3	Front delamination factor 120	Front delamination factor 121	Front delamination factor 122	Front delamination factor 240	Front delamination factor 241	Front delamination factor 242
24	20000	3	60	1,045	1,055	1,038	1,066	1,315	1,098	1,849	1,229	1,460
36	20000	3	60	1,080	1,046	1,064	1,250	1,287	1,209	1,181	1,490	1,180
40	20000	3	60	1,008	1,018	1,043	1,101	1,134	1,296	1,315	1,230	1,487
29	20000	5	100	1,045	1,044	1,028	1,094	1,057	1,173	1,122	1,203	1,289
30	20000	5	100	1,072	1,056	1,076	1,227	1,118	1,092	1,223	1,055	1,147
38	20000	5	100	1,026	1,044	1,058	1,115	1,214	1,119	1,118	1,277	1,556
16	20000	7	140	1,087	1,094	1,062	1,228	1,383	1,222	1,207	1,049	1,114
42	20000	7	140	1,037	1,041	1,039	1,166	1,121	1,191	1,301	1,438	1,217
43	20000	7	140	1,063	1,078	1,045	1,180	1,537	1,096	1,090	1,073	1,077
15	30000	3	90	1,087	1,068	1,079	1,555	1,422	1,701	1,299	1,400	1,168
23	30000	3	90	1,046	1,074	1,114	1,834	1,094	1,193	1,815	1,561	1,178
35	30000	3	90	1,043	1,020	1,059	1,107	1,364	1,228	1,730	1,113	1,710
17	30000	5	150	1,059	1,091	1,043	1,180	1,140	1,118	1,251	1,323	1,149
21	30000	5	150	1,048	1,107	1,052	1,148	1,116	1,388	1,091	1,142	1,215
37	30000	5	150	1,046	1,040	1,055	1,163	1,183	1,107	1,120	1,246	1,433
27	30000	7	210	1,027	1,073	1,100	1,155	1,175	1,079	1,079	1,427	1,247
33	30000	7	210	1,051	1,027	1,032	1,112	1,232	1,081	1,056	1,387	1,254
34	30000	7	210	1,029	1,044	1,038	1,092	1,190	1,150	1,247	1,062	1,313
19	40000	3	120	1,028	1,046	1,025	1,380	1,505	1,079	1,125	1,277	1,202
20	40000	3	120	1,051	1,038	1,074	1,223	1,338	1,115	1,132	1,100	1,621
31	40000	3	120	1,053	1,045	1,102	1,630	1,666	1,308	1,302	1,203	1,762
28	40000	5	200	1,043	1,065	1,029	1,206	1,008	1,613	1,139	1,335	1,126
32	40000	5	200	1,026	1,013	1,107	1,266	1,376	1,204	1,137	1,331	1,666
41	40000	5	200	1,038	1,032	1,016	1,279	1,163	1,400	1,094	1,423	1,088
22	40000	7	280	1,061	1,047	1,054	1,481	1,057	1,083	1,103	1,481	1,096
26	40000	7	280	1,077	1,109	1,212	1,159	1,267	1,103	1,188	1,191	1,596
39	40000	7	280	1,015	1,033	1,017	1,372	1,038	1,600	1,773	1,263	1,349

Appendix 1-2. Rear side delamination factors for bare CFRP laminate micro-drilling experiments.

Run Order	Spindle Speed (rpm)	Feed (µm/rev)	Feed Rate (mm/min)	Rear delamination factor 1	Rear delamination factor 2	Rear delamination factor 3	Rear delamination factor 120	Rear delamination factor 121	Rear delamination factor 122	Rear delamination factor 240	Rear delamination factor 241	Rear delamination factor 242
24	20000	3	60	1,072	1,192	1,174	1,537	1,297	1,181	1,405	1,764	1,438
36	20000	3	60	1,308	1,462	1,360	1,212	2,015	1,449	1,574	1,246	1,191
40	20000	3	60	1,594	1,233	1,729	1,427	1,459	1,258	1,719	1,599	1,693
29	20000	5	100	1,042	1,135	1,322	1,302	1,234	1,125	1,355	1,371	1,419
30	20000	5	100	1,040	1,110	1,253	1,181	1,354	1,190	1,363	1,297	1,681
38	20000	5	100	1,050	1,313	1,538	1,561	1,509	1,361	1,552	1,419	1,658
16	20000	7	140	1,416	1,333	1,392	1,518	1,997	1,352	1,655	1,870	1,386
42	20000	7	140	1,189	1,451	1,204	1,358	1,292	1,155	1,254	1,315	1,313
43	20000	7	140	1,030	1,171	1,462	1,301	1,121	1,666	1,684	1,445	1,230
15	30000	3	90	1,551	1,175	1,107	1,386	1,485	1,051	1,409	1,507	1,601
23	30000	3	90	1,109	1,346	1,527	1,753	1,157	1,338	1,579	1,627	1,159
35	30000	3	90	1,383	1,242	1,221	1,447	1,536	1,387	1,403	1,327	1,474
17	30000	5	150	1,291	1,420	1,099	1,134	1,240	1,317	1,556	1,255	1,225
21	30000	5	150	1,121	1,194	1,128	1,245	1,642	1,161	1,220	1,466	1,418
37	30000	5	150	1,089	1,099	1,149	1,592	2,074	1,977	2,016	2,051	1,366
27	30000	7	210	1,078	1,251	1,061	1,496	1,280	1,254	1,263	1,516	1,343
33	30000	7	210	1,293	1,147	1,573	1,363	1,725	1,878	1,609	1,148	1,338
34	30000	7	210	1,182	1,166	1,257	1,238	1,388	1,519	1,715	1,413	1,286
19	40000	3	120	1,261	1,223	1,115	1,498	1,171	1,122	1,246	1,422	1,404
20	40000	3	120	1,163	1,166	1,169	1,360	1,354	1,043	1,179	1,347	1,425
31	40000	3	120	1,080	1,426	1,232	1,380	1,555	1,436	1,410	1,345	1,204
28	40000	5	200	1,474	1,219	1,441	1,225	1,370	1,567	1,224	1,443	1,371
32	40000	5	200	1,093	1,110	1,129	1,829	1,472	1,308	1,356	1,804	1,521
41	40000	5	200	1,080	1,087	1,220	1,257	1,487	1,190	1,406	1,362	1,503
22	40000	7	280	1,180	1,244	1,108	1,320	1,415	1,314	1,415	1,403	1,386
26	40000	7	280	1,109	1,039	1,061	1,213	1,248	1,234	1,444	1,217	1,207
39	40000	7	280	1,163	1,085	1,146	1,254	1,413	1,399	1,348	1,492	1,285

Appendix 1-3. Front side damage factors for CFRP laminate with Aluminum-Phenolic support plate micro-drilling experiments.

Run Order	Spindle Speed (rpm)	Feed (µm/rev)	Feed Rate (mm/min)	Front delamination factor 1	Front delamination factor 2	Front delamination factor 3	Front delamination factor 120	Front delamination factor 121	Front delamination factor 122	Front delamination factor 240	Front delamination factor 241	Front delamination factor 242
53	20000	3	60	1,203	1,194	1,162	1,154	1,118	1,144	1,209	1,234	1,261
60	20000	3	60	1,266	1,191	1,212	1,135	1,216	1,192	1,192	1,205	1,213
64	20000	3	60	1,140	1,237	1,155	1,180	1,187	1,165	1,200	1,170	1,202
45	20000	5	100	1,175	1,018	1,121	1,197	1,210	1,171	1,219	1,237	1,220
49	20000	5	100	1,190	1,198	1,167	1,234	1,228	1,213	1,230	1,240	1,260
59	20000	5	100	1,242	1,218	1,258	1,224	1,255	1,199	1,300	1,246	1,216
50	20000	7	140	1,018	1,204	1,229	1,154	1,176	1,196	1,254	1,157	1,187
57	20000	7	140	1,189	1,184	1,257	1,205	1,222	1,189	1,207	1,204	1,247
58	20000	7	140	1,275	1,205	1,274	1,257	1,196	1,155	1,199	1,225	1,207
46	30000	3	90	1,162	1,256	1,202	1,183	1,154	1,202	1,189	1,225	1,211
54	30000	3	90	1,230	1,014	1,123	1,181	1,128	1,194	1,172	1,201	1,144
66	30000	3	90	1,122	1,188	1,163	1,188	1,157	1,134	1,180	1,188	1,182
56	30000	5	150	1,196	1,043	1,121	1,164	1,173	1,168	1,225	1,198	1,178
65	30000	5	150	1,355	1,272	1,240	1,176	1,201	1,209	1,222	1,252	1,256
70	30000	5	150	1,139	1,223	1,175	1,199	1,184	1,206	1,207	1,271	1,186
52	30000	7	210	1,207	1,217	1,180	1,184	1,225	1,259	1,200	1,211	1,317
67	30000	7	210	1,167	1,198	1,196	1,171	1,163	1,163	1,159	1,169	1,182
69	30000	7	210	1,130	1,134	1,171	1,156	1,156	1,235	1,207	1,199	1,211
48	40000	3	120	1,115	1,125	1,337	1,214	1,119	1,153	1,160	1,208	1,174
55	40000	3	120	1,147	1,170	1,130	1,173	1,152	1,184	1,182	1,239	1,176
61	40000	3	120	1,081	1,245	1,186	1,259	1,194	1,151	1,219	1,197	1,169
47	40000	5	200	1,171	1,033	1,150	1,185	1,177	1,163	1,171	1,177	1,202
51	40000	5	200	1,175	1,110	1,099	1,159	1,158	1,178	1,248	1,147	1,165
68	40000	5	200	1,206	1,263	1,223	1,197	1,150	1,202	1,175	1,175	1,189
44	40000	7	280	1,020	1,131	1,227	1,148	1,181	1,222	1,206	1,170	1,211
62	40000	7	280	1,147	1,204	1,189	1,173	1,195	1,198	1,223	1,202	1,180
63	40000	7	280	1,228	1,122	1,198	1,155	1,164	1,203	1,191	1,236	1,195

Appendix 1-4. Rear side delamination factors for CFRP laminate with Aluminum-Phenolic support plate micro-drilling experiments.

Run Order	Spindle Speed (rpm)	Feed (µm/rev)	Feed Rate (mm/min)	Rear delamination factor 1	Rear delamination factor 2	Rear delamination factor 3	Rear delamination factor 120	Rear delamination factor 121	Rear delamination factor 122	Rear delamination factor 240	Rear delamination factor 241	Rear delamination factor 242
53	20000	3	60	1,489	1,273	1,284	1,584	1,487	1,107	1,384	1,520	1,484
60	20000	3	60	1,295	1,294	1,331	1,154	1,582	1,399	1,355	1,601	1,408
64	20000	3	60	1,581	1,490	1,254	1,672	1,485	1,450	1,398	1,215	1,559
45	20000	5	100	1,046	1,313	1,386	1,657	1,375	1,318	1,228	1,208	1,198
49	20000	5	100	1,408	1,385	1,247	1,346	1,530	1,559	1,302	1,394	1,760
59	20000	5	100	1,246	1,404	1,263	1,319	1,506	1,619	1,343	1,486	1,708
50	20000	7	140	1,132	1,470	1,110	1,845	1,507	1,411	1,613	1,333	1,516
57	20000	7	140	1,349	1,308	1,463	1,707	1,364	1,700	1,753	1,250	1,293
58	20000	7	140	1,849	1,248	1,192	1,288	1,238	1,376	1,309	1,552	1,616
46	30000	3	90	1,308	1,353	1,223	1,415	1,416	1,233	1,847	1,522	1,469
54	30000	3	90	1,080	1,176	1,265	1,298	1,314	1,216	1,163	1,222	1,441
66	30000	3	90	1,367	1,205	1,331	1,470	1,412	1,260	1,320	1,640	1,350
56	30000	5	150	1,270	1,082	1,231	1,313	1,375	1,516	1,439	1,555	1,566
65	30000	5	150	1,688	1,201	1,166	1,376	1,275	1,454	1,391	1,315	1,384
70	30000	5	150	1,322	1,240	1,205	1,473	1,177	1,484	1,365	1,299	1,268
52	30000	7	210	1,029	1,470	1,142	1,269	1,376	1,326	1,456	1,450	1,297
67	30000	7	210	1,172	1,435	1,255	1,219	1,304	1,239	1,319	1,480	1,244
69	30000	7	210	1,143	1,226	1,328	1,550	1,318	1,278	1,097	1,330	1,167
48	40000	3	120	1,309	1,121	1,298	1,212	1,221	1,561	1,423	1,391	1,326
55	40000	3	120	1,542	1,152	1,268	1,504	1,487	1,393	1,364	1,479	1,914
61	40000	3	120	1,208	1,275	1,297	1,255	1,452	1,542	1,279	1,390	1,241
47	40000	5	200	1,131	1,245	1,487	1,752	1,566	1,428	1,304	1,137	1,188
51	40000	5	200	1,208	1,083	1,288	1,407	1,344	1,419	1,190	1,671	1,366
68	40000	5	200	1,140	1,172	1,256	1,306	1,484	1,067	1,513	1,565	1,556
44	40000	7	280	1,039	1,138	1,139	1,335	1,098	1,157	1,357	1,234	1,247
62	40000	7	280	1,296	1,249	1,183	1,296	1,312	1,176	1,345	1,833	2,579
63	40000	7	280	1,360	1,184	1,467	1,525	1,470	1,595	1,331	1,230	1,436

Appendix 1-5. Front side damage factors for CFRP laminate with Brass-Wood support plate micro-drilling experiments.

Run Order	Spindle Speed (rpm)	Feed (µm/rev)	Feed Rate (mm/min)	Front delamination factor 1	Front delamination factor 2	Front delamination factor 3	Front delamination factor 120	Front delamination factor 121	Front delamination factor 122	Front delamination factor 240	Front delamination factor 241	Front delamination factor 242
77	20000	3	60	1,006	1,068	1,024	1,263	1,263	1,162	1,142	1,178	1,181
81	20000	3	60	1,030	1,031	1,063	1,165	1,181	1,143	1,262	1,278	1,456
75	20000	5	100	1,023	1,039	1,035	1,125	1,157	1,167	1,198	1,170	1,233
82	20000	5	100	1,021	1,031	1,069	1,094	1,125	1,138	1,193	1,255	1,218
79	20000	7	140	1,009	1,033	1,073	1,083	1,113	1,134	1,269	1,218	1,101
89	20000	7	140	1,032	1,055	1,046	1,094	1,138	1,094	1,186	1,202	1,332
80	30000	3	90	1,023	1,037	1,087	1,226	1,118	1,153	1,140	1,203	1,225
83	30000	3	90	1,037	1,032	1,044	1,103	1,128	1,170	1,164	1,308	1,254
73	30000	5	150	1,014	1,013	1,068	1,141	1,228	1,187	1,179	1,237	1,224
86	30000	5	150	1,025	1,035	1,040	1,181	1,195	1,185	1,182	1,162	1,408
74	30000	7	210	1,030	1,033	1,031	1,101	1,106	1,115	1,235	1,156	1,112
88	30000	7	210	1,022	1,028	1,043	1,101	1,154	1,143	1,152	1,197	1,205
78	40000	3	120	1,075	1,056	1,044	1,173	1,153	1,157	1,259	1,096	1,205
85	40000	3	120	1,017	1,023	1,029	1,107	1,196	1,117	1,284	1,257	1,305
76	40000	5	200	1,041	1,060	1,038	1,072	1,086	1,133	1,228	1,308	1,253
87	40000	5	200	1,157	1,057	1,040	1,133	1,181	1,209	1,130	1,188	1,408
72	40000	7	280	1,021	1,045	1,017	1,146	1,127	1,157	1,171	1,165	1,209
84	40000	7	280	1,030	1,080	1,040	1,249	1,163	1,087	1,166	1,134	1,235

Appendix 1-6. Rear side delamination factors for CFRP laminate with Brass-Wood support plate micro-drilling experiments.

Run Order	Spindle Speed (rpm)	Feed (µm/rev)	Feed Rate (mm/min)	Rear delamination factor 1	Rear delamination factor 2	Rear delamination factor 3	Rear delamination factor 120	Rear delamination factor 121	Rear delamination factor 122	Rear delamination factor 240	Rear delamination factor 241	Rear delamination factor 242
77	20000	3	60	1,133	1,165	1,152	1,369	1,270	1,527	1,508	1,418	1,334
81	20000	3	60	1,243	1,062	1,132	1,399	1,517	1,392	1,247	1,273	1,921
75	20000	5	100	1,206	1,251	1,243	1,786	1,354	1,503	1,704	1,453	1,332
82	20000	5	100	1,080	1,282	1,252	1,323	1,181	1,456	1,202	1,315	1,256
79	20000	7	140	1,109	1,300	1,229	1,379	1,671	1,183	1,498	1,497	1,405
89	20000	7	140	1,188	1,126	1,251	1,496	1,284	1,328	1,628	1,320	1,270
80	30000	3	90	1,417	1,327	1,318	1,495	1,565	1,249	1,280	1,398	1,440
83	30000	3	90	1,199	1,185	1,285	1,313	1,342	1,264	1,226	1,436	1,591
73	30000	5	150	1,397	1,188	1,127	1,664	1,311	1,170	1,297	1,354	1,617
86	30000	5	150	1,271	1,382	1,265	1,785	1,423	1,370	1,695	1,367	1,655
74	30000	7	210	1,051	1,281	1,160	1,512	1,216	1,526	1,703	1,413	1,280
88	30000	7	210	1,042	1,345	1,186	1,537	1,336	1,382	1,730	1,513	1,673
78	40000	3	120	1,101	1,361	1,216	1,192	1,287	1,473	1,609	1,247	1,276
85	40000	3	120	1,263	1,113	1,387	1,441	1,363	1,758	1,557	1,714	1,289
76	40000	5	200	1,290	1,144	1,332	1,288	1,292	1,162	1,597	1,238	1,296
87	40000	5	200	1,225	1,174	1,187	1,639	1,273	1,507	1,254	1,211	1,369
72	40000	7	280	1,233	1,254	1,228	1,221	1,207	1,197	1,650	1,726	1,482
84	40000	7	280	1,168	1,158	1,170	1,855	2,090	1,792	1,693	1,650	1,596

Appendix 2-1. Front side hole diameters for bare CFRP laminate micro-drilling experiments.

Run Order	Spindle Speed (rpm)	Feed (µm/rev)	Feed Rate (mm/min)	Diameter front 1	Diameter front 2	Diameter front 3	Diameter front 120	Diameter front 121	Diameter front 122	Diameter front 240	Diameter front 241	Diameter front 242
24	20000	3	60	507,2	504,6	502,5	478,0	486,9	493,9	505,1	496,9	495,6
36	20000	3	60	509,2	510,0	505,9	495,0	510,9	510,2	489,1	498,3	502,4
40	20000	3	60	497,9	496,9	496,0	487,8	490,7	495,2	497,3	490,2	486,3
29	20000	5	100	499,3	496,9	498,4	496,2	491,5	507,6	510,6	505,5	503,2
30	20000	5	100	511,5	510,2	517,4	499,9	509,1	502,7	499,8	495,8	511,9
38	20000	5	100	504,7	504,1	501,2	510,6	524,1	503,2	494,0	505,9	528,0
16	20000	7	140	507,4	502,3	507,3	502,2	499,3	499,2	495,6	495,3	494,1
42	20000	7	140	505,5	503,7	504,3	486,0	496,3	489,8	506,8	507,1	499,8
43	20000	7	140	498,8	503,4	502,0	492,4	505,5	490,6	490,9	499,7	510,5
15	30000	3	90	506,3	501,6	502,7	492,1	499,6	520,0	499,6	502,4	511,3
23	30000	3	90	503,8	506,0	504,4	504,8	502,3	506,3	488,3	496,9	503,2
35	30000	3	90	500,5	500,4	500,4	488,2	500,4	492,5	498,4	492,5	498,8
17	30000	5	150	507,4	510,3	505,2	505,2	503,0	499,9	502,3	496,4	490,1
21	30000	5	150	511,7	507,1	500,5	498,5	491,6	494,0	490,5	505,5	497,2
37	30000	5	150	508,1	502,3	507,2	490,6	500,0	499,1	495,7	500,3	493,9
27	30000	7	210	506,5	508,1	500,3	497,2	499,9	495,5	494,8	509,4	488,7
33	30000	7	210	505,8	497,8	496,5	491,4	489,4	493,6	497,4	498,0	495,1
34	30000	7	210	500,9	501,5	501,6	502,1	511,4	492,7	497,6	498,4	513,2
19	40000	3	120	499,5	498,9	495,9	495,8	483,4	498,0	501,4	510,2	494,3
20	40000	3	120	504,8	501,9	506,9	496,5	501,4	497,9	481,1	492,9	484,6
31	40000	3	120	498,3	502,4	499,8	497,5	506,5	485,6	483,1	482,9	485,2
28	40000	5	200	502,0	500,0	498,8	499,8	491,8	496,5	489,4	482,8	502,9
32	40000	5	200	502,4	502,0	501,8	495,4	501,9	493,4	497,8	496,2	497,6
41	40000	5	200	505,0	502,0	502,3	506,4	498,7	497,1	500,2	505,3	496,1
22	40000	7	280	507,8	503,3	506,2	493,9	494,2	490,3	491,0	487,2	487,4
26	40000	7	280	505,6	508,4	506,1	500,8	492,4	511,3	517,0	486,4	493,6
39	40000	7	280	500,9	490,1	494,1	494,1	493,9	506,2	489,9	485,4	482,9

Appendix 2-2. Rear side hole diameters for bare CFRP laminate micro-drilling experiments.

Run Order	Spindle Speed (rpm)	Feed (µm/rev)	Feed Rate (mm/min)	Diameter rear 1	Diameter rear 2	Diameter rear 3	Diameter rear 120	Diameter rear 121	Diameter rear 122	Diameter rear 240	Diameter rear 241	Diameter rear 242
24	20000	3	60	489,8	494,0	486,9	478,3	472,1	465,1	471,9	477,1	489,0
36	20000	3	60	498,9	492,3	491,9	490,1	488,2	488,8	500,0	491,1	482,4
40	20000	3	60	492,9	496,8	488,2	501,4	482,6	482,9	483,2	491,6	480,6
29	20000	5	100	489,4	492,0	493,4	487,7	502,8	478,1	488,6	482,5	488,7
30	20000	5	100	494,3	503,0	503,8	489,5	492,0	486,3	496,2	481,3	478,4
38	20000	5	100	497,3	506,3	504,6	485,5	468,2	470,7	482,1	479,6	480,0
16	20000	7	140	495,5	500,0	497,1	483,5	529,7	488,0	503,2	482,0	492,5
42	20000	7	140	505,0	495,2	496,8	497,7	488,4	484,2	477,6	479,3	483,8
43	20000	7	140	500,9	500,7	500,6	465,3	484,5	479,4	488,5	483,4	478,3
15	30000	3	90	496,9	495,8	486,7	487,1	466,5	520,0	486,6	491,7	471,8
23	30000	3	90	490,1	491,3	485,9	468,2	476,1	467,3	482,8	478,0	479,1
35	30000	3	90	492,0	496,3	496,0	477,1	481,8	474,4	470,1	475,3	478,3
17	30000	5	150	495,8	499,8	489,6	484,5	481,6	482,2	480,0	475,1	485,0
21	30000	5	150	498,6	495,7	482,5	478,6	481,4	486,4	481,7	483,3	474,1
37	30000	5	150	493,2	492,8	485,8	481,0	472,8	478,3	491,4	476,3	485,4
27	30000	7	210	493,5	493,0	482,2	484,5	477,2	484,7	480,7	499,6	492,0
33	30000	7	210	505,5	491,6	499,1	495,5	488,5	500,8	489,5	485,5	490,8
34	30000	7	210	497,0	498,6	499,3	481,4	477,7	489,2	478,9	479,7	491,6
19	40000	3	120	495,7	493,5	495,0	469,7	475,8	470,9	476,7	496,1	475,8
20	40000	3	120	498,2	501,0	499,4	477,0	486,6	486,6	472,9	492,3	482,7
31	40000	3	120	488,2	484,5	487,9	480,2	496,8	484,6	489,5	490,5	485,9
28	40000	5	200	496,3	491,8	491,5	505,5	481,9	488,0	481,6	475,4	488,5
32	40000	5	200	493,3	486,1	494,0	478,7	490,8	487,6	481,4	490,7	485,8
41	40000	5	200	496,1	505,8	499,9	494,9	476,1	490,7	478,4	483,2	482,7
22	40000	7	280	483,5	484,1	489,9	478,0	476,3	490,2	485,8	491,0	477,6
26	40000	7	280	479,4	491,4	482,3	482,3	486,5	479,2	494,9	483,2	492,7
39	40000	7	280	490,5	491,2	497,4	480,9	478,5	484,4	487,4	477,3	479,5

Appendix 2-3. Front side hole diameters for CFRP laminate with Aluminum-Phenolic support plate micro-drilling experiments.

Run Order	Spindle Speed (rpm)	Feed (µm/rev)	Feed Rate (mm/min)	Diameter front 1	Diameter front 2	Diameter front 3	Diameter front 120	Diameter front 121	Diameter front 122	Diameter front 240	Diameter front 241	Diameter front 242
53	20000	3	60	514,6	513,8	513,9	502,5	504,1	507,5	503,9	507,8	501,3
60	20000	3	60	509,8	517,0	512,6	517,6	507,9	513,2	511,6	504,5	502,8
64	20000	3	60	505,2	512,5	512,0	516,1	514,7	501,7	505,2	507,6	515,6
45	20000	5	100	499,7	496,1	498,3	499,9	499,0	496,3	505,0	502,0	505,0
49	20000	5	100	516,6	506,4	507,4	505,7	510,2	507,6	506,9	508,1	507,4
59	20000	5	100	509,7	504,5	510,9	498,8	502,7	503,9	520,0	502,9	502,0
50	20000	7	140	496,3	508,9	512,7	503,7	497,3	495,5	496,6	504,3	503,4
57	20000	7	140	507,3	506,3	517,2	500,6	500,9	503,3	498,0	504,9	504,2
58	20000	7	140	530,2	510,1	530,0	513,7	510,2	504,8	506,1	518,3	506,2
46	30000	3	90	498,0	500,9	509,7	506,4	500,2	506,6	511,2	509,7	501,1
54	30000	3	90	525,4	499,0	500,9	497,4	503,1	504,3	497,8	499,4	500,4
66	30000	3	90	507,1	508,2	503,3	499,2	499,6	502,9	512,1	509,8	503,9
56	30000	5	150	503,4	500,9	501,2	510,1	510,0	504,8	503,1	505,5	499,9
65	30000	5	150	509,6	513,4	518,5	508,3	503,1	506,0	511,8	508,5	505,0
70	30000	5	150	504,8	510,1	510,4	504,2	503,6	506,7	510,5	509,1	506,0
52	30000	7	210	511,4	512,6	504,8	510,8	512,1	527,2	502,1	506,6	506,6
67	30000	7	210	510,1	524,5	512,9	508,4	499,7	505,7	497,1	503,9	515,9
69	30000	7	210	510,5	503,3	522,9	501,9	508,2	523,0	504,6	502,0	507,0
48	40000	3	120	493,9	498,6	519,3	501,1	499,0	493,8	495,7	506,4	506,3
55	40000	3	120	504,9	500,8	503,8	499,0	504,1	505,5	501,1	503,2	511,1
61	40000	3	120	508,0	509,8	515,6	502,3	506,9	507,3	510,1	511,2	503,2
47	40000	5	200	507,6	499,0	502,3	500,2	505,4	512,6	509,8	505,4	504,8
51	40000	5	200	509,1	502,1	504,4	506,3	504,9	501,9	504,6	510,6	510,9
68	40000	5	200	514,6	521,1	504,8	502,0	504,8	502,4	502,5	501,6	503,5
44	40000	7	280	499,9	506,1	501,2	504,2	498,0	498,1	504,4	503,6	501,7
62	40000	7	280	502,7	519,4	513,7	510,2	509,6	511,0	510,3	504,2	504,3
63	40000	7	280	521,8	514,1	525,3	499,5	498,4	495,3	511,5	507,7	505,8

Appendix 2-4. Rear side hole diameters for CFRP laminate with Aluminum-Phenolic support plate micro-drilling experiments.

Run Order	Spindle Speed (rpm)	Feed (µm/rev)	Feed Rate (mm/min)	Diameter rear 1	Diameter rear 2	Diameter rear 3	Diameter rear 120	Diameter rear 121	Diameter rear 122	Diameter rear 240	Diameter rear 241	Diameter rear 242
53	20000	3	60	516,0	504,0	506,9	491,4	487,9	480,4	486,2	496,1	521,1
60	20000	3	60	506,4	506,1	507,6	474,1	482,4	483,3	493,0	485,6	479,4
64	20000	3	60	506,7	505,3	494,6	499,7	492,0	490,2	473,0	482,9	483,4
45	20000	5	100	491,1	483,9	498,3	522,3	490,7	484,5	497,2	480,8	472,3
49	20000	5	100	497,2	490,7	497,3	491,8	497,9	499,6	497,5	494,7	517,6
59	20000	5	100	495,0	493,8	490,5	489,9	502,2	494,1	500,5	492,4	505,4
50	20000	7	140	495,4	509,2	497,6	492,0	481,8	490,3	490,4	493,2	487,5
57	20000	7	140	495,2	487,5	493,6	499,6	491,8	492,0	495,1	485,6	502,5
58	20000	7	140	495,6	494,3	498,4	489,8	491,0	496,6	494,3	494,9	487,1
46	30000	3	90	500,6	501,2	495,4	486,8	494,7	488,6	486,8	477,5	488,0
54	30000	3	90	493,8	487,6	487,1	483,5	492,8	480,2	501,3	488,2	477,9
66	30000	3	90	504,7	499,7	500,6	493,1	498,5	489,7	483,2	481,5	492,6
56	30000	5	150	490,1	494,8	493,8	490,2	496,8	493,4	495,3	497,1	490,1
65	30000	5	150	477,5	494,2	494,8	491,0	485,1	492,8	497,5	489,0	503,4
70	30000	5	150	498,3	499,7	490,1	502,6	491,4	491,6	479,9	473,9	481,4
52	30000	7	210	490,8	497,8	494,5	502,1	507,1	495,5	493,6	507,0	490,7
67	30000	7	210	497,8	497,6	498,4	486,8	479,3	482,2	492,1	484,6	501,8
69	30000	7	210	498,1	495,6	495,0	490,0	490,6	494,4	482,5	482,4	485,1
48	40000	3	120	492,4	492,9	487,6	503,0	486,1	482,9	477,5	477,6	476,0
55	40000	3	120	492,6	490,4	495,5	497,0	501,7	476,1	508,6	482,4	485,3
61	40000	3	120	505,9	496,1	500,5	484,1	493,7	491,7	481,0	494,9	490,0
47	40000	5	200	503,6	508,5	505,5	492,0	513,0	495,2	483,3	491,0	493,8
51	40000	5	200	496,3	493,5	493,9	494,9	499,4	489,1	482,8	486,2	476,6
68	40000	5	200	486,2	485,2	492,6	489,3	478,1	480,6	484,7	494,2	471,0
44	40000	7	280	496,8	500,5	490,3	494,5	495,1	485,9	493,0	489,8	484,9
62	40000	7	280	509,3	499,1	502,6	490,5	485,6	484,4	493,8	499,6	501,8
63	40000	7	280	494,5	490,5	492,2	487,2	493,0	491,5	480,2	482,3	482,9

Appendix 2-5. Front side hole diameters for CFRP laminate with Brass-Wood support plate micro-drilling experiments.

Run Order	Spindle Speed (rpm)	Feed (µm/rev)	Feed Rate (mm/min)	Diameter front 1	Diameter front 2	Diameter front 3	Diameter front 120	Diameter front 121	Diameter front 122	Diameter front 240	Diameter front 241	Diameter front 242
77	20000	3	60	495,6	494,9	498,4	497,0	489,7	494,2	488,2	490,9	490,7
81	20000	3	60	500,7	495,7	496,0	493,8	497,5	498,0	498,5	498,6	503,8
75	20000	5	100	505,0	506,1	507,5	498,4	498,8	497,0	494,9	498,7	495,0
82	20000	5	100	496,5	492,4	489,4	485,4	489,8	496,2	504,4	491,1	495,0
79	20000	7	140	497,5	497,2	503,6	494,1	499,7	504,7	509,2	501,9	498,0
89	20000	7	140	500,1	511,2	500,3	495,4	493,5	493,3	510,1	504,6	498,1
80	30000	3	90	497,3	504,1	503,8	518,9	496,0	496,7	500,4	501,7	497,2
83	30000	3	90	505,1	495,3	500,3	497,4	495,1	496,0	495,9	496,1	493,5
73	30000	5	150	499,0	498,7	503,0	501,8	496,3	493,4	490,7	491,3	489,6
86	30000	5	150	505,7	505,7	495,9	493,8	503,9	503,0	486,4	495,1	519,0
74	30000	7	210	507,0	493,0	494,9	503,6	508,7	505,9	494,7	496,8	499,9
88	30000	7	210	504,1	497,6	503,9	497,3	503,4	502,1	496,7	504,7	503,1
78	40000	3	120	508,0	503,5	505,0	500,2	498,4	496,7	489,6	493,2	491,9
85	40000	3	120	492,6	495,5	496,4	494,2	495,3	496,0	495,7	492,3	489,3
76	40000	5	200	500,1	495,8	492,9	494,0	490,5	495,6	495,3	505,3	491,1
87	40000	5	200	502,5	506,3	497,9	495,6	503,0	501,4	489,8	496,9	506,8
72	40000	7	280	504,1	496,9	499,3	506,5	501,9	508,3	499,7	504,8	505,0
84	40000	7	280	503,9	512,5	504,0	513,8	509,1	506,5	500,7	504,9	523,0

Appendix 2-6. Rear side hole diameters for CFRP laminate with Brass-Wood support plate micro-drilling experiments.

Run Order	Spindle Speed (rpm)	Feed (µm/rev)	Feed Rate (mm/min)	Diameter rear 1	Diameter rear 2	Diameter rear 3	Diameter rear 120	Diameter rear 121	Diameter rear 122	Diameter rear 240	Diameter rear 241	Diameter rear 242
77	20000	3	60	494,4	480,0	488,4	470,8	477,1	480,1	477,8	504,0	484,9
81	20000	3	60	496,2	495,1	499,6	483,3	481,1	486,4	480,8	489,6	480,8
75	20000	5	100	502,3	500,1	502,2	486,1	494,6	483,5	508,5	488,1	487,1
82	20000	5	100	496,9	509,4	516,1	493,9	495,7	494,6	472,5	480,9	481,9
79	20000	7	140	497,0	501,1	501,3	483,6	491,3	490,6	481,6	473,4	478,8
89	20000	7	140	492,4	501,8	489,4	489,9	492,3	497,8	493,2	493,8	492,0
80	30000	3	90	499,2	502,9	498,9	490,5	484,2	488,7	482,8	470,0	468,6
83	30000	3	90	490,9	496,7	495,4	472,3	479,2	471,4	479,3	482,7	490,9
73	30000	5	150	501,6	501,0	490,1	491,4	494,9	493,3	482,0	484,4	479,2
86	30000	5	150	499,0	497,4	497,4	486,4	498,8	486,0	488,9	481,1	498,9
74	30000	7	210	500,1	500,4	494,5	497,0	490,1	489,7	487,9	482,1	488,5
88	30000	7	210	504,7	496,8	495,3	483,4	496,6	486,3	491,1	480,5	498,2
78	40000	3	120	499,5	504,6	496,9	495,8	499,8	493,4	486,1	477,8	477,2
85	40000	3	120	498,3	497,6	493,7	483,7	477,9	489,6	476,0	465,6	473,3
76	40000	5	200	482,9	489,3	493,6	477,3	473,2	480,2	478,4	478,7	474,0
87	40000	5	200	499,9	500,5	495,3	480,7	490,7	485,1	486,3	484,8	487,8
72	40000	7	280	499,3	499,3	500,2	493,2	494,0	490,3	493,8	485,7	500,5
84	40000	7	280	498,4	494,4	495,1	480,2	492,9	498,4	482,5	485,1	485,0

Appendix 3-1. Front side roundness errors for bare CFRP laminate micro-drilling experiments.

Run Order	Spindle Speed (rpm)	Feed (µm/rev)	Feed Rate (mm/min)	Roundness front 1	Roundness front 2	Roundness front 3	Roundness front 120	Roundness front 121	Roundness front 122	Roundness front 240	Roundness front 241	Roundness front 242
24	20000	3	60	4,8	5,1	7,7	14,4	5,0	12,3	18,3	4,2	14,3
36	20000	3	60	2,8	4,4	4,8	7,1	10,2	12,4	15,2	35,0	27,7
40	20000	3	60	2,9	1,7	5,3	10,6	8,1	11,1	18,7	6,3	17,9
29	20000	5	100	5,1	5,9	5,6	9,4	8,6	12,9	8,6	12,5	18,1
30	20000	5	100	7,8	6,5	6,9	12,2	10,0	7,6	6,1	8,0	16,7
38	20000	5	100	4,1	6,8	6,4	12,0	7,0	12,1	7,9	13,0	11,3
16	20000	7	140	3,0	6,8	5,6	12,5	8,2	5,6	13,7	5,3	12,3
42	20000	7	140	0,9	2,8	4,5	19,3	28,7	16,7	18,8	9,4	22,7
43	20000	7	140	5,9	6,6	4,3	11,9	14,4	6,8	17,8	7,8	11,9
15	30000	3	90	8,1	6,1	5,4	9,9	10,4	13,4	19,2	14,1	15,0
23	30000	3	90	6,9	6,8	7,3	7,1	15,4	9,6	9,4	13,3	8,4
35	30000	3	90	5,4	4,9	4,9	4,7	27,1	12,9	16,7	8,8	12,1
17	30000	5	150	6,4	6,0	4,9	4,9	12,3	6,9	21,3	16,6	17,4
21	30000	5	150	4,8	6,8	5,7	5,8	5,6	11,2	18,5	23,3	12,9
37	30000	5	150	10,3	4,9	7,2	20,3	13,1	11,7	9,5	9,7	12,8
27	30000	7	210	5,2	5,8	3,6	3,5	10,0	14,7	7,0	17,1	11,1
33	30000	7	210	8,1	8,3	2,9	16,2	16,7	5,6	5,0	4,3	9,7
34	30000	7	210	3,3	9,7	7,7	16,7	18,6	10,6	5,2	9,6	17,1
19	40000	3	120	6,2	7,1	2,2	17,6	17,2	11,0	21,0	16,5	6,6
20	40000	3	120	3,9	8,2	15,6	6,4	13,0	2,8	8,3	13,4	13,1
31	40000	3	120	7,3	4,8	6,4	7,9	23,1	14,9	12,5	5,7	16,1
28	40000	5	200	6,2	5,4	7,0	5,4	5,9	10,3	8,9	19,3	7,3
32	40000	5	200	5,6	2,9	6,7	6,9	13,6	6,4	19,2	8,7	11,6
41	40000	5	200	4,9	3,7	5,4	7,6	14,1	9,2	9,0	13,3	12,0
22	40000	7	280	6,6	5,1	6,9	20,7	10,4	14,5	12,4	24,5	8,0
26	40000	7	280	6,4	5,5	3,8	11,1	14,8	13,3	14,5	13,0	14,9
39	40000	7	280	4,5	12,9	4,8	9,9	17,6	12,1	5,6	18,3	7,2

Appendix 3-2. Rear side roundness errors for bare CFRP laminate micro-drilling experiments.

Run Order	Spindle Speed (rpm)	Feed (µm/rev)	Feed Rate (mm/min)	Roundness rear 1	Roundness rear 2	Roundness rear 3	Roundness rear 120	Roundness rear 121	Roundness rear 122	Roundness rear 240	Roundness rear 241	Roundness rear 242
24	20000	3	60	5,1	8,1	18,4	10,9	20,6	8,3	18,3	18,2	13,9
36	20000	3	60	13,3	12,9	11,7	10,8	9,5	23,6	11,1	12,8	13,4
40	20000	3	60	8,0	11,4	6,2	16,7	20,0	28,3	6,1	16,6	10,3
29	20000	5	100	19,3	6,5	6,4	18,7	4,5	13,0	12,6	17,6	20,5
30	20000	5	100	8,6	7,0	8,4	10,5	12,2	9,8	16,9	18,7	13,2
38	20000	5	100	3,3	9,6	11,4	17,4	26,2	17,0	6,0	21,8	10,8
16	20000	7	140	9,2	6,4	11,8	13,7	7,6	8,2	14,5	14,4	10,4
42	20000	7	140	7,8	12,5	20,7	10,6	19,5	8,9	30,0	32,4	9,9
43	20000	7	140	10,9	6,2	8,0	21,8	16,9	13,4	21,2	13,1	17,9
15	30000	3	90	7,0	8,0	22,5	17,7	57,3	13,4	21,6	9,1	5,4
23	30000	3	90	19,9	9,8	20,1	18,7	21,0	22,3	23,5	23,6	12,7
35	30000	3	90	5,1	11,4	2,2	7,5	14,1	14,2	25,9	17,3	16,6
17	30000	5	150	7,1	3,9	17,9	6,4	21,1	16,7	21,7	18,8	28,8
21	30000	5	150	5,1	4,7	13,1	8,3	10,1	11,8	11,0	19,4	25,8
37	30000	5	150	9,4	4,3	16,7	9,4	14,2	11,5	15,4	26,1	8,9
27	30000	7	210	7,9	10,3	15,3	8,1	19,8	7,0	6,5	16,4	19,5
33	30000	7	210	7,7	12,7	5,2	5,7	8,2	7,2	11,6	12,7	3,3
34	30000	7	210	7,2	4,5	11,1	10,2	23,3	15,9	8,5	14,8	11,4
19	40000	3	120	8,9	13,6	7,7	31,7	19,8	27,6	25,4	19,9	31,6
20	40000	3	120	7,3	6,1	6,3	23,4	13,2	13,2	14,5	13,3	13,7
31	40000	3	120	17,0	5,8	8,3	18,8	16,2	14,6	16,6	18,8	13,7
28	40000	5	200	9,1	7,5	10,6	7,1	16,8	11,0	24,4	13,4	8,7
32	40000	5	200	13,5	8,5	7,7	3,8	10,0	9,2	23,2	20,8	14,3
41	40000	5	200	11,4	6,2	3,6	11,6	12,8	5,9	17,1	15,2	16,6
22	40000	7	280	12,2	13,4	7,7	8,5	27,7	7,1	23,2	10,0	17,0
26	40000	7	280	22,6	4,1	18,5	18,5	11,3	11,5	9,8	12,0	8,8
39	40000	7	280	11,1	12,9	7,3	8,5	18,2	21,0	12,1	14,4	14,7

Appendix 3-3. Front side roundness errors for CFRP laminate with Aluminum-Phenolic support plate micro-drilling experiments.

Run Order	Spindle Speed (rpm)	Feed (µm/rev)	Feed Rate (mm/min)	Roundness front 1	Roundness front 2	Roundness front 3	Roundness front 120	Roundness front 121	Roundness front 122	Roundness front 240	Roundness front 241	Roundness front 242
53	20000	3	60	3,4	2,1	5,5	9,9	2,6	2,1	5,4	4,5	1,5
60	20000	3	60	8,9	5,4	7,6	8,3	8,9	10,5	6,7	4,7	2,4
64	20000	3	60	5,0	2,9	2,2	5,3	9,6	2,5	5,1	6,9	15,1
45	20000	5	100	6,5	3,7	3,6	5,1	4,2	1,8	5,4	6,3	10,8
49	20000	5	100	11,1	3,9	4,9	2,6	2,3	2,5	11,4	5,2	5,2
59	20000	5	100	5,3	9,7	5,1	1,6	1,7	9,1	7,0	5,4	6,7
50	20000	7	140	1,9	7,1	8,3	1,7	3,2	6,3	5,7	4,5	5,6
57	20000	7	140	2,3	4,5	9,3	4,5	4,5	1,9	3,8	5,7	6,6
58	20000	7	140	10,2	8,7	6,7	9,3	7,3	5,1	2,3	1,8	10,7
46	30000	3	90	4,4	5,8	4,2	8,8	5,1	8,6	6,2	5,8	6,2
54	30000	3	90	8,4	8,8	3,6	5,0	5,5	6,2	5,6	4,6	3,3
66	30000	3	90	0,6	3,9	3,2	3,2	4,0	4,4	7,7	4,7	5,5
56	30000	5	150	4,8	2,6	5,9	3,4	3,8	6,0	5,8	11,4	7,6
65	30000	5	150	11,0	6,2	5,6	8,0	4,6	5,3	6,1	7,2	5,9
70	30000	5	150	2,4	4,2	5,5	4,0	4,6	4,5	5,7	8,5	6,7
52	30000	7	210	3,2	7,3	4,6	4,5	5,4	7,1	2,3	4,7	4,3
67	30000	7	210	4,1	6,1	2,4	4,2	2,3	3,1	2,6	3,5	4,4
69	30000	7	210	3,9	6,0	6,2	2,3	7,1	1,5	3,3	3,9	5,4
48	40000	3	120	2,4	4,0	8,2	5,2	5,4	5,8	6,9	1,3	4,5
55	40000	3	120	3,8	6,0	8,7	9,2	7,4	5,7	6,3	5,1	8,6
61	40000	3	120	4,0	3,2	5,1	5,3	4,5	9,2	10,6	2,8	2,7
47	40000	5	200	4,5	5,9	5,0	4,9	6,0	1,5	8,7	2,8	5,0
51	40000	5	200	2,6	4,1	7,9	4,0	5,6	4,9	3,5	2,5	7,4
68	40000	5	200	5,2	6,2	4,2	3,8	5,6	3,9	5,4	6,5	1,8
44	40000	7	280	3,7	4,4	3,2	9,1	3,5	3,4	3,2	4,5	13,0
62	40000	7	280	3,9	7,3	6,4	6,4	3,1	3,0	3,6	5,7	4,6
63	40000	7	280	7,3	4,3	3,5	4,1	4,7	7,2	3,4	4,4	2,4

Appendix 3-4. Rear side roundness errors for CFRP laminate with Aluminum-Phenolic support plate micro-drilling experiments.

Run Order	Spindle Speed (rpm)	Feed (µm/rev)	Feed Rate (mm/min)	Roundness rear 1	Roundness rear 2	Roundness rear 3	Roundness rear 120	Roundness rear 121	Roundness rear 122	Roundness rear 240	Roundness rear 241	Roundness rear 242
53	20000	3	60	4,3	5,6	15,0	27,3	17,3	18,0	15,5	34,6	53,0
60	20000	3	60	4,7	12,2	12,4	18,1	10,1	14,1	31,9	19,6	31,1
64	20000	3	60	22,3	8,8	18,2	29,0	27,4	32,0	34,6	24,7	11,6
45	20000	5	100	13,2	7,9	15,5	20,3	13,3	5,0	12,1	21,1	23,3
49	20000	5	100	13,0	7,7	9,2	11,5	10,7	11,4	17,1	17,6	26,6
59	20000	5	100	6,7	12,8	14,4	14,9	23,2	31,2	30,4	25,0	17,6
50	20000	7	140	9,0	21,2	34,0	31,4	12,1	7,2	8,0	26,0	12,0
57	20000	7	140	9,8	14,5	5,9	17,1	33,6	32,9	14,9	9,3	25,2
58	20000	7	140	11,3	7,5	12,1	24,7	13,4	19,3	8,8	24,5	36,5
46	30000	3	90	23,2	9,4	15,7	11,6	12,2	11,1	18,6	34,8	8,3
54	30000	3	90	8,8	10,6	8,7	23,1	15,1	36,0	11,5	11,8	32,7
66	30000	3	90	10,4	7,2	2,2	16,0	13,2	11,1	18,8	13,9	32,1
56	30000	5	150	12,4	15,8	11,4	28,2	37,5	26,6	11,6	19,6	16,9
65	30000	5	150	41,7	10,1	21,2	19,9	18,7	24,1	18,6	17,4	15,1
70	30000	5	150	8,5	7,5	18,8	37,2	34,4	7,8	15,8	24,3	25,1
52	30000	7	210	14,3	6,2	18,4	33,5	28,2	14,4	19,2	25,8	12,2
67	30000	7	210	5,0	7,4	7,5	4,7	12,0	10,6	8,8	19,2	21,3
69	30000	7	210	7,7	11,9	5,0	23,5	21,7	8,5	21,1	17,3	17,4
48	40000	3	120	7,4	6,2	11,1	23,7	12,5	4,8	12,2	5,8	15,1
55	40000	3	120	5,6	13,2	12,2	18,2	25,4	18,3	31,6	25,2	18,5
61	40000	3	120	10,5	3,8	13,4	12,6	22,6	23,9	16,3	15,0	17,2
47	40000	5	200	9,0	17,7	25,3	24,0	29,8	21,0	16,9	7,8	20,4
51	40000	5	200	7,5	12,6	8,3	10,1	17,0	4,9	17,9	25,2	13,2
68	40000	5	200	12,9	17,1	7,2	17,0	15,3	12,1	27,9	39,6	23,1
44	40000	7	280	12,9	5,1	10,8	18,9	22,6	12,1	16,7	6,6	15,5
62	40000	7	280	8,1	9,6	5,5	10,5	10,9	11,8	4,1	17,3	37,6
63	40000	7	280	13,4	13,0	9,2	14,2	22,0	20,9	11,0	11,6	12,3

Appendix 3-5. Front side roundness errors for CFRP laminate with Brass-Wood support plate micro-drilling experiments.

Run Order	Spindle Speed (rpm)	Feed (µm/rev)	Feed Rate (mm/min)	Roundness front 1	Roundness front 2	Roundness front 3	Roundness front 120	Roundness front 121	Roundness front 122	Roundness front 240	Roundness front 241	Roundness front 242
77	20000	3	60	2,8	4,1	9,7	4,9	6,8	5,8	7,2	6,9	5,6
81	20000	3	60	6,9	1,6	5,1	7,9	9,6	7,1	6,4	6,5	9,8
75	20000	5	100	4,7	5,1	7,6	8,0	8,0	4,6	4,3	5,4	4,7
82	20000	5	100	6,2	4,9	3,3	8,4	6,4	5,8	3,8	6,8	8,5
79	20000	7	140	5,3	2,4	8,6	6,0	3,5	8,7	6,4	3,3	11,7
89	20000	7	140	2,0	4,9	4,6	0,9	5,4	4,2	9,4	11,8	7,2
80	30000	3	90	7,7	8,0	7,1	12,3	8,0	5,4	6,4	5,8	5,4
83	30000	3	90	3,1	6,8	3,6	8,2	6,0	3,1	4,9	9,2	4,7
73	30000	5	150	4,5	7,8	7,1	6,8	13,0	6,4	4,2	3,8	6,1
86	30000	5	150	5,5	4,8	8,7	4,8	7,7	9,2	3,0	7,2	29,9
74	30000	7	210	9,2	1,5	5,7	7,3	6,4	7,2	12,7	8,2	4,2
88	30000	7	210	4,4	7,1	7,9	4,0	6,8	2,8	4,2	7,7	4,2
78	40000	3	120	9,0	7,3	8,4	7,7	7,5	7,5	5,4	4,1	7,2
85	40000	3	120	3,2	7,4	7,1	8,3	8,2	4,2	2,2	9,1	7,2
76	40000	5	200	8,5	2,9	6,0	2,1	5,4	4,6	10,8	18,6	7,9
87	40000	5	200	6,3	4,1	7,6	2,3	4,0	2,7	4,8	4,3	13,2
72	40000	7	280	6,0	4,6	8,6	8,4	2,9	5,8	6,1	3,3	3,1
84	40000	7	280	4,4	2,1	3,7	4,3	9,5	5,4	10,6	8,7	8,1

Appendix 3-6. Rear side roundness errors for CFRP laminate with Brass-Wood support plate micro-drilling experiments.

Run Order	Spindle Speed (rpm)	Feed (µm/rev)	Feed Rate (mm/min)	Roundness rear 1	Roundness rear 2	Roundness rear 3	Roundness rear 120	Roundness rear 121	Roundness rear 122	Roundness rear 240	Roundness rear 241	Roundness rear 242
77	20000	3	60	7,1	10,0	8,2	7,9	39,9	9,9	4,1	37,5	23,6
81	20000	3	60	7,5	12,1	7,7	20,3	20,7	15,4	33,6	11,4	21,3
75	20000	5	100	6,1	9,6	7,9	27,4	8,8	8,9	43,7	14,7	22,0
82	20000	5	100	5,2	10,8	22,7	3,6	16,1	14,6	7,4	17,9	12,1
79	20000	7	140	7,1	8,4	12,4	19,4	25,7	9,0	15,7	12,7	15,2
89	20000	7	140	16,7	3,3	8,3	15,0	7,1	17,0	22,3	28,5	10,0
80	30000	3	90	9,0	12,3	9,8	14,7	12,9	7,5	8,9	36,7	26,7
83	30000	3	90	6,3	6,6	9,2	26,9	18,1	15,8	5,3	25,4	28,6
73	30000	5	150	8,2	9,8	6,4	24,2	17,0	13,1	13,0	32,1	20,7
86	30000	5	150	8,2	9,7	10,0	19,1	7,8	17,0	6,2	23,3	29,5
74	30000	7	210	5,3	8,5	15,1	11,8	6,7	26,7	9,2	43,8	10,0
88	30000	7	210	5,8	11,9	5,5	29,2	23,5	16,7	14,4	11,4	29,3
78	40000	3	120	4,2	5,4	13,1	28,8	20,1	12,4	14,0	17,7	22,6
85	40000	3	120	7,5	9,1	7,3	15,9	24,1	8,3	23,5	24,3	10,5
76	40000	5	200	14,2	6,6	7,0	12,7	26,3	22,4	24,1	25,7	20,7
87	40000	5	200	13,5	12,2	7,6	20,3	26,1	16,4	10,3	16,6	10,6
72	40000	7	280	7,3	6,5	5,9	5,7	18,0	12,2	17,1	11,5	4,4
84	40000	7	280	7,9	9,0	4,4	25,8	17,3	16,3	5,2	15,5	29,6

Appendix 4-1. Front side fiber overlap areas for bare CFRP laminate micro-drilling experiments.

Run Order	Spindle Speed (rpm)	Feed (µm/rev)	Feed Rate (mm/min)	Front Fiber Overlap Area 1	Front Fiber Overlap Area 2	Front Fiber Overlap Area 3	Front Fiber Overlap Area 120	Front Fiber Overlap Area 121	Front Fiber Overlap Area 122	Front Fiber Overlap Area 240	Front Fiber Overlap Area 241	Front Fiber Overlap Area 242
24	20000	3	60	194200	191010	192836	178662	180649	185440	182182	183080	179566
36	20000	3	60	198728	198466	197380	185543	196839	194936	179356	188728	189279
40	20000	3	60	189727	191613	186859	175963	181503	187844	182925	182135	174118
29	20000	5	100	189447	185597	190732	169842	175953	181673	190452	184767	192771
30	20000	5	100	198507	200339	203770	189034	198770	195235	193086	186905	192613
38	20000	5	100	192741	192837	192060	195311	207016	194566	181325	185708	203737
16	20000	7	140	191372	194673	197050	187513	187053	184335	182124	188205	186235
42	20000	7	140	195053	192903	192042	173345	170870	172848	187568	186732	125483
43	20000	7	140	189115	191819	193616	184302	196393	183696	175516	187469	194379
15	30000	3	90	195889	189148	194430	189153	187701	199781	186411	185884	190984
23	30000	3	90	194131	196377	190861	192480	192901	199881	181124	184299	191860
35	30000	3	90	192300	190298	187752	179986	183775	181591	185885	173014	182973
17	30000	5	150	194485	200014	197281	189380	187532	187547	175625	188201	178960
21	30000	5	150	202330	200792	195519	194264	190090	183944	179357	185007	183428
37	30000	5	150	197964	193361	198551	179749	185229	188508	181807	183621	191004
27	30000	7	210	194652	195819	194216	181605	194777	186754	181088	189411	180109
33	30000	7	210	195567	188540	188117	185245	176572	180028	188442	183875	187947
34	30000	7	210	196590	189238	192588	189898	195051	182893	185625	188313	200423
19	40000	3	120	192884	194703	191918	180849	184108	191104	192777	203942	190464
20	40000	3	120	196911	195493	197721	188274	192898	189503	171609	185722	181448
31	40000	3	120	186326	189024	188952	189618	191876	185351	174869	178962	180764
28	40000	5	200	189046	190519	191504	190982	184134	184116	176871	177996	175927
32	40000	5	200	194622	192392	192913	184332	190334	188868	185176	180818	180733
41	40000	5	200	193043	193919	195476	193239	190885	183102	190442	185813	187052
22	40000	7	280	200426	198096	197618	188921	178968	186063	180505	180245	178096
26	40000	7	280	193579	197518	199110	188330	185009	198003	197099	176500	182494
39	40000	7	280	190398	183369	187895	180214	182968	180881	175341	173046	164888

Appendix 4-2. Rear side fiber overlap areas for bare CFRP laminate micro-drilling experiments.

Run Order	Spindle Speed (rpm)	Feed (µm/rev)	Feed Rate (mm/min)	Rear Fiber Overlap Area 1	Rear Fiber Overlap Area 2	Rear Fiber Overlap Area 3	Rear Fiber Overlap Area 120	Rear Fiber Overlap Area 121	Rear Fiber Overlap Area 122	Rear Fiber Overlap Area 240	Rear Fiber Overlap Area 241	Rear Fiber Overlap Area 242
24	20000	3	60	179281	186744	178346	147079	164684	138147	130687	113485	136025
36	20000	3	60	168865	131320	159961	115816	89588	138624	129175	160447	151501
40	20000	3	60	180645	187783	156019	160327	161814	107463	136119	114280	148474
29	20000	5	100	172740	182317	178655	149911	141790	177704	169895	102250	95475
30	20000	5	100	188013	190427	184535	175269	175950	169837	132797	164734	149179
38	20000	5	100	185433	190510	166244	161024	136805	159835	162004	116728	72237
16	20000	7	140	189829	144808	160525	165638	92344	168544	16850	97586	108614
42	20000	7	140	163258	186863	182915	169904	161132	176327	169207	140702	134440
43	20000	7	140	185268	192174	184546	148414	177769	168173	151560	129650	116087
15	30000	3	90	184959	179515	183863	129070	99397	128292	122185	113471	133888
23	30000	3	90	176965	181892	179379	142867	153408	143551	107255	122094	121640
35	30000	3	90	182113	181126	183808	163545	122290	139501	122276	124706	137076
17	30000	5	150	138736	70822	184719	155274	172630	119413	174971	142524	184828
21	30000	5	150	121342	174801	163732	165324	137511	167130	169648	160503	166161
37	30000	5	150	178362	176111	180139	141674	53635	74010	130415	101383	148511
27	30000	7	210	182964	186555	178184	124926	155982	164356	128302	117268	109436
33	30000	7	210	188809	179077	194001	174330	177101	165747	166888	179465	168161
34	30000	7	210	183548	179951	181104	145139	158010	114881	155298	152609	143507
19	40000	3	120	175060	183479	189421	118216	152580	116645	131225	133398	57362
20	40000	3	120	191872	187117	188073	144363	158016	159717	141954	121367	121449
31	40000	3	120	182050	172788	178575	138391	76953	150640	114388	73270	136529
28	40000	5	200	169782	181876	162962	172859	170836	129106	158030	168659	129537
32	40000	5	200	111016	107637	172987	57921	164959	142163	113784	104475	109145
41	40000	5	200	185452	189150	186951	145226	163191	183155	142515	135508	112705
22	40000	7	280	181962	178661	181726	139652	127846	135765	99879	142874	158215
26	40000	7	280	175439	179020	173786	138308	112784	173793	146413	149583	68544
39	40000	7	280	181084	182080	185729	174764	171329	161414	111236	125044	165906

Appendix 4-3. Front side fiber overlap areas for CFRP laminate with Aluminum-Phenolic support plate micro-drilling experiments.

Run Order	Spindle Speed (rpm)	Feed (µm/rev)	Feed Rate (mm/min)	Front Fiber Overlap Area 1	Front Fiber Overlap Area 2	Front Fiber Overlap Area 3	Front Fiber Overlap Area 120	Front Fiber Overlap Area 121	Front Fiber Overlap Area 122	Front Fiber Overlap Area 240	Front Fiber Overlap Area 241	Front Fiber Overlap Area 242
53	20000	3	60	200880	201827	199338	193754	193757	194806	190391	192856	189251
60	20000	3	60	199530	199307	200443	190749	194394	198034	192418	191821	190814
64	20000	3	60	196554	200212	197468	198013	195702	191698	192616	195496	196738
45	20000	5	100	183340	189625	192080	191378	187875	185206	191180	190424	189405
49	20000	5	100	199132	192989	197010	190692	196727	189274	191269	195277	195122
59	20000	5	100	196857	192591	198961	187756	190352	189357	201392	188439	192417
50	20000	7	140	186857	194260	199193	192237	189020	186499	188392	193750	189877
57	20000	7	140	193657	194829	199721	188161	186270	193414	188552	192698	191941
58	20000	7	140	209786	198978	204721	195201	191841	194727	194304	202641	192170
46	30000	3	90	190392	192608	196896	193236	187987	191894	194864	189769	189984
54	30000	3	90	207482	188085	191104	182247	192642	190891	185586	190493	190524
66	30000	3	90	199068	196488	194458	189273	189301	192013	198999	195164	192486
56	30000	5	150	191649	189446	184843	194570	192045	193824	191243	191641	190130
65	30000	5	150	186671	198090	202877	197288	192385	194588	198799	198443	192607
70	30000	5	150	192969	200819	200267	194172	193935	196799	195476	195591	191849
52	30000	7	210	197705	198589	195811	197851	204082	198400	191366	190613	195171
67	30000	7	210	201505	204288	200666	197131	190908	193526	188506	192660	198860
69	30000	7	210	197651	195072	209394	189809	197909	207533	188840	188768	194836
48	40000	3	120	186491	189574	201889	186220	186266	182283	185663	193599	190829
55	40000	3	120	192770	192718	190013	190411	192179	194073	191949	190951	191461
61	40000	3	120	195575	194334	193526	187607	193738	195678	193673	197115	192602
47	40000	5	200	196685	191030	193319	187655	194114	197512	193561	189011	195123
51	40000	5	200	199241	191523	190208	184274	189894	190123	194038	195888	198312
68	40000	5	200	204822	207099	194914	192535	196420	193292	192498	191628	193821
44	40000	7	280	190771	192138	195689	192862	192575	191954	192410	187634	187683
62	40000	7	280	189210	202498	193381	195843	196714	195521	195637	190853	191640

Appendix 4-4. Rear side fiber overlap areas for CFRP laminate with Aluminum-Phenolic support plate micro-drilling experiments.

Run Order	Spindle Speed (rpm)	Feed (µm/rev)	Feed Rate (mm/min)	Rear Fiber Overlap Area 1	Rear Fiber Overlap Area 2	Rear Fiber Overlap Area 3	Rear Fiber Overlap Area 120	Rear Fiber Overlap Area 121	Rear Fiber Overlap Area 122	Rear Fiber Overlap Area 240	Rear Fiber Overlap Area 241	Rear Fiber Overlap Area 242
53	20000	3	60	177366	173190	193969	147845	135730	170306	160938	134416	132911
60	20000	3	60	182543	192485	184444	163696	199413	175418	132686	143812	138178
64	20000	3	60	179774	183775	181779	172810	172385	163828	157536	170679	166944
45	20000	5	100	173895	161893	177879	156319	156512	160451	179317	167815	161142
49	20000	5	100	176890	181034	185323	162163	157374	158633	179236	169424	139834
59	20000	5	100	187856	186564	184927	175515	156218	156196	175585	175224	173863
50	20000	7	140	187218	171885	180431	171318	172788	179154	177798	178996	174271
57	20000	7	140	182646	181525	180695	143358	149346	162242	170496	179247	186046
58	20000	7	140	180672	184626	185889	161659	180603	177207	194596	171953	136068
46	30000	3	90	183263	171407	176851	150583	177680	173420	102993	137309	142699
54	30000	3	90	180158	174519	174147	160659	159047	158458	165728	167939	153493
66	30000	3	90	193269	189181	185427	178350	181715	170095	167018	169494	138197
56	30000	5	150	173164	181190	172911	165955	142335	151098	172544	147245	151860
65	30000	5	150	149752	182497	181066	168206	163909	153258	181272	167426	175444
70	30000	5	150	187868	189046	174563	165022	159868	178081	155629	164104	168092
52	30000	7	210	178877	180580	180487	170820	172649	180323	171696	179518	179755
67	30000	7	210	184277	184728	188174	147163	162102	164636	165160	167848	178883
69	30000	7	210	182984	182144	174597	168840	170225	175572	176096	175194	164150
48	40000	3	120	180217	177698	171307	147466	170650	155844	161867	152162	160944
55	40000	3	120	179711	178623	177276	120583	134585	150017	158124	163227	164646
61	40000	3	120	190624	187953	186101	160317	141757	130532	160611	150190	156812
47	40000	5	200	183411	180431	185914	169874	136934	156907	164620	178623	169897
51	40000	5	200	184021	174293	186905	154358	170301	173766	175502	142928	157047
68	40000	5	200	176619	174854	181305	166746	173558	169576	128395	121106	160224
44	40000	7	280	178759	182961	179134	147244	166562	172052	161650	159880	163944
62	40000	7	280	193979	189802	190853	169579	173749	172523	147788	151231	153673
63	40000	7	280	179146	182383	173485	152991	176242	160589	155440	175400	176469

Appendix 4-5. Front side fiber overlap areas for CFRP laminate with Brass-Wood support plate micro-drilling experiments.

Run Order	Spindle Speed (rpm)	Feed (µm/rev)	Feed Rate (mm/min)	Front Fiber Overlap Area 1	Front Fiber Overlap Area 2	Front Fiber Overlap Area 3	Front Fiber Overlap Area 120	Front Fiber Overlap Area 121	Front Fiber Overlap Area 122	Front Fiber Overlap Area 240	Front Fiber Overlap Area 241	Front Fiber Overlap Area 242
77	20000	3	60	188696	188083	189869	188143	180227	184128	179374	183263	182537
81	20000	3	60	183665	189579	187403	185691	189151	185160	186676	189282	186828
75	20000	5	100	193842	192236	193875	186547	186388	187173	184814	185188	183576
82	20000	5	100	183859	181863	180183	178325	179657	187550	193541	182497	183296
79	20000	7	140	186692	191253	191666	187282	191258	191454	197766	190913	184275
89	20000	7	140	184688	191619	193226	188573	187714	187668	197458	187982	183600
80	30000	3	90	189981	197869	202164	201393	188245	186404	190599	190154	188194
83	30000	3	90	194227	189239	191157	187862	186610	187320	183373	185084	184182
73	30000	5	150	185292	182989	193715	191190	185670	189333	180228	183325	181673
86	30000	5	150	192341	199240	191111	183476	190049	193314	180182	183899	195690
74	30000	7	210	194464	185465	187728	189571	195469	198123	185977	185088	189578
88	30000	7	210	195462	189607	196049	189890	190122	190443	188924	193689	193013
78	40000	3	120	191634	184490	185535	189174	188008	186533	181106	181937	181624
85	40000	3	120	184737	186371	186869	184786	186375	187581	184546	173337	179988
76	40000	5	200	187050	183166	181026	185478	182151	185329	187116	200591	183179
87	40000	5	200	193888	191690	186637	188544	192746	192210	183451	186186	194875
72	40000	7	280	191643	190479	186361	194658	193199	195523	187721	194404	193133
84	40000	7	280	193079	199428	193744	201164	199184	194574	191697	195338	204284

Appendix 4-6. Rear side fiber overlap areas for CFRP laminate with Brass-Wood support plate micro-drilling experiments.

Run Order	Spindle Speed (rpm)	Feed (µm/rev)	Feed Rate (mm/min)	Rear Fiber Overlap Area 1	Rear Fiber Overlap Area 2	Rear Fiber Overlap Area 3	Rear Fiber Overlap Area 120	Rear Fiber Overlap Area 121	Rear Fiber Overlap Area 122	Rear Fiber Overlap Area 240	Rear Fiber Overlap Area 241	Rear Fiber Overlap Area 242
77	20000	3	60	179862	162582	173595	141003	149066	137780	123871	105003	130331
81	20000	3	60	183502	181658	188130	165450	160015	158720	148816	173936	144668
75	20000	5	100	182748	185049	165849	147130	168630	174294	142181	164291	166822
82	20000	5	100	148872	199359	189785	184585	185383	168465	165045	136660	171072
79	20000	7	140	186894	189489	187234	164453	161652	180064	169385	148356	160894
89	20000	7	140	174122	185281	179091	150609	177711	177828	174671	160019	177899
80	30000	3	90	187986	188831	186249	154291	145036	177938	157419	147495	124687
83	30000	3	90	180067	184556	186313	135544	143259	164539	132129	153898	118438
73	30000	5	150	183502	172479	166464	155216	176595	182139	165958	130734	146569
86	30000	5	150	189326	185023	184999	157702	161584	173758	173803	129934	116842
74	30000	7	210	184806	184700	182568	174583	151464	147640	157387	169661	177752
88	30000	7	210	184910	187359	184100	157675	154965	163431	143445	161316	147035
78	40000	3	120	179973	179114	186238	173055	174351	164285	146317	143507	161559
85	40000	3	120	184407	184527	182502	169284	143880	151955	137821	134166	162923
76	40000	5	200	174564	178922	184375	166265	157618	155096	123296	145966	165290
87	40000	5	200	172420	185396	187219	162555	127628	171515	168395	171321	161761
72	40000	7	280	177494	180621	186032	174073	178035	155858	133406	152144	146093
84	40000	7	280	178066	179962	184324	120100	154050	155617	176397	156799	139489

CURRICULUM VITAE

AHMET DOĞRUSADIK

Date of Birth: 13.04.1986

ahmet_ds@hotmail.com
Mobile: 0554 582 05 05

EDUCATION

MSc Istanbul Technical University
2007-2009 Department of Mechanical Engineering
Thesis Title: Experimental investigation of methods used in determining the fatigue lives of notched members (in Turkish)

BCs Sakarya University
2003-2007 Department of Mechanical Engineering

WORK EXPERIENCE

2007 – Present Otoman Makina San. ve Tic. Ltd. Şti.

PUBLICATIONS

1. Dogrusadik, A., Kentli, A., Bakkal, M., Cakan, M. (Submitted) Investigation on temperatures generated in CFRP laminates due to micro-drilling process.
2. Dogrusadik, A., Kentli, A. (Under Review) Experimental investigation of support plates' influences on tool wear in micro-drilling of CFRP laminates.
3. Dogrusadik, A., Kentli, A. (Under Review) Effects of support plates on hole form quality in micro-drilling of CFRP laminates.
4. Dogrusadik, A., Kentli, A. (2017) Comparative assessment of support plates' influences on delamination damage in micro-drilling of CFRP laminates. Composite Structures, 173, 156-167.